JKU

**JOHANNES KEPLER
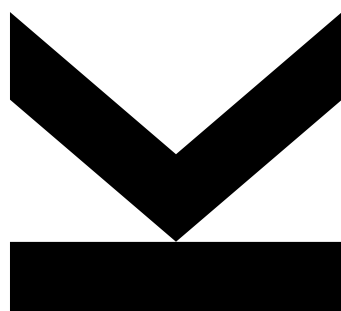UNIVERSITY LINZ**

Submitted by
DI. Halime Coskun Aljabour

Submitted at
**Linz Institute for Organic
Solar Cells (LIOS)/ Institute
of Physical Chemistry (IPC)**

Supervisor and
First Examiner
**o. Univ. Prof. Mag. Dr. DDr.
h.c. Niyazi Serdar Sariciftci**

Second Examiner
Prof. Dr. Christian Paulik

November 2018

Conducting, Functional Polymers from Bio-Organic Molecules for Catalysis

Doctoral Thesis

to obtain the academic degree of

Doktorin der technischen Wissenschaften

in the Doctoral Program

Technical Sciences

STATUTORY DECLARATION

I hereby declare that the thesis submitted is my own unaided work, that I have not used other than the sources indicated, and that all direct and indirect sources are acknowledged as references.
This printed thesis is identical with the electronic version submitted.

Linz, 19.11.2018

Signature

Acknowledgements

Foremost, I would like to express my special appreciation and thanks to the institute head Prof. Niyazi Serdar Sariciftci for supervision during my time as PhD-candidate. I greatly appreciate your extended supporting and sponsoring of my studies and research. From the day on, I did my physical chemistry exam with you, you never let me go and you always inspired me never to give up. Your guidance, involvement, motivation, and immense knowledge throughout this hard and exciting journey is invaluable to me. Your inputs on my career have been memorable. For all these, I sincerely thank you from the bottom of my heart.

Besides my supervisor, I would like to thank my dissertation committee: Prof. Wolfgang Buchberger, Prof. Christian Paulik, and Prof. Sabine Hild, for their co-operation and being beside me at the end of this long lasting marathon.

A very warm acknowledgement goes to Dr. Philipp Stadler, who guided me in all the time of my research. Especially, I am grateful to him for enlightening me in scientific topics. I sincerely thank him for his insightful comments and encouragements, which lead to the fruitful completion of this research.

My extended thanks also goes to the internal and external collaboration partners during this period. Without their precious support and expertise, it would not be possible to conduct many of the experiments and theoretical calculations for this thesis.

I thank the whole institute's members for their motivation, for the stimulating discussions and for all the entertainment, we have had in the last couple of years.

Last but not the least, I owe thanks to a very special person to me, my husband, Abdalaziz, for his endless love, support and encouragement during my doctoral studies. You were always with me at times I thought that it is impossible to continue. I highly value your contribution and deeply appreciate your belief in me. In addition, I am extremely thankful to my father-in-law and mother-in-law, Suliman and Buthayna, for their kindness, motivation and support not only during my studies but always all the time.

Finally, I would like to thank my family: my parents, Tuncay and Filiz and my sisters, Betül and Tuba for supporting me spiritually throughout writing this thesis. You always gave me the strength, courage and patience to work through all these years. You were standing beside me with all your love and never-ending support. It is my fortune to have such a lovely and caring family, standing always beside me and supporting any decision I made.

Abstract

The utilization of bio-inspired, polymer-based materials in the field of catalysis can help to resolve relevant energy questions in the 21th century. This work is dedicated to the design and engineering of electrocatalysts for carbon dioxide reduction reaction (CO2RR) and hydrogen evolution reaction (HER) using bio-derived, hydrogen-bonded systems, that exhibit heterogenous catalytic activity. These will be important as sustainable systems, which are shown here to exhibit tremendous performance. In light of today´s dependence on expensive and rare noble metals, it is of outmost interest to develop alternative polymeric and non-metallic contenders, which will replace metals and thus increase the catalyst material pool and the catalyst versatility. The here demonstrated electrocatalytic polymers are low-cost and bio-inspired, have low environmental impact and at the same time offer similar stability as noble metals but also tunable physical-electronic properties. Combined with their bio-compatibility they will be a future emerging material class in the field of electrocatalysis.

The focus of this thesis has been to generate polymers with superior catalytic activity and therefore their electronic properties have been improved, in particular their intrinsically low capability to transport electrons. In their initial state, most biopolymers are insulators. In this work, a novel synthesis path is shown to create doped conductive biopolymers with excellent catalytic activity and long-term stability.

The synthesis of two conductive and electrocatalytic biopolymers is presented: these are first polydopamine (PDA) as a derivative of the naturally occurring pigment eumelanin, and, second, polyguanine (PG), a purine base and component of the desoxyribonucleic acid (DNA), which adopted an emeraldine-related structure. Both biopolymers have been applied as electrocatalysts for CO2RR and/or HER. The synthesis pathway from the monomers to the conductive and functional biopolymers is described using a facile one-step oxidative chemical vapor deposition (o-CVD) technique. This has been the crucial effort to unit polymerization and doping leading to the desired electrically conductive biopolymers in a single step reaction without compromising on the organic functionality remaining unchanged on the polymer backbone.

Besides replacing the metal catalysts by organic units, the main motivation in this work was to mimic natural phenomena by using artificial biopolymers. Therefore, polydopamine was firstly applied as an electrocatalyst for CO2RR to convert the anthropogenic carbon dioxide emissions into useful chemical feedstock. The catalytic effect driven by hydrogen-bonded functional motifs resulted in significant electrocatalytic performance with almost > 90 % Faraday efficiency and a geometric current density of 18 mA cm^{-2} at 210 mV overpotential. Besides the CO_2 reduction productions leading to CO and formate, hydrogen was also produced as a side-product at neutral pH. This result gave the hint, that hydrogen could be evolved by the PDA catalyst, when the polymer is further re-designed.

In the next approach, such structurally modified PDA was applied in HER in an acidic medium showing excellent HER performance with a Tafel slope of 80 mV dec^{-1} and an overpotential of -190 mV vs. reversible hydrogen electrode (RHE) at 10 mA cm^{-2} and stable catalytic activity demonstrated by an initial 168 hours electrolysis. More important, scaled continuous-flow electrolysis was exhibited, producing 1 L of molecular hydrogen within less than 9 hours using 2.3 mg of biopolymer electrocatalyst.

In order to confirm the proof-of-principle of catalytic activity in biopolymers containing organic themes, an alternative concept was sought: polyguanine (PG) is synthesized similarly to PDA and utilized it as HER electrocatalyst. It's ability to bind protons similar to the emeraldine form of polyaniline led to a signficiant HER activity with a Tafel slope as low as 80 mV dec^{-1} at an overpotential of -290 mV vs. RHE at 10 mA cm^{-2} and 80 hours of continuous electrolysis.

The idea of employing biopolymers in various heterogenous electrocatalytic applications reveals that these emerging materials will be promising candidates for future sustainable energy conversion catalysts.

Kurzfassung

Die Verwendung von bio-inspirierten und Polymer-basierten Materialien in der Katalyse kann eine Notwendigkeit im 21. Jahrhundert werden. Diese Arbeit widmet sich dem Design und der Konstruktion von Elektrokatalysatoren für die Kohlenstoffdioxid-Reduktionsreaktion (CO2RR) und der Wasserstoffentwicklungsreaktion (HER) unter Verwendung aus biologischer Produktion stammenden, Wasserstoff-gebundenen Systemen, die auch heterogene katalytische Aktivität zeigen. Heute basieren die besten Elektrokatalysatoren hauptsächlich auf teuren und seltenen Edelmetallen und es ist von besonderem Interesse, alternative Katalysatormaterialien zu entwickeln, die diese Metalle ersetzen können und somit den Katalysatorpool und dessen Vielfalt erhöht. Für die Biopolymer-Katalysatoren sprechen die niedrigen Kosten für die Herstellung, ihre biologische Herkunft und damit verbunden ihre Umweltfreundlichkeit, aber auch ihre Leistungsdaten, vor allem ihre hohe katalytische Aktivität und Stabilität, kombiniert mit einstellbaren elektronischen-physikalischen Eigenschaften als auch die Kombination von Bioabbaubarkeit und Biokompatibilität. Das alles macht die Materialklasse der Biopolymere hochinteressant als künftige Katalysatormaterialien.

Eine entscheidende Einschränkung hinsichtlich der Anwendung dieser Materialien - ihre intrinsisch geringe Elektronenleitfähigkeit – wurde in dieser Arbeit überwunden: ein integriertes Dotierungsverfahren, das die Polymere von ihrem isolierenden Grundzustand in einen leitenden Zustand versetzt und damit entscheidend ihre katalytische Aktivitäten verbessert, wurde implementiert.

In dieser Studie wird eine neuartige Synthese von zwei Biopolymeren präsentiert: Polydopamin (PDA), die zur natürlich vorkommenden Pigmentfamilie von Eumelanin gehört, und von Polyguanin (PG), einer wichtigen Purinkomponente der Desoxyribonukleinsäure (DNA). Beide Polymere werden für die CO2RR und/oder HER verwendet. Die funktionellen, leitfähigen Polymere werden durch einfache oxidative chemische Dampfphasenabscheidung (o-CVD) hergestellt. Diese Technik ermöglicht die vereinte Polymerisation und Dotierung von Dopamin und Guanin in einer einstufigen Reaktion, ohne dass die organischen Funktionalitäten, die im Polymerrückgrat verbleiben, beeinträchtigt werden.

Neben der Ersetzung der Metallkatalysatoren durch organische Funktionalitäten, war die Hauptmotivation in dieser Arbeit, natürliche Phänomene durch die Verwendung künstlicher Biopolymere nachzuahmen. Daher wurde Polydopamin zunächst als Elektrokatalysator für CO2RR verwendet, um die anthropogene Kohlenstoffdioxidemissionen in nützliche Chemikalien umzuwandeln. Die katalytische Wirkung von wasserstoffverbrückten funktionellen Motiven führte zu einer außerordentlich guten elektrokatalytischen Leistung mit nahezu > 90% Faraday-Effizienz und einer geometrischen Stromdichte von 18 mA cm^{-2} bei 210 mV Überspannung. Neben den CO_2-Reduktionsprodukten (CO und Formiat) wurde auch Wasserstoff als Nebenprodukt bei

neutralem pH erzeugt. Dies gab den Hinweis, dass Wasserstoff durch den PDA-Katalysator entwickelt werden könnte, wenn die richtigen Bedingungen zusammentreffen würden.

Im nächsten Ansatz wurde strukturell modifiziertes PDA in HER in einem sauren Medium angewendet, wobei die HER-Leistung mit einer Tafel-Steigung von 80 mV dec^{-1} zufriedenstellend war und ein Überpotential von -190 mV gegen reversible Wasserstoffelektrode (RHE) bei 10 mA cm^{-2} gefunden wurde zusammen mit enormer Katalysatorstabilität von 168 Stunden Dauerbetrieb. Noch wichtiger war die skalierte kontinuierliche Elektrolyse, die 1 L molekularen Wasserstoff in weniger als 9 Stunden mit 2.3 mg Biopolymer-Elektrokatalysator erzeugte.

Um den prinzipiellen Nachweis der katalytischen Aktivität in Biopolymeren mit organischen Themen zu bestätigen, wurde nach ein zweites und ähnliches Konzept gesucht. Polyguanin wurde auf die gleiche Weise synthetisiert und charakterisiert. Die Verwendung von PG für HER ist durch die enge Protonenbindung naheliegend und PG liefert vergleichbare Ergebnisse in der elektrokatalytischen HER mit einer Tafel-Steigung von 80 mV dec^{-1} und einem Überpotential von -290 mV vs. RHE bei10 mA cm^{-2} und mehr als 80 Stunden kontinuierliche Elektrolyse.

Die Idee, Biopolymere in verschiedenen heterogenen elektrokatalytischen Anwendungen einzusetzen, zeigt, dass diese neu entstehenden Materialien vielversprechende Kandidaten für eine nachhaltigere Energieumwandlung sein werden.

CONDUCTING, FUNCTIONAL POLYMERS FROM BIO-ORGANIC MOLECULES FOR CATALYSIS

Table of Contents

1. Introduction

1.1. Role of Electrocatalysts in Catalysis

The role of electrocatalysts in various branches of catalysis is indispensable. Over the last few decades, the research field had developed, concerned with the design and development of proper electrocatalysts, reflected in large number of publications.[1-15]

One great need for electrocatalyst application exists in the field of renewable energy. Basically, the idea of renewable energy sources (i.e. wind, solar, hydropower, biomass and geothermal energy) relies on becoming independent on the fossil fuels, such as coal, oil and natural gas, since the combustion of the fossil fuels generates carbon dioxide (CO_2). CO_2 is considered as the main and most problematic greenhouse gas. The atmospheric CO_2 concentration is increasing tremendously every year and hence an immediate action is needed to stop this rise, which is also responsible for climate change and global warming on earth.[1-19] Two approaches are well established in handling this issue: (i) the carbon capture and sequestration (CCS), which captures and stores CO_2 at underground facilities, and (ii) the carbon capture and utilization (CCU), which deals with the transformation and reduction of the CO_2 in to useful chemicals and thus CO_2 is used as a future non-fossil carbon feedstock (Figure 1). However, the electroreduction of the carbon dioxide (CO_2) requires the utilization of advanced electrocatalysts due to the high chemical stability of the CO_2.[20-21]
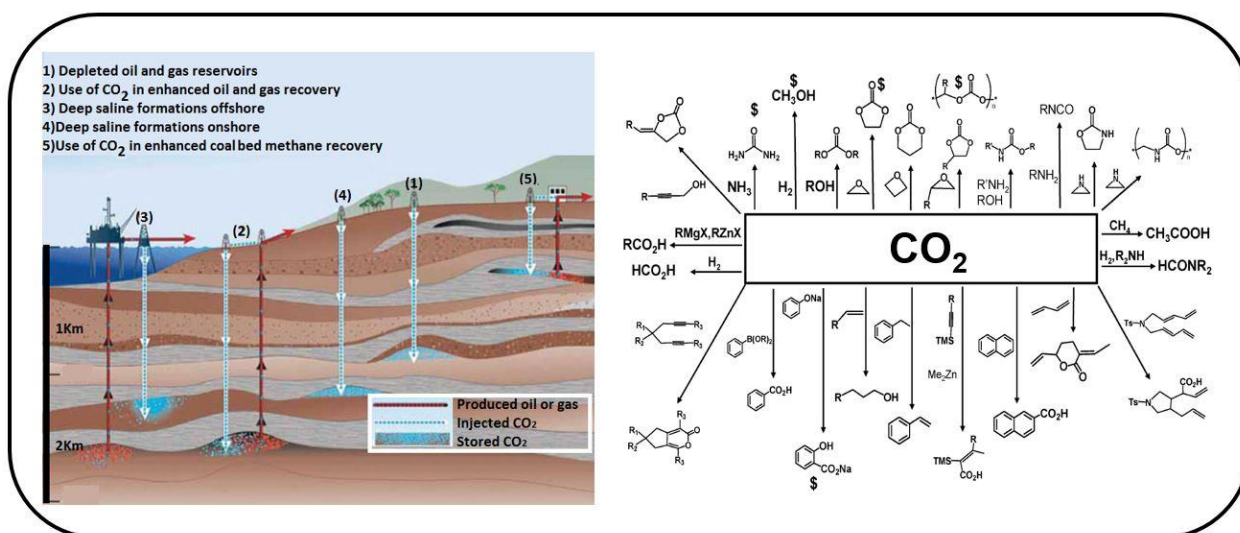
Figure 1. Two approaches to deal with the increasing atmospheric CO_2 concentration. The carbon capture and sequestration (CCS on the left), the carbon capture and utilization (CCU on the right).[20-22]

The research and development in alternative and renewable energy sources have the priority if we intend to meet the growing energy demand of the modern world society outside of the fossil sources.[23] Ecological responsible technologies are important.

Hydrogen (H_2) gas, recovered from water electrolysis, is thought to be the successor for replacing fossil fuels owing to its energy density and carbon neutrality.[24-43] In addition, the produced H_2 gas

reacts with CO_2 to create artificial synthetic natural gas methane (SNG) which is also a large effort on the "power-to-gas" strategies for CO_2 capture and utilization (CCU).[44-46]

However, the approach of water electrolysis for hydrogen evolution requires optimum energy conversion with minimum cathodic overpotentials. To guarantee such energy-efficient conversion, electrocatalysts are requisite.

Presently, Pt-based electrocatalysts are the most-active catalysts for the both catalytic cycles in CO2RR and HER.[9, 19, 25, 37, 41, 47] Nonetheless, high costs and limited abundance of Pt restricts its extensive application. Instead, the implementation of the transition metal carbides, oxides, nitrides, selenides and phosphides but also conductive polymers, such as polythiophene, polypyrrole and polyaniline have been widely studied.[18, 29, 48-52] Indeed, there is an important scientific movement in quest of replacing expensive and rare metal catalysts by alternatives. In Tables 1 and 2, the state-of-the-art CO2RR and HER electrocalatysts are listed, respectively.

Catalyst	Applied Potential	Over-potential	Current Density	Time	F.E.	Ref.
graphene confined Sn quantum sheets	-2.0V vs SCE	N/A	30 mA cm^{-2}	50 h	90% (CO)	8
Cu_xO–Sn	-0.8V vs RHE	0.69V	4.5 mA cm^{-2}	12 h	90% (HCOO)	53
nanoparticles-Ag	-0.6V vs RHE	<0.5V	18 mA cm^{-2}	2 h	92% (HCOO)	11
nano-SnO_2	-1.8V vs SCE	0.34V	10.2 mA cm^{-2}	18 h	94 % (HCOO)	54
partially oxidized bulk Co	-0.85V vs SCE	0.24V	~10 mA cm^{-2}	40 h	90 % (HCOO)	5

Table 1 State-of-the-art electrocatalysts for CO and formate.

Electrocatalyst	Over-potential	Current Density	Stability	Tafel slope	Ref.
Pt (control)	50 mV	10 mA cm^{-2}	reproduced	33 mV dec^{-1}	[52]
Molybdenum phosphide	140mV	10 mA cm^{-2}	50 h	~48 mV dec^{-1}	[52]
Molybdenumdisulfide/Copper sulfide.	100mV	10 mA cm^{-2}	10 days	~40 mV dec^{-1}	[55]

Table 2 HER electrocatalysts state-of-the art including Pt as reference.

The aim of this work was to design alternative molecular catalysts, which operate comparatively efficient as metal catalysts due to the support of hydrogen-bonded, functional themes in their polymeric structure. Therefore, two candidates of conductive and functional polymers from bio-organic molecules were developed and utilized as electrocatalysts in CO2RR and HER in this thesis.

1.2. Conductive and Functional Bio-organic Polymers as Heterogenous Electrocatalysts

As introduced previously, the main motivation of this thesis was to develop conductive and functional, bio-organic polymers for electrocatalysis. However, a general and brief search of previous catalysis studies reveal that predominantly metals are top-rated. Closer investigations of these studies show that the catalytic activation always runs over metallic centers.[5, 35, 53, 56-58] There exist also catalysts with non-metallic centers, which rely on organic functionalities such as carbonyl, amine or hydroxyl groups, for example in enzymatic processes. This was the central inspiration in our work to mimic such themes from enzymology and to create organic-functional catalytic centers with on-par active catalytic sites. Such electrocatalytic organic matter could substitute metals.[59]

In particular, we refer here to the catalytic triades, where a description used in enzymology for sequential bio-catalysis. The central and frequent motif in the triade is the hydrogen-bonded function consisting of amine-carbonyl and amine-hydroxy groups. We mimic this process in the artificially synthesized biopolymers possessing these hydrogen-bonded themes. They are incorporated in the conjugated-conductive matrix and therefore we hypothesized that they work as electrocatalytic centers similar as in the enzymes. However, for this we had to overcome the poor electrical conductivity of present state-of-the art biopolymers. Most of the bio-organic

polymers such as polydopamines are insulators. Therefore, we sought to implement doping in order to improve their conductivity without affecting their hydrogen-bonded functions. [59-60]

1.3. Doping Mechanisms for Conductivity

In conjugated matter, doping is by definition the charge injection by a redox-reaction. This leads to enhanced electrical conductivity and changes in their optoelectronic properties. In general there exist four main types of doping: (i) photochemical, (ii) interfacial, (iii) chemical and (iv) electrochemical doping (Figure 2).[61]
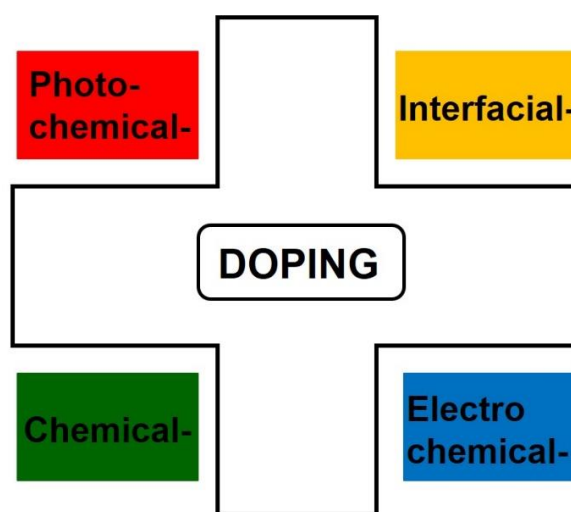
Figure 2. An illustration of the four doping mechanisms of conjugated polymers.[61]

Depending on which application is desired for the organic-conjugated system, the most suitable doping technique can be applied. Since, for the polymers attention was given to the phenomenon of electrical conductivity, we found it convenient to integrate the chemical doping in the polymerization process. In general, conducting polymers use oxidative polymerization – an oxidant-induced synthesis reaction cascade – to unit doping and polymerization in one single step. This approach was used in all of the investigated materials presented in this work. Whether a conjugated polymer can be chemically doped depends on the redox properties of the material: oxidation results in p-type doping; reduction in n-type doping. Accordingly, a p-type chemical doping can be written as:

$$P + ½ I_2 \rightarrow P^+ + I^- \qquad\qquad\qquad (1)$$

where P is the π-conjugated polymer and iodine the oxidation agent.[61] The polymers presented here will use only p-doping.

1.4. Biopolymers

1.4.1. Polydopamine (PDA)

Natural monomer units, such as hydrogen-bonded pigment molecules, represent an emerging class of conjugated semiconductors proposed for manifold bio-compatible applications.[59-60, 62-67]

Among other bio-related conjugated systems, polydopamines (PDAs) are frequently used conjugated biopolymers. Polydopamine illustrates a family of synthetic bio-inspired pigments offering high functional activity combined with semiconducting properties. To date, it represents one of the main synthetic biopolymers used mainly because of its simple synthesis in aqueous solutions.[59-60]

Polydopamines adopt indole-based conjugated-functional repeating units reminiscent to eumelanines – a group of natural pigments built from 5,6-dihydroxy-indoles and derivatives thereof (Figure 3). Consequently, early research has focused bio-mechanical applications.[68-75] Meanwhile, the synthesis pathways have eased and polydopamines are applied in manifold coatings, template layers and catalyst carriers.[71] The dominant synthesis to date uses oxidative polymerization of dopamine in aqueous solutions.[62, 71, 76-78] Thereby, ambient oxygen serves as C-C coupling agent making the synthesis straightforward (i.e. self-polymerization in a glass beaker). However, the downside of aqueous synthesis is resulting complex structures such as disrupted conjugation. Studies have shown that entire building blocks of hydrogen bond networks (H-aggregates) are formed within polydopamine and inhibit covalent coupling among the monomers. Hence, aqueous polydopamines are often inprocessable and show limited applicability in electronic devices.[62, 68, 71] In addition, the establishment of consistent growth parameters like temperature, pressure, local pH is difficult, as minor changes in ambient conditions significantly alter the final molecular structure.[68, 70-71, 79] In order to promote the covalent polymerization, monomer intermediate formation has to occur under controlled oxidative conditions. Discretely, these are the oxidation of dopamine (DA) to dopamine-quinone (DAQ), the intramolecular cyclization to leucodopaminechrome (LDC) and thereafter the formation and polymerization of indole and its derivatives (Figure 3).[59-60, 71]
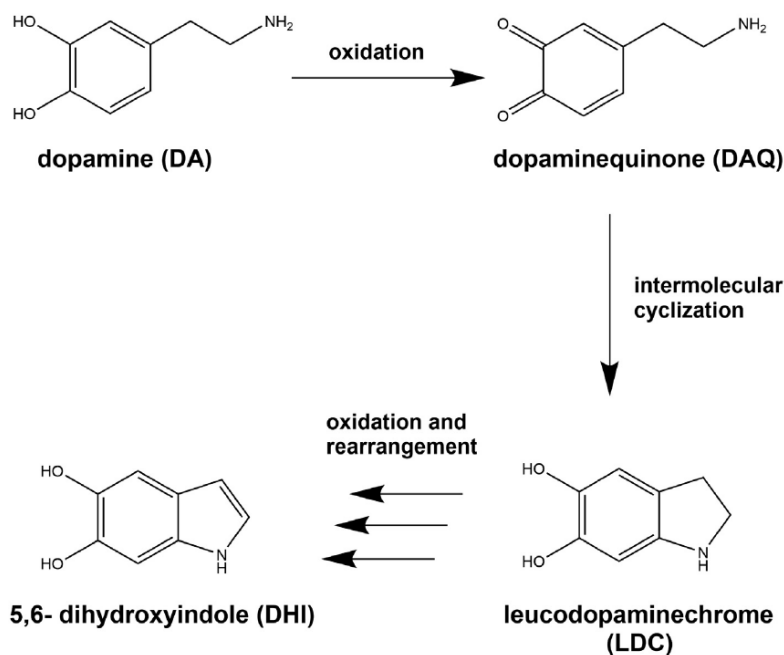
Figure 3. The potential chemical structures of the polydopamine (PDA) building blocks. Intermediate steps during PDA formation undergo numerous oxidation and rearrangement reactions. Reprinted/modified from [60].©

To overcome polydopamine´s affinity to build up H-aggregates, a synthesis strategy is pursued that adopts insights from classic conductive polymers.[68, 71, 80] The aim was to generate conjugated and conductive polydopamine from dopamine by using oxidative chemical vapor deposition. This technique is able use stronger oxidation reagent (as compared to ambient O_2) in combination with acidic surrounding to enforce oxidative C-C coupling. The goal was to arrive at the desired functionalized polyparaphenylene (PPP) type of backbone (Figure 17).[59-60]

Finally, the resulting polymer formed a polyparaphenylene (PPP) core with periodically repeating patterns of functional groups. The evidence of (i) indole (condensed secondary amine in an aromatic system with oxidized keto functions), (ii) dopamine, and, in the greatest quantity, (iii) oxidized dopamine (carbonyl function) was found (Figures 3 and 24). These dominated other intermediates, which are compounds thereof. The precise nature of the repeating unit in the polymer was identified by detailed spectral investigations.[59-60]

1.4.2. Polyguanine (PG)

Adenine, guanine, thymine and cytosine are the nucleobases of the deoxyribonucleic acid (DNA). These are hydrogen-bonded nitrogenous bases having the building block ability in the stabilization of the DNA double- helix by base pairing through hydrogen-bonding (adenine-thymine; guanine-cytosine). [81-84]

Besides adenine, guanine is an important purine component in both DNA and RNA (ribonucleic acid). Guanine is responsible not only for the genetic information storage but also for protein biosynthesis, energy transduction across the cells and the regulation of cell metabolism. Therefore, the balance of guanine in human body is highly critical, since abnormal guanine concentrations lead to serious diseases. That is why the detection of guanine occupied for a long period the research community. Many chromatographic, spectroscopic and electrochemical studies were conducted for the detection of guanine mainly under physiological conditions. [82-83, 85-91]

One remarkable fact is that, the application of guanine as an active material in devices has been barely investigated. Only recently, some attempts were made in the fabrication of pentacene-guanine organic field effect transistors to enhance the device performances. Here, guanine was utilized as an organic dielectric layer, deposited by thermal evaporation above 230 °C at ultra high vacuum with a deposition rate of 2 nm/ min. [92]

In this thesis, an innovation in guanine research is initiated. Similarly as in PDA case, guanine monomer was implemented in the oxidative chemical vapor deposition synthesis in order to form polyguanine (PG). Guanine was oxidatively polymerized from the vapor phase in combination with sulfuric acid as an oxidant. Since the guanine monomer possess a primary amine functionality in its structure, it is hypothesized that the amine group gets initialized for the polymerization by oxidation. Next, the generated radical cations couple and finally the propagation reactions take place forming a conductive and oxidatively doped polyguanine at the end of the o-CVD synthesis. The proposed polymerization steps are shown in Figure 4.[84]
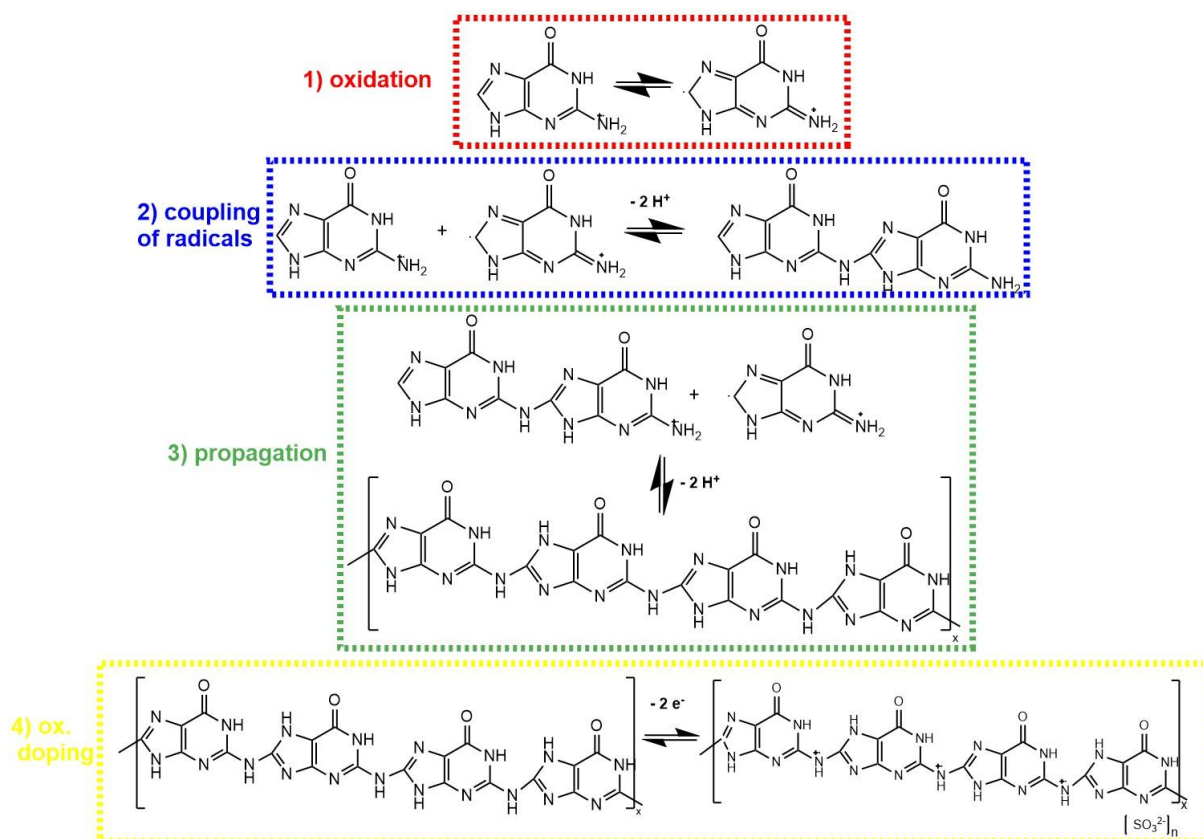
Figure 4. Proposed polymerization mechanism of polyguanine starting with an initiation of the primary amine group by oxidation, followed by the coupling reaction of the radical cations and finally the propagation reaction. After the polymerization reaction, oxidative doping take place in sulfuric acid environment all in a facile one- step reaction. Reprinted/modified from [84].©

2. Experimental

2.1. Materials

All of the materials used in this thesis are summarized in Table 3.

Materials	Purity	Supplier
Carbon felt	-	SGL group-the Carbon Company
Sapphire substrate	-	CrysTec Kristalltechnologie
Acetone	technical	VWR Chemicals
Isopropanol	AnalaR Normapur	VWR Chemicals
Hellmanex	-	VWA
Gold	99.99%	Ögussa
Nitrogen	-	JKU
Dopaminehydrochloride	98%	Sigma Aldrich
Calciumhydride	95%	Sigma Aldrich
Sodiumhydroxide	99%	Merck
Sulfuric acid	95-98%	J.T.Baker
Sodium sulfate	≥ 99.0%	Sigma Aldrich
Poly(methyl methacrylate)	-	Sigma Aldrich
Tetrabutylammoniumhexafluorophophate	> 99.0%	Fluka
Acetonitrile	> 99.9%	Roth
Ag/AgCl (3M KCl), (MF2079)	-	BASI
Carbon Dioxide	> 99.995%	Linde
Indium solder	99.999%	Sigma Aldrich
Guanine	≥ 99.0%	Fluka
Trifluoromethanesulfonic acid	98%	Sigma Aldrich
Polyaniline (emeraldine base)	-	Sigma Aldrich

Table 3 Materials used in this thesis.

2.2. Methods

2.2.1. Oxidative chemical vapor deposition (o-CVD)

2.2.1.1. Introduction into the Technique

Chemical vapor deposition is a widely used, powerful material-processing technique. In the past, CVD was mainly applied not only for the solid-thin film coatings on surfaces, but also for the synthesis of highly pure bulk materials and powders as well as composites. A great literature is provided on the application of CVD reporting on a wide range of materials. The books by Hitchman, Jensen and Shermen focus more on silicon application of CVD while those by Stringfellow, Jones and O`Brien show interest in semiconductor applications.[93-95]

Recently, oxidative chemical vapor deposition (o-CVD) is utilized for the synthesis of conducting polymers. Hence, by this technique new and novel possibilities as well as the production of high quality and reproducible films in a facile one-step synthesis are enabled.[96-97]

Usually, o-CVD requires two conditions: the presence of a monomer and the presence of an oxidant, which acts as an initiator of the polymerization reaction. In this study, both the monomers and the oxidant were supplied in their vapor form to conduct the synthesis. Bringing the chemicals to the vapor phase at optimum conditions required some engineering, since the tuning of the evaporation- or sublimation-rates of all reactants was not straightforward. Especially, the adjusting of the evaporation/ sublimation temperatures and thus the positioning of the reactants is crucial while performing o-CVD. In this thesis, sulfuric acid (with dissolved sodium sulfate) were utilized as oxidation agent and corresponding salt in the synthesis, respectively, in order to shift the balance towards SO_3^- and SO_4^{2-} in the gas phase.[59-60]

Although, the limitations concerning the o-CVD technique are few, some can be listed as follows: one important aspect is that only volatile materials find application in o-CVD. Any non-volatile reactant will not participate in the reaction. However, this point can also be advantageous, since contaminations such as iron can be excluded. Another problematic issue, which limits the synthesis, is the presently limited scalability of the synthesis. Additionally, critical parameters influencing the reaction are temperature and the gas-flow. The reaction parameters can vary and require empiric experience to reach high-quality homogeneous polymer films.
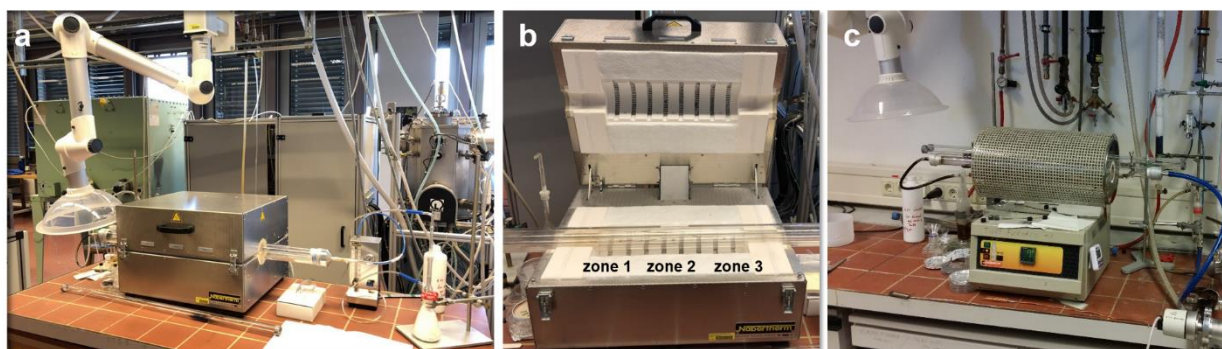
Figure 5. Tube furnaces for oxidative Chemical Vapor Deposition (o-CVD). (a and b) The Nabertherm company furnace for the o-CVD of polyguanine, (c) the Carbolite company furnace for the PDA synthesis by o-CVD.

Two different tube furnaces were used during the realization of this work. Nabertherm company furnace was principally used for the synthesis of polyguanine (Figure 5, a and b), while the Carbolite company furnace was employed for the synthesis of polydopamine (Figure 5, c). The Nabertherm company furnace is fully automatized and thus enables precise temperature control over three different zones. The Carbolite company furnace on the other hand, is home-made and simply adapted for o-CVD conditions without temperature-controlled reaction zones, provides however, the formation of highly reproducible and homogenously covered films. The technical properties of both furnaces are listed in Table 4.

Parameter	Carbolite Company	Nabertherm Company
Temperature	0-1200 °C	0-1100 °C
Gas Flow	0-5 L min^{-1}	0-600 L h^{-1}
Tube diameter	Up to 30 mm	Up to 50 mm
Opening	-	+
Movement	+	-
Bubbling	+	-
Programming	-	+
In-situ control	+	±
Reproducibility	+	+

Table 4 Technical properties of both furnace systems used in this thesis.

2.2.1.2. Synthesis of Polydopamine by o-CVD

In this work o-CVD was adapted for PDA. The gaseous dopamine free base was contacted with sulfuric acid. The latter serves as acidic oxidation agent and directs the synthesis to deposit conjugated and conductive PDA thin films. In this manner, it was possible to define film thickness and deposition on various substrates such as glass, sapphire or carbon-materials (Figure 6) for potential (catalytic) applications.[59-60]

The oxidative chemical vapor deposition (o-CVD) was carried out on glass substrates (20mm x 20mm) and sapphire (10mm x 10mm x 0.5mm) purchased from CrysTecKristall technology with Cr/Au electrodes utilized for the characterization of the polymer films. For the conductivity measurements, the metal contacts were deposited on sapphire by PVD through a 4-in-line contact mask. First, the substrates were cleaned using ultra-sonic bath 15 minutes each in acetone, isopropyl alcohol, Hellmanex-detergent (Hellma, 70 °C) and deionized water. For the polymer deposition, dopamine hydrochloride (Sigma Aldrich) was dried in an oven at 150 °C overnight in presence of CaH_2 (95%, Sigma Aldrich) to remove residual water. The polymerization and doping reaction was carried out in a tube furnace (Carbolite company; glass tube length: 45 cm; tube diameter: 2.4 cm; reaction temperature: 300 °C) under nitrogen atmosphere with a carrier gas-flow of 3 L min^{-1}. A solution of sulphuric acid (95-97%, J.T. Baker) and sodium sulphate (≥99.0%, Sigma Aldrich) was utilized as oxidation agent. In the vaporized state, the sodium sulfate enhances the oxidation power by increasing the amount of SO_3 in the gas phase. The reaction times were varied to reach the desired film thickness. For electrical characterization the samples were stored under inert conditions to avoid humidity and are sealed by drop casting a polymethyl methacrylate (PMMA) film on top of the active area.[59-60]
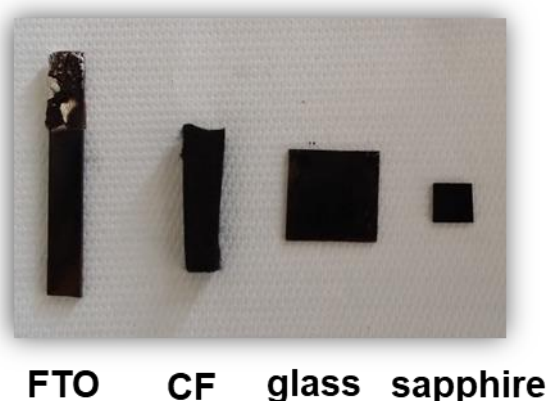

Figure 6. Polydopamine synthesized by o-CVD in the Carbolite company furnace on various substrates.

2.2.1.3. Synthesis of Polyguanine by o-CVD

Oxidative chemical vapor deposition (o-CVD) was used for the deposition of polyguanine (PG) directly on carbon felt (CF) (10 mm x 10 mm, SGL Group, The Carbon Company). These electrodes were applied in electrochemical studies. For conductivity measurements we utilized sapphire substrates (10 mm x 10 mm x 0.5 mm, CrysTec Kristalltechnologie) with Cr/Au (8 nm/80 nm) electrodes in the van der Pauw geometry. We treated all substrates with acetone, isopropanol, Hellmanex-detergent (Hellma, 70 °C) and deionized water prior usage. Chromium/gold electrodes were deposited by PVD through a shadow mask. For the PG-synthesis, guanine (Sigma Aldrich) was dried 15 minutes at 100 °C. For the polymerization we used oxidative chemical vapor deposition technique. The equipment consisted of a tube furnace (Nabertherm company; glass tube length: 110 cm; tube diameter: 2.5 cm). In the zone 2, the temperature was set constant to 360 °C, in order to evaporate guanine. Nitrogen (100 L h^{-1}) was used as carrier gas in a laminar flow. The entire process was carried out at atmospheric pressure (1 atm). In the zone 1, sulphuric acid (95-97 %, J.T. Baker) and sodium sulphate (≥99.0 %, Sigma Aldrich) were placed. Upon heating up to 240 °C, the acid was vaporized and reacted immediately with the gas-phase guanine. The desired substrates were placed in between zones 2 and 1 so that the polyguanine deposition could take place. The complete reaction zone (between zone 1 and 2) was covering a space of 17 cm.[84]
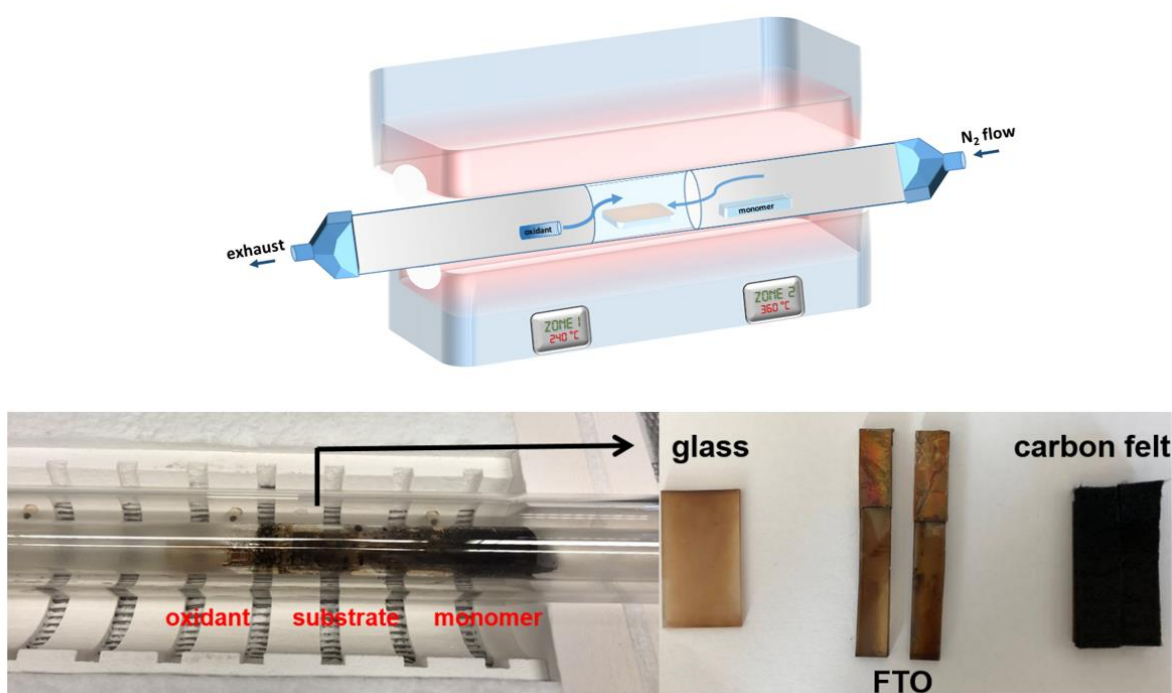

Figure 7. Nabertherm Tube Furnace for oxidative chemical vapor deposition of guanine. The guanine monomer was placed at zone 2, the sulphuric acid at zone 1 and the substrate in between the zones 1 and 2 (top). Synthesis of polyguanine on various substrates (below).

2.2.2. Scanning Electron Microscopy (SEM)

For the visualization of the polymer films on electrodes in nanoscale, scanning electron microscopy (SEM) was an essential tool. A JEOL JSM-6360LV scanning electron microscope (Figure 8) was used for the characterization of all the samples. Images were taken with a working distance (WD) of 10-15 mm and an acceleration voltage between 7-15 kV.
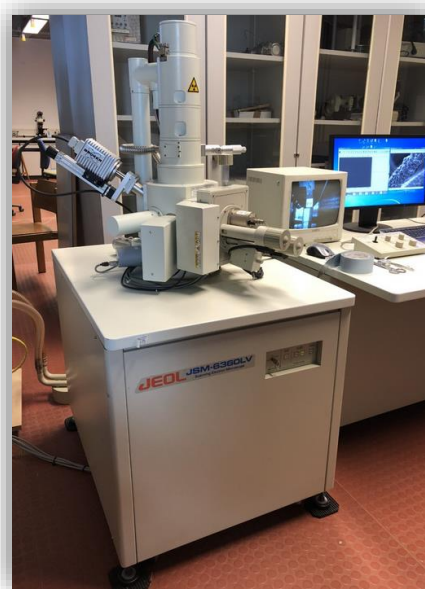

Figure 8. A photo of the Scanning Electron microscopy (SEM).

2.2.3. Spectroscopic Characterization

2.2.3.1. X-ray photoelectron spectroscopy (XPS)

The chemical surface composition of the as-prepared polymer films was evaluated on the basis of X-ray photoelectron spectroscopy (Figure 9). For this surface-sensitive measurement, polymer films were grown on chromium (8nm) / gold (80nm) deposited glass substrates. A Theta probe from Thermo Fisher Scientific was applied with an Al Kα (1486.7 eV) source. The charge was compensated by a dual flood gun (1 to 2 eV electrons and Ar^+ ions), and the lens mode was set to standard. The energy pass amounted to 200 eV for the survey scan and 50 eV for HR scans, with energy steps of 1 and 0.1 eV, respectively. The Avantage v5.32 software package was used for data analysis.[59-60] All XPS measurements in this thesis were conducted by Mag.[a] DI.[in] Theresia Greunz and DI. Andreas Hinterreiter under the supervision of Assoc.Univ-Prof. DI.Dr. David Stifter.

Figure 9. A photo of X-ray photoelectron spectroscopy (XPS) located at ZONA laboratory.

2.2.3.2. Fourier-Transform Infrared Spectroscopy (FTIR)

FTIR was an important instrument for the spectroscopic characterization and identification of the synthesized biopolymers in this thesis. FTIR measurements were performed on Bruker Vertex 80 spectrophotometers equipped with a Platinum ATR module (Figure 10). The resolution was set to 4 cm^{-1} for all the measurements in a spectral range between 8000-600 cm^{-1}. Furthermore, the setup includes a Globar (IR source), a Michelson Interferometer with a KBr beam splitter, the chamber for sample installation and a Mercury Cadmium Telluride (MCT) detector. Before each measurement, background single channel measurements were taken with air and blank glass substrate. For the characterization of thin films, a glass coated with a thin film of material was placed with the active site facing downwards on the module where it touches the diamond reflection element. Therefor the lever was let down onto the sample in order to remove any trapped air to avoid optical and atmospheric interference. In this manner the characterization of thin films in absorbance, transmittance or reflectance modes with high precision was possible. OPUS 7.2.139.1294 software was used for the visualization of all the spectra.
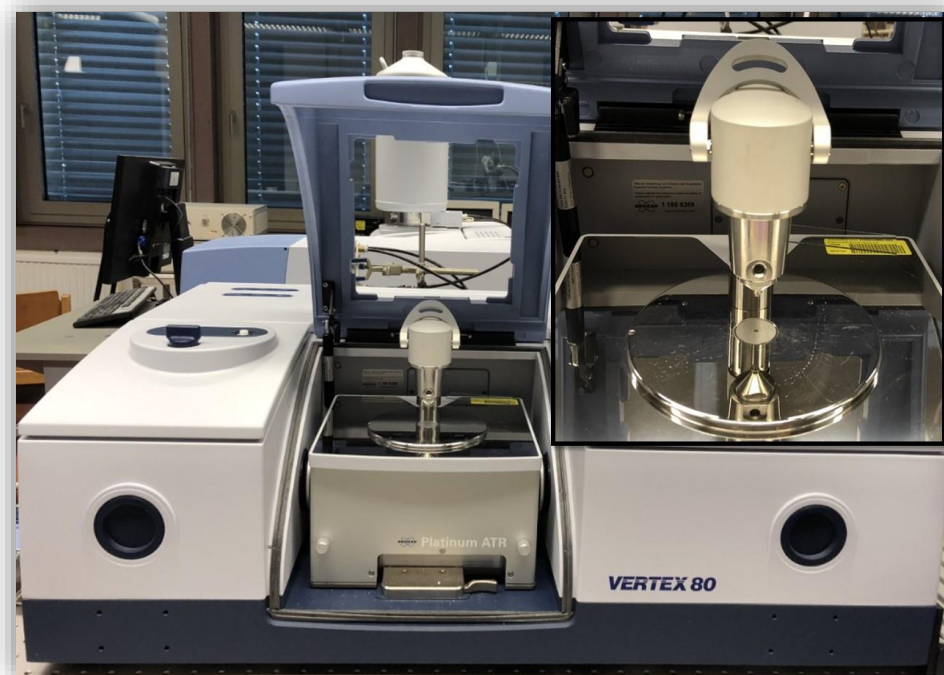
Figure 10. A photo of the ATR-FTIR instrument. Magnified photo reveals the actual measurement area with the diamond reflection element below the lever.

As the complementary technique to the infrared spectroscopy, we used Raman spectroscopy for further detailed analysis of the biopolymers. This technique enables the observation of rotational and vibrational modes in a system and thus is employed to identify structural fingerprints. The Raman spectra were recorded at room temperature with a WITec Alpha 300 R-Raman- System (WITec GmbH, Ulm, Germany) instrument. Nd:YAG laser (532 nm) was applied for the excitation and thermoelectrically cooled CCD (DU970N-BV) detector was used for all recordings. A grating of 600 mm^{-1} was used with a resolution of 4 cm^{-1}. For all three molecules 20× Zeiss EC Epiplan (Carl Zeiss Jena GmbH, Germany) objective lens was used, while the laser intensity, integration time and accumulations were changed for the monomer (10 mW, 15 sec., 10), solution synthesized PDA (5 mW, 2 sec., 3), and o-CVD PDA (5 mW, 3 sec., 20), respectively.[60]

2.2.3.3. In-situ ATR-FTIR Spectroelectrochemistry

Mechanistic insights and information about the intermediate processes were gained by in situ spectroelectrochemistry (isSEC) in the fingerprint regime (Figure 11). This technique provided the exploration of the detailed sequence of the electrosynthesis as a function of the applied potential.[59]

The in situ spectroelectrochemical (attenuated total reflection (ATR)–FTIR) measurements were performed on a Bruker IFS 66/S spectrometer equipped with an MCT detector. Before starting the experiments, the detector was cooled down with liquid nitrogen to ensure high sensitivity. For the

in situ technique, a sealed electrochemical cell (Figure 11) with platinum as CE, polydopamine as WE, and Ag/AgCl quasi reference electrode was mounted in the spectrometer.[59]
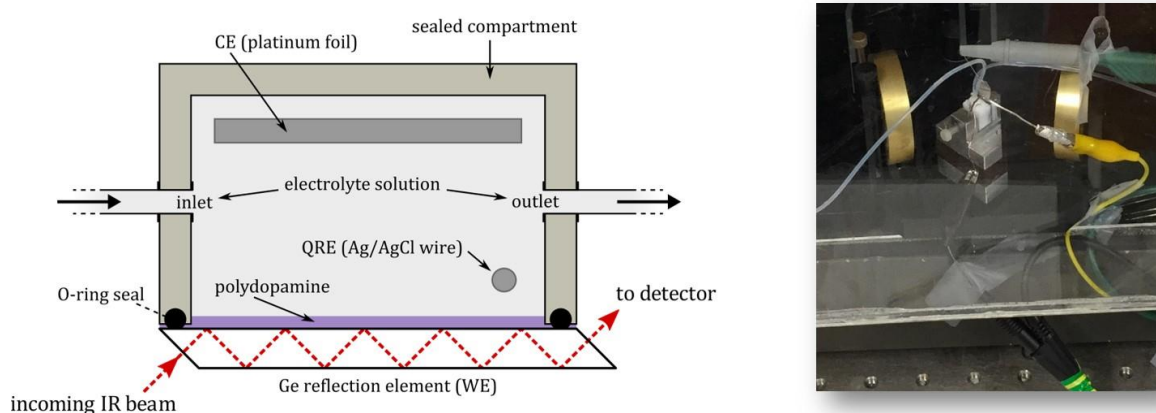

Figure 11. The schematic of the sealed Teflon compartment for the in-situ spectroelectrochemistry measurements (left). A photo taken after the sealed compartment is mounted in the spectrometer. Reprinted/modified from [59]. ©

The system was continuously flushed with 0.1 M TBA-PF$_6$ in acetonitrile. Polydopamine was deposited onto a germanium crystal as a reflection element. During the spectroscopic recording, the cyclic voltammogram (CV) was captured between 0 and −2000 mV versus Ag/AgCl. The resulting differential spectra were calculated in the –ΔT/T configuration and plotted against the wavenumber.[59] The differencial spectra were calculated according to the formula below, where T_0 is the biopolymer in the ground state and T_1 are spectra recorded under electrochemical bias:

$$-\Delta T/T = \frac{T_0 - T_1}{T_1} \qquad\qquad (2)$$

2.2.4. Electrical and Electrochemical Characterization

2.2.4.1.Physical Property Measurement System (PPMS)

The physical property measurement system from the DynaCool company (Figure 12) was utilized for the electrical characterization of the functional biopolymers. Therefore, the materials of interest were deposited on sapphire substrates. In order to avoid humidity, the films were protected by a poly (methyl methacrylate) (PMMA) layer and contacted by using indium solder. In this way, the electrical conductivity of polydopamine and polyguanine were recorded as a function of time, as a function of temperature and at different aqueous surroundings.
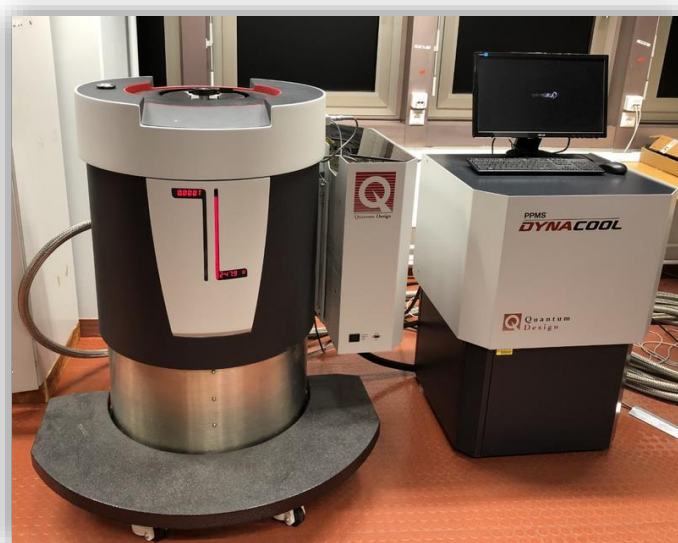

Figure 12. DynaCool - Physical Property Measurement System (PPMS).

2.2.4.2. Electrochemistry

Cyclic voltammetry is a useful electrochemical technique for the characterization of the electrocatalyst behavior of a material. This technique helps for the visualization of the electrochemical catalytic activity of substances depending on reduction and oxidation properties. Typically, an electrochemical system consists of a working electrode (WE), a counter electrode (CE), a reference electrode (RE) and an electrolyte solution. A cyclic voltammogram (CV) is obtained by using a potentiostat, which can be considered as a current-to-voltage converter, together with a data acquisition system. The working principle of this method is the following: the potential of the WE is varied linearly by time, while a constant potential is maintained at the RE. The current only flows between the WE and the CE. The RE has no contribution to the current but only keeps the potential constant. The resulting cyclic voltammogram is than generated by the data acquisition system. ECM Win 2.2.1.7 software was used as a data acquisition system for all the measurements. [1, 59, 98]

For the investigational purposes through this thesis, a three-electrode-system was applied in an H- Cell configuration, as shown in Figure 13.

Figure 13. Electrochemical setup for CO2RR (left) and HER (right) experiments in an H-Cell configuration. Reprinted/modified from [59]. ©

To evaluate polydopamine as an electrocatalyst for CO_2 reduction, we conducted electrochemical studies in a standard three-electrode arrangement in an H-cell configuration. A PDA-coated CF was used as a working electrode (WE), Pt as a counter electrode (CE), and Ag/AgCl as a quasi reference electrode (QRE). All were suspended in a 0.1 M tetrabutylammonium hexafluorophosphate (TBA-PF$_6$) in acetonitrile-water (1 volume% H_2O, 0.55 M) as the electrolyte solution. This system offers high CO_2 solubility with approximately 0.27 M.[59] The working electrode and the quasi reference electrode were placed in one compartment of the H-cell, and the counter electrode in the other. The compartments were connected by a bridge with a membrane (glass frit, porosity no. 2) in between. The Ag/AgCl QRE was calibrated against Fc/Fc$^+$ as an internal reference ($E_{1/2,\ ferrocene,NHE}$= 640 mV). All results are given relative to the NHE. The half-wave potential $E_{1/2}$ for ferrocene/ ferrocenium (Fc/Fc$^+$) was found at 400 mV versus QRE and 240 mV versus NHE.[59] The conversion was carried out accordingly by using the following equation:

$$E_{1/2,\ ferrocene,\ Ag/AgCl} = (E_{red.} + E_{ox.}) / 2 \tag{3}$$

$$E_{1/2,\ ferrocene,\ Ag/AgCl} = (300\ mV + 500\ mV) / 2 = \underline{400\ mV\ vs.\ Ag/AgCl} \tag{4}$$

and

$$E_{NHE} = E_{1/2,ferrocene,\ NHE} - E_{1/2,\ ferrocene,\ Ag/AgCl} \tag{5}$$
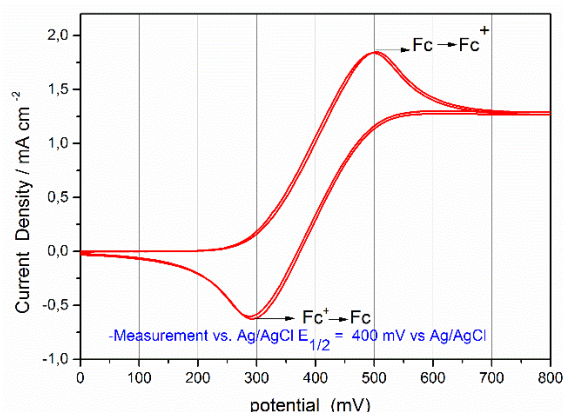
Figure 14. Cyclic voltammogram of ferrocene/ferrocenium redox couple in organic solvent, recorded versus Ag/AgCl.

All electrochemical experiments were carried out in a glove box atmosphere to avoid moisture absorption. CO_2 was introduced to the glove box via a plastic tube from a bottle that contained 99.995% pure CO_2, and all chemicals used in the electrochemical experiments were stored only in the glove box. The compartments of the H-cell were purged with N_2 and CO_2 to achieve complete saturation of the system and prevent possible electrolyte exchange between the compartments that would lead to a change in the CO_2 concentration in the environment. The headspace volume was kept constant (20 mL). Before each experiment, the cell was flushed with N_2 and then CO_2 for 30 min. [1, 59, 98]

For the electrochemical HER measurements the electrodes was rinsed with the electrolyte (1 M TA) and then directly installed as working electrode. The as prepared structurally modified polydopamine (DHI-PDA), PG and blank carbon felt electrodes were electrochemically characterized for hydrogen evolution using an H-Cell configuration. The electrochemical experiments were performed using a JAISSLE Potentiostat Galvanostat IMP 88 PC. Carbon-felt as well as the catalyst coated electrodes were set as working electrodes, Ag/AgCl (3 M KCl, +197mV vs. SHE) was set as reference electrode and Pt as counter electrode. A 1 M trifluoromethanesulfonic acid as electrolyte solution was used. The H-cell was separated by a diaphragm. Before chronoamperometry, the sealed compartments of the cell were purged with N_2 gas for at least 1 h. All results are given relative to the RHE, applying the following conversion:

$$E_{RHE} = E_{Ag/AgCl} + 0.059 \, pH + E^0_{Ag/AgCl}, \tag{6}$$

where $E^0_{Ag/AgCl}$ is 0.197 V at 25 °C. Polarographic scans and chronoamperometric scans were conducted under stirring the electrolyte solution in the cathode system and under nitrogen inert gas with a scan rate of 50 mV s^{-1}.

2.2.4.3. Electrochemical Impedance Spectroscopy (EIS)

The electrochemical setup was characterized by systematic impedance analysis using an IVIUM CompactStat (Netherlands). In general, the electrochemical impedance spectroscopy (EIS) is a powerful technique, which enables a deep understanding of different mechanisms going on in the electrochemical system. Interesting cell parameters, such as the capacitance of the working electrode, the actual electrochemically active area, and different resistance values (resistance of the electrolyte solution, resistance of the working electrode, resistance of the glass frit membrane) can be extracted either by Nyquist or Bode plots.[99-100] All EIS measurements mentioned in this thesis were conducted by Dr. Abdalaziz Aljabour and Prof. Dr. Achim Walter Hassel through a collaborative framework.

2.2.5. Product Analysis

2.2.5.1. Gas Chromatography (GC)

The capability of the o-CVD synthesized conductive and functional biopolymers as electrocatalysts in CO2RR and HER, for the formation of gaseous products (i.e. carbon monoxide (CO) and hydrogen (H_2)) was evaluated by gas chromatography. For this reason, a Thermo Fischer Trace GC Ultra Gas Chromatograph was applied, equipped with a thermal conductivity detector (TCD). The chromatograph consisted of two channels with nitrogen and helium carrier gases, for an enhanced visibility of detectable products such as CO, H_2, O_2 and N_2. For the analysis of the insoluble CO gas, 2-ml samples were taken from the headspace by means of a gas-tight syringe and injected manually into the TRACE Ultra Gas Chromatograph (Thermo Fisher Scientific). Helium was used as carrier gas at a flow rate of 20 ml min^{-1}. The thermal conductivity detector was kept at 200°C. [1, 59, 98]

Figure 15. A photo of the Gas Chromatography employed for the analysis of gaseous products (i.e CO and H_2).

2.2.5.2. Ion Chromatography (IC)

Formate is an anionic CO_2 reduction product. It can be detected through the analysis of the electrolyte solution after a constant potential electrolysis by capillary ion chromatography (CAP-IC). In this study, a CAP-IC with Dionex ICS 5000, conductivity detector, AG19, CAP, 0.4 x 50 mm pre-column, AS19, CAP, 0.4 x 250 mm main column and potassium hydroxide (KOH) as an eluent was used for the analysis. Samples were diluted 1:10 with highly purified 18 MΩ water for the

injection. Injection was performed by injecting 1 ml of diluted sample with a syringe. A conductivity detector was used for signal detection.[59, 98]

Figure 16. A photo of the Capillary Ion Chromatography for the detection of anionic compounds.

3. Results and Discussions

3.1. Polydopamine in CO_2 Reduction Reaction (CO2RR)

The electrocatalytic conversion of CO_2 has become of strategic interest: for generating renewable carbon feedstock and synthetic fuels and to mitigate the anthropogenic climate change.[1-15, 59] Electrocatalysis uses catalysts that reductively recycle CO_2 to CO and hydrocarbons. In large scale such process will be helpful to generate an anthropogenic carbon cycle. However, the expected throughput of present emissions requires high-performance and inexpensive materials to catalyze at CO2RR at sufficient high energy efficiency.[59] Therefore a major aim is to reduce overpotentials and at the same time to reach significant turnover. This will be requisite to justify the use of renewable energy to convert CO_2 to CO and the corresponding hydrocarbons.[59]

Various scarce transition metal catalysts are presently utilized to electrosynthesize fuels and carbon feedstock yielding readily efficient energy yields.[7, 10-14, 16-19, 59] However, in light of present emission, a significant scale-up will be necessary in the near future to apply for industrial use. This requires in particular alternative, more abundant and inexpensive electrocatalysts with a least comparable, but desirably better performance than the state-of-the-art. We believe that rare elements create risk of local shortage and socioecological impacts such as wars. We therefore sought to eliminate metals entirely in our electrocatalyst material design. Such green concepts are nature-inspired and attract interest. Organic electrocatalysts represent such materials class.[9, 59, 101-106]

Renewable material approach uses themes from enzymology, in particular discrete chemical functions that are actively contributing in a bio-catalytic reaction cascade. Using such motifs on electroactive organic carriers is our contribution to electrochemically reduce CO_2 at high faradaic and energy efficiency.[59]

The enzymology offers manifold functional themes that can be incorporated into the organic electrocatalyst structures.[59, 103-104, 106] Enzyme related moieties are abundant in polydopamine (PDA) – the previously described biopolymer is a direct derivative of natural eumelanins and fully decorated with hydrogen-bonded motifs.[58] PDA's possesses a 1:1 ratio of hydrogen bond per monomer so that it reaches a functional density similar to various inorganic contenders.[59, 70, 107-118] The electrocatalytic functions are adjacently-placed amines and hydroxyl or carbonyl groups, that are consistently associated via the characteristic hydrogen bonds.[119] Their intimiate structure activates an inter- and intramolecular coordination across the entire system and features ultimately a nucleophilic sequence, in particular under negative polarization with strong possibility to bind and electroreduce CO_2.[59]

In the following chapters, the application of o-CVD synthesized PDA electrocatalyst in CO2RR is provided.

3.1.1. Structural and spectroscopic Characterization of PDA

We utilize o-CVD to grow conductive polydopamines as described above in chapter 2.2.1.2. Prior art on conductive polymer synthesis is conducted mainly in solution by electrochemical grown and a few other related techniques.[76, 107-108, 118, 120] As discussed, the detrimental aspect of solution-based synthesis is the limited control over some ambient parameters such as the precise temperature or the precise O_2 partial pressure. Also, it has been reported that the local pH can change during synthesis which impacts the synthesis e.g. by favoring the competing H-aggregation. This can disrupt the conjugation of the final polymer. We demonstrated that a classic solution route reported earlier yields solution-PDA.[59-60, 71] We use this as reference system to compare our results in the context of utilizing the o-CVD processed PDA (o-CVD PDA) (Figure 17).[59-60]
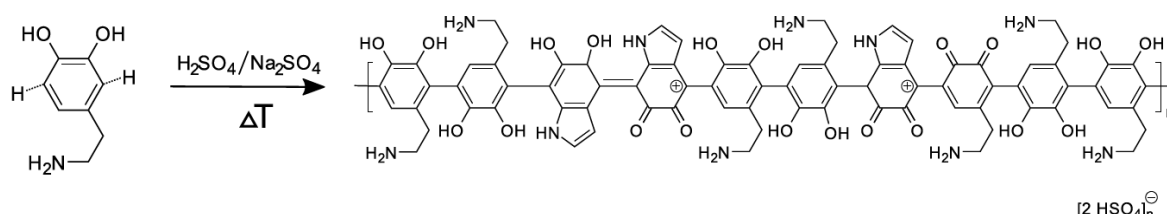

Figure 17. After the reaction is completed, the monomer is transferred into a doped and conjugated polymer consisting of indole and quinone derivatives of the dopamine monomer. Reprinted/modified from [60].©

o-CVD offers the possibility to growth polydopamine rapidly as compared to other related synthesis techniques (Figure 18). Typical deposition rates can be up to 5–6 nm per minute so that within 4 h thin films with high homogeneity as used for electrocatalysis can be deposited.[60] We found that acidic media help to protonate the dopamine and can deactivate thereby the competing H-bond aggregations observed under neutral or basic conditions. This is an important step also to preserve the functionality of the polydopamine, most dominantly to protect the amine. In parallel o-CVD lead to conductive PDA - the conducting biopolymer forms by the in-situ progressing p-doping reaction included in the polymerization.[60] The results are defined and reproducible conductive biopolymers. We were able to demonstrate o-CVD conducted on plain glass, sapphire and silicon but also on mesh-type or sponge-type carrier electrodes such as carbon fibers. These are used later to generate high-surface area PDA electrode with the help of vapor infiltration (Figure 6).[60]
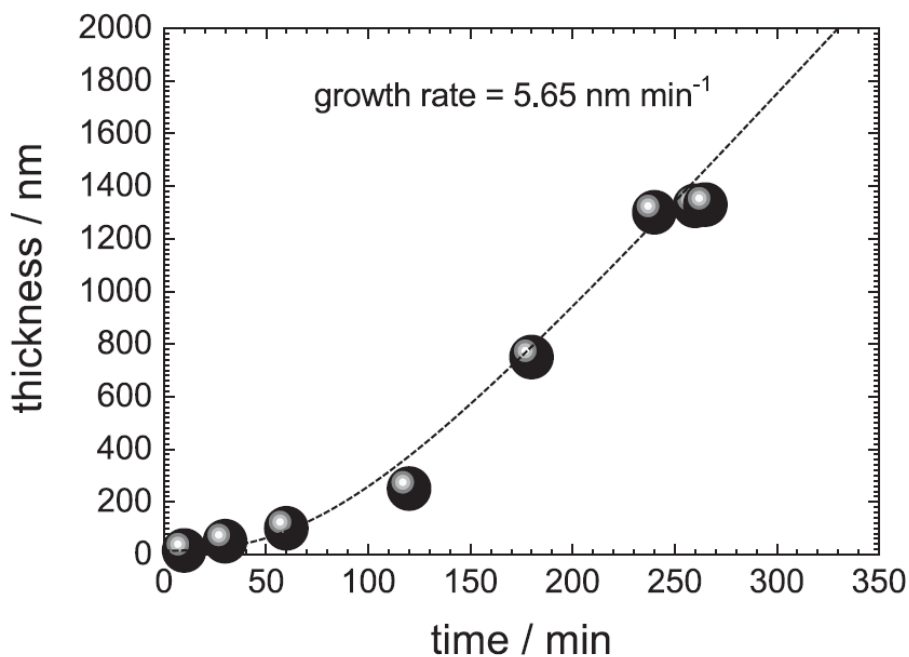
Figure 18. Determination of the film thickness of the o-CVD synthesized PDA as a function of the deposition time. Reprinted/modified from [60].©

X-ray photoelectron spectroscopy (XPS) was used to evaluate the chemical surface composition of PDA on Au (reference) and CF. The elemental response was presented in survey scans and high-resolution (HR) scans (Figures 19-23, PDA on Au). Sulfur was analyzed by its S2p and S2s levels: It gave a higher response as expected.[59] This corresponded to a higher content of sulfuric acid or sulfate. For nitrogen, the N1s level suggested two chemical environments, predominantly the primary amine: $-R-NH_2$ (401.8 ± 0.3 eV). Al secondary amines–R-NH-R– (399.9 ± 0.1 eV) were (less pronounced) present on the surface. The C1s spectrum was fitted using three moieties: CH_x (284.4 ± 0.1 eV), C–O/C–N (286.1 ± 0.2 eV), and C=O (287.7 ± 0.4 eV). Oxygen O1s feature consisted of three major contributions: O=C (531.0 ± 0.2 eV), HSO_4^- (531.7 ± 0.2 eV), and O–C (533.0 ± 0.2 eV). All the relevant HR scans for the elements C, N, O, and S are presented in Figures 20-23. The potential chemical structure of PDA proposed on this basis is shown in Figure 24.[59]
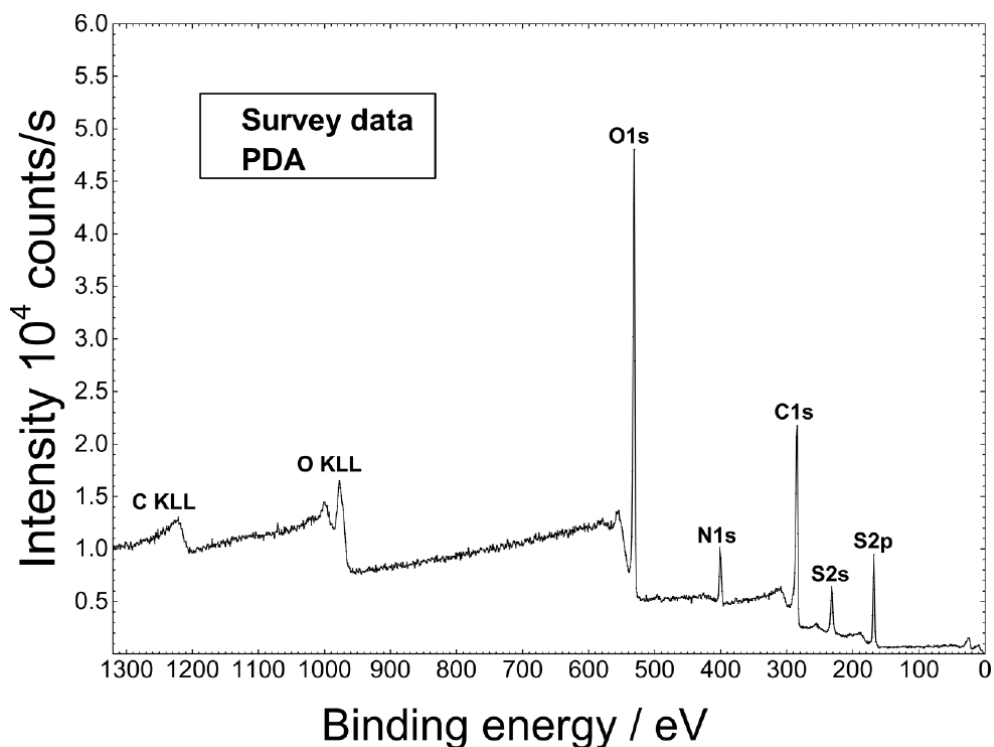
Figure 19. The survey scan of conductive PDA measured by XPS. Based on the survey scan and subsequent high-resolution scans the elemental concentration was determined (C1s, N1s, O1s and S2p). The following XPS spectra were measured by Mag.ª DI.ᶦⁿ Theresia Greunz under the supervision of Assoc.Univ-Prof. DI.Dr. David Stifter. Reprinted/modified from [59]. ©
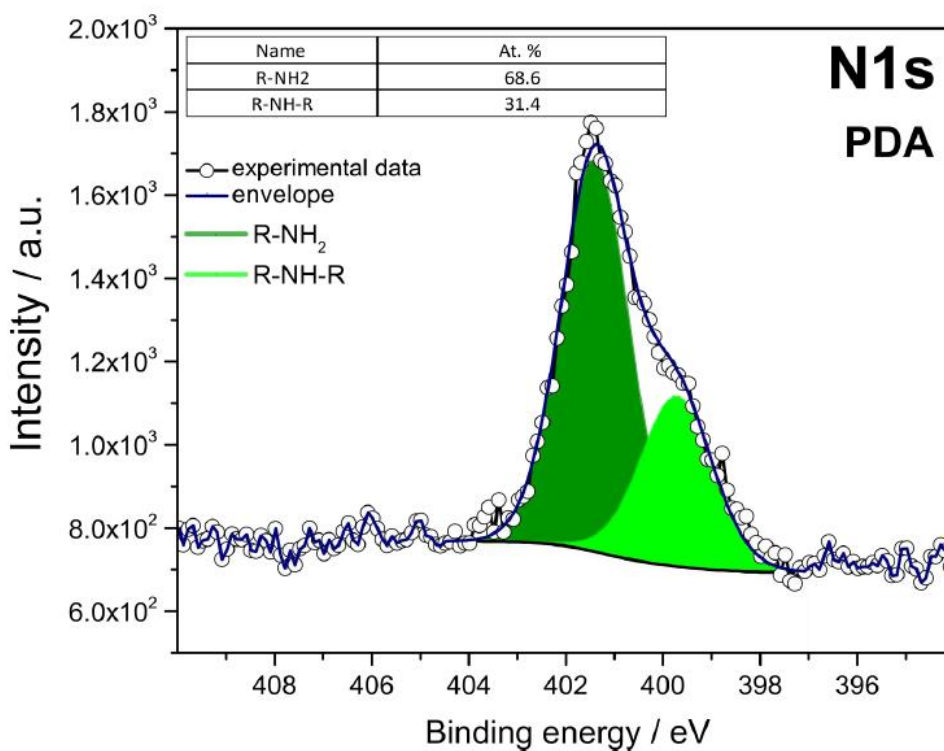
Figure 20. The nitrogen spectrum provides insight into the structure of polydopamine. Primary amine ($-NH_2$) is predominant in the structure (68.6 %), as shown in the synthesis path. Reprinted/modified from [59]. ©
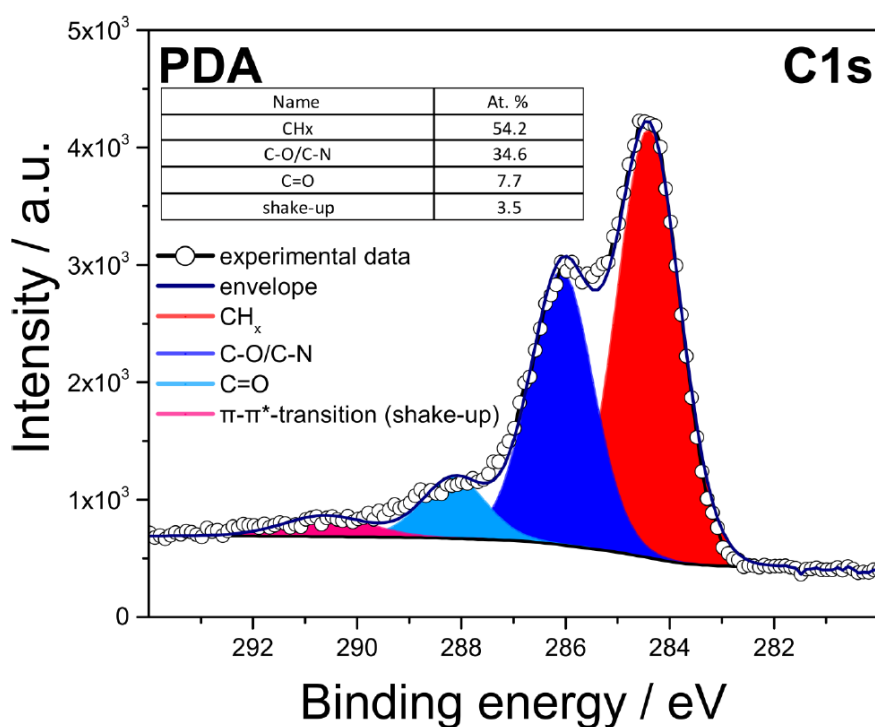
Figure 21. The carbon peak demonstrates the various structural moieties in conductive and conjugated polydopamine (CH$_x$, C-O and C-N or carbonyl and the conjugated core). Reprinted/modified from [59]. ©
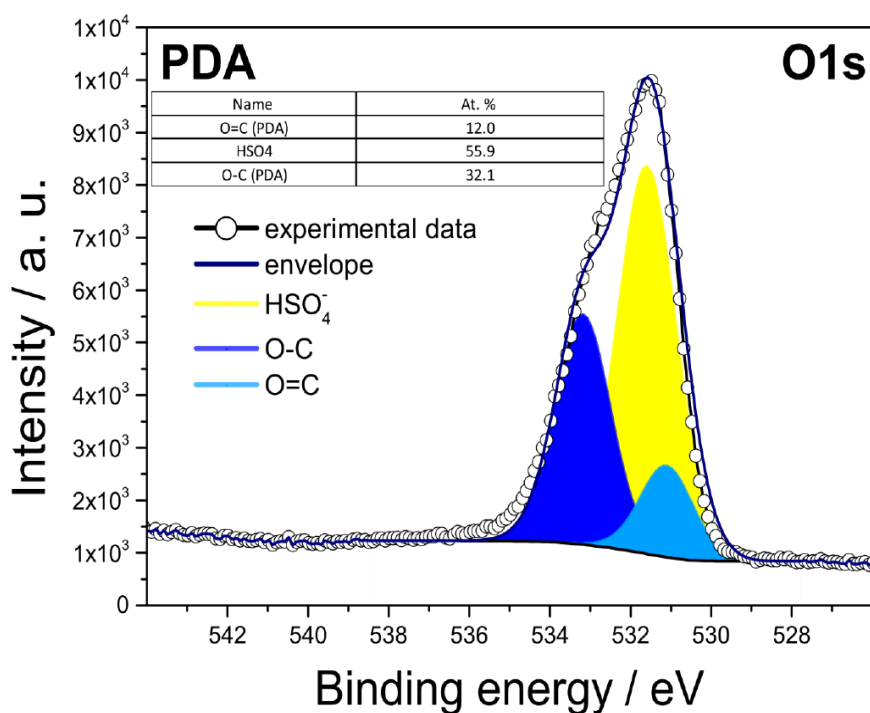
Figure 22. The peaks of the oxygen atom display the surrounding either related to sulfate anions or the dopamine ring with the carbonyl- and hydroxyl functionalities. Reprinted/modified from [59]. ©
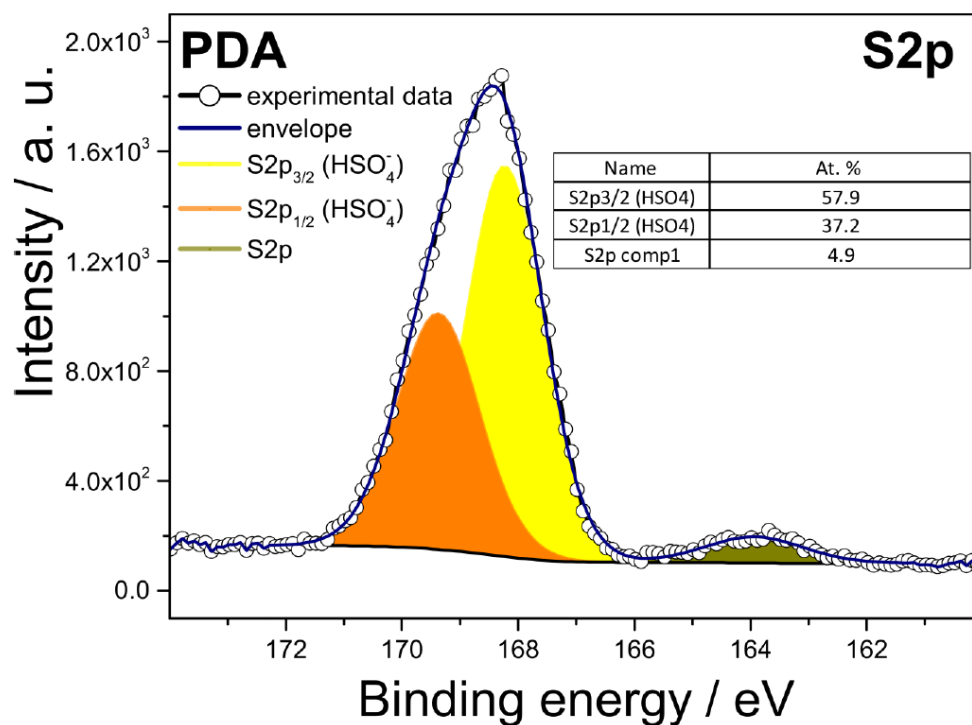
Figure 23. The sulfur in o-CVD synthesized, conductive polydopamine is associated with the presence of bisulfate and/or sulfate. Reprinted/modified from [59]. ©
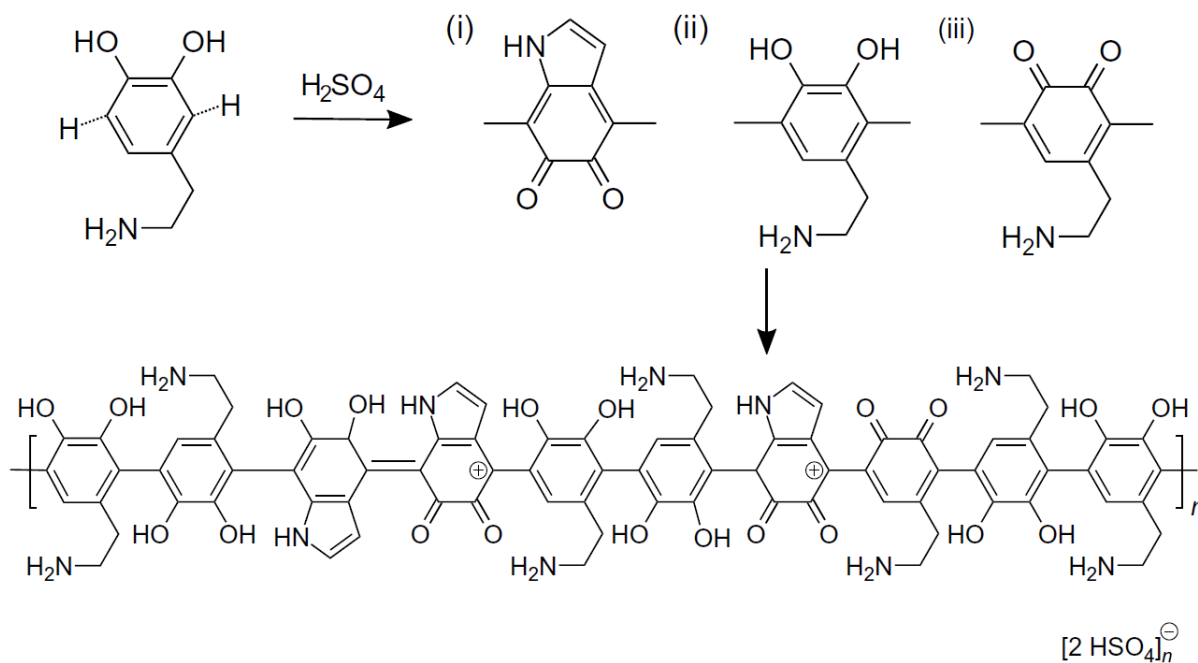
Figure 24. The synthesis pathway of the conductive polydopamine. Reaction of dopamine from the vapor phase combined with the sulfuric acid to conductive PDA mainly involves building blocks like (i) condensed and oxidized diketoindole, (ii) dopamine, and (iii) oxidized dopamine, resulting in the final product with periodically repeating units. Reprinted/modified from [59]. ©

We used Raman and FTIR spectroscopy to elucidate the vibronic regimes, in particular to explore the detailed structural properties of doped o-CVD PDA including its functional groups on top of the complex IR-electronic interactions.[60] We hypothesized that the functional groups are integrated in the conjugated system. This leads to the desired *functions-on-conjugation*. To examine such entanglement in detail, we related the FTIR and Raman spectra of dopamine hydrochloride to o-CVD PDA and solution-grown PDA (Figures 25-27).[60]
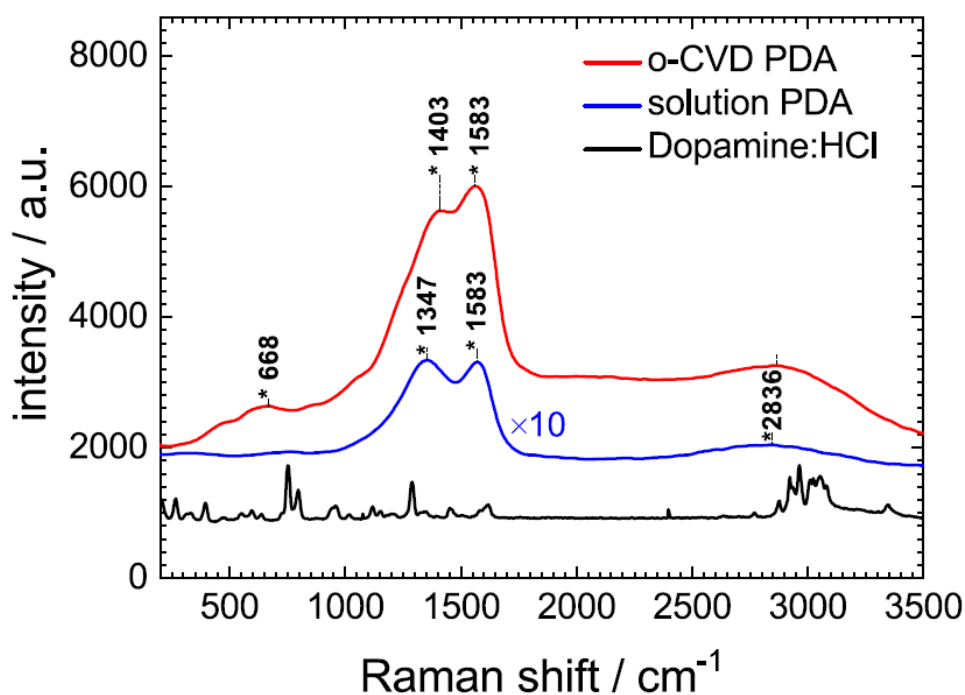
Figure 25. The Raman spectra of the three components: dopamine hydrochloride (black), solution PDA (blue, 10-fold expansion) and o-CVD synthesized PDA (red). The signals at 1403 cm^{-1} and 1583 cm^{-1} appear more intense in o-CVD PDA in comparison to solution PDA. Interestingly, these peaks at 1403 cm^{-1} and 1583 cm^{-1} are the aromatic C-N and C-C vibrations. Reprinted/modified from [60].©

Previous Raman spectroscopic studies have focused on the characterization of functional sites.[121-122] Here, Raman was used to determine the distinct spectral differences between solution- and o-CVD PDA: While the monomer possessed pronounced peaks at 1616 cm^{-1}, 1455 cm^{-1}, 1349 cm^{-1} and 1287 cm^{-1} (with the first three assigned as aromatic C-C stretching-vibration and with the latter as aromatic C-H vibration).[60] These peaks changed after polymerization - we found three weak bands at 2836 cm^{-1}, 1583 cm^{-1} and 1347 cm^{-1} in the solution-PDA, while in o-CVD PDA exactly these bands become more intense (1583 cm^{-1} and 1403 cm^{-1}). We related them to C-C vibrations of the corresponding aromatic units. The increased intensity indicates that H-aggregation is less dominant in o-CVD PDA and C-C coupling is effectively present.[60] Similarly, we observed the aromatic C-N bonds to increase in o-CVD PDA (Figure 25).[122] In parallel weaker peaks at 2854 cm^{-1} and 668 cm^{-1} indicate less aromatic O-H and (aromatic) stretching-deformation pointing at improved C-C polymerization without effectively H-aggregation (Figure 25).[60]

Similar to Raman, the FTIR spectroscopy showed the interplay of hydrogen bonds and the conjugated network.[60] We were interested to elucidate the changes between solution- and o-CVD in order to explore, whether C-C coupling was dominating the structure i.e. the building of functionalized polyparaphenylenes (PPP) as the fundamental polymer backbone.[60] The FTIR spectra of dopamine hydrochloride (Figure 26) showed broad and intense bands at 3000–3400 cm^{-1}. These were hallmarks of intermolecular hydrogen bonds, particularly (aromatic) O-H stretching vibrations.[75] Compared to the amine NH_2 functionality, the hydrochloride adduct shifted to lower wavenumbers, i.e. the N-H bands emerged at 2700 cm^{-1} and 2250 cm^{-1}, respectively features below 1700 cm^{-1} are aromatic C=C and C-H vibrations.[60] In solution-PDA (blue line) the vibrational features between 3400 and 2954 cm^{-1} and 3000–2100 cm^{-1} remained similarly intense and blurry, but weakened compared to the monomer. They were related to the aromatic O-H stretch vibrations and the corresponding amines at 1593 cm^{-1} and 1498 cm^{-1}, respectively (Figure 27).[60, 70, 75, 123-124]
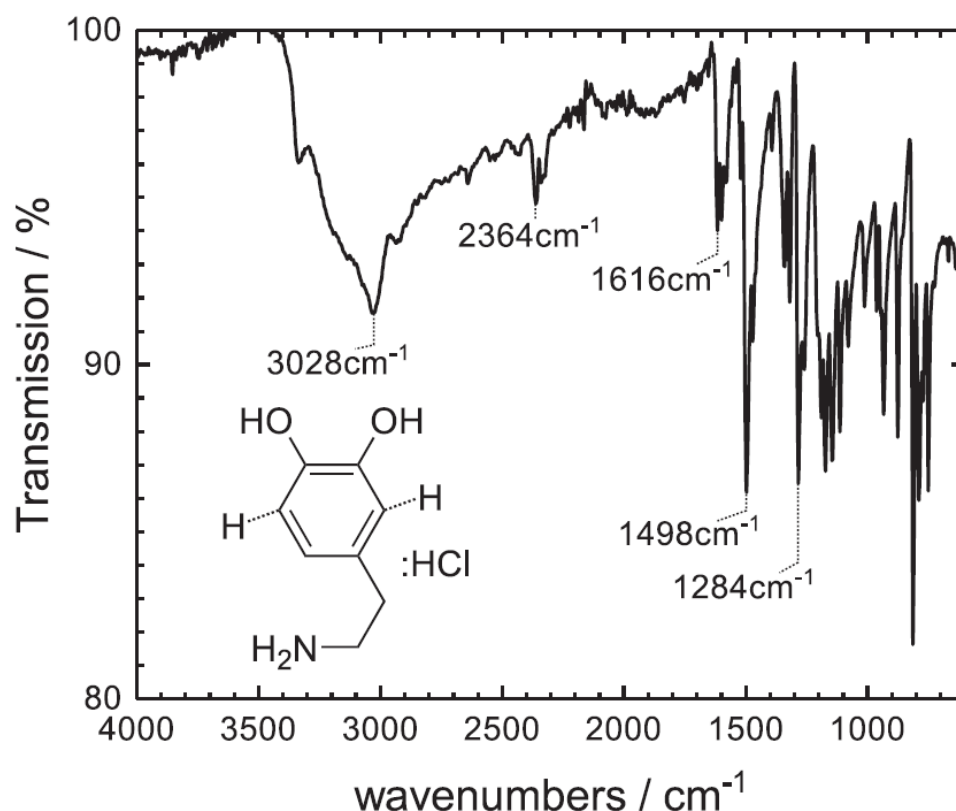
Figure 26. The FTIR spectrum of the PDA monomer. Reprinted/modified from [60].©

The spectrum of o-CVD PDA (red line) showed united and broad spectral features between 3000-3400 cm^{-1} and between 2856–1623 cm^{-1}.[60] We interpreted them as N-H or O-H vibrations from hydrogen bonds. On top, significant vibrations between 1660–1425 cm^{-1} were characteristic conjugated, cyclic C=N groups.[60, 75, 123-124] The intense carbonyl bands emerged between 1590 and 1640 cm^{-1}. They corresponded to a prevalent oxidation of O-H groups to ketones. In the lower mid-IR regime we observed the signature infrared-activated vibrations (IRAVs) which emerged in

conductive polymers characteristically between 857 and 1075 cm^{-1}. Such features provide evidence of strong doping.[60]

We found the fingerprint FTIR regime is distinctively different in o-CVD PDA as compared to the solution PDA. Some peaks occurred at higher intensity. Qualitatively, we confirmed presence of doping-induced IRAV only in o-CVD PDA. Similar features were found in functional fingerprints such as the C=N and carbonyl vibrations.[60]
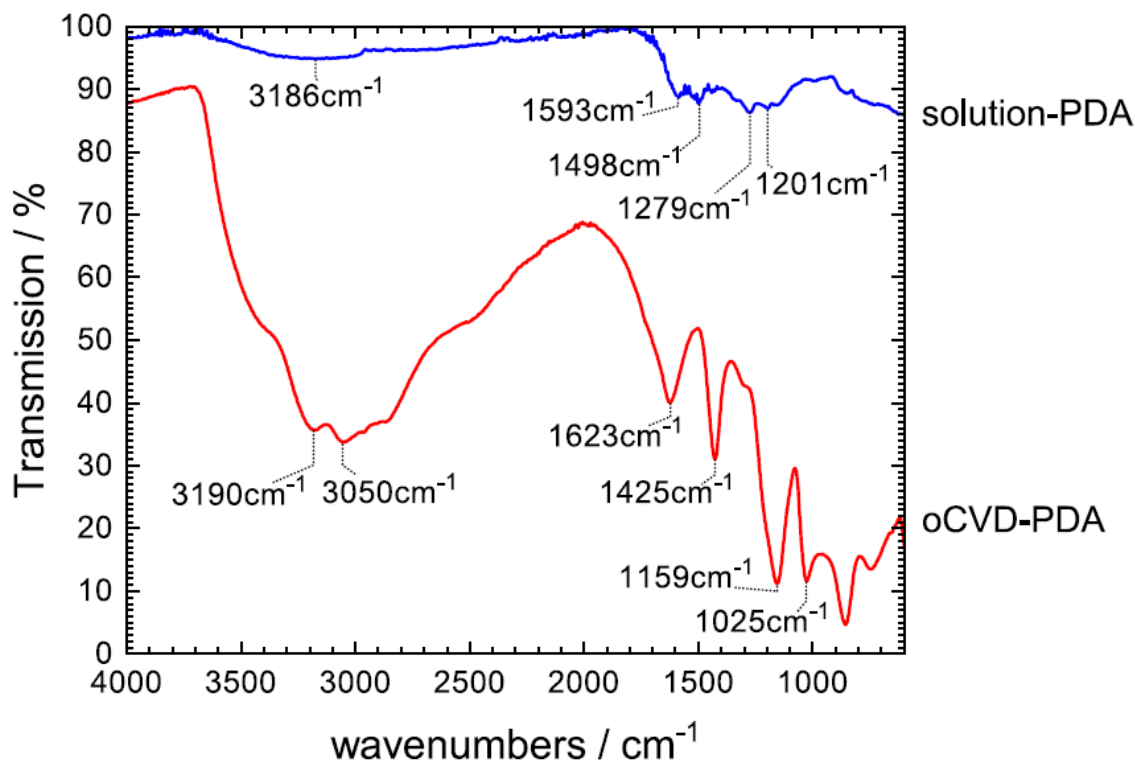
Figure 27. The FTIR spectrum of solution synthesized PDA indicated in blue color and o-CVD PDA in red color. Reprinted/modified from [60].©

A crosscheck for presence of delocalized charges (p-doping) was provided by 4-probe electrical conductivity. In solution PDA prior art has reported protonic motion, but no evidence of strong electronic conductivity. The intrinsic polymers absorb in the UV and possess a wide-bandgap at the order of 3.0 to 3.5eV.[60] This is high for organic semiconductors. In addition the low order (amorphous phases) limit the electrical transport. The signature of protonic motion in eumelanins is the pronounced temperature dependence and the need for ambient humidity. In dry inert atmosphere, eumelanins and solution polydopamines exhibit highly insulating properties at 10^{-13} S/m. Only under humid atmosphere, these values can increase up to 10^{-5} S/m (e.g. at 100% humid atmosphere).[71, 125-126] Especially, Meredith et al.[58, 72] proposed melanin as electronic-ionic hybrid conductors, predominantly the protons responsible for transport phenomena.[59-60, 73]

A persistent and substantially higher conductivity was observed in o-CVD PDA. Conductivities up to 0.4 S cm^{-1} at 300 K measured frequently in a timeframe of 1000 minutes (17 hours) (Figure 28)

under inert atmosphere gave strong evidence of electronic motion. Ionic contribution to the transport phenomena played a subordinate role.[59-60]

Figure 28. The four-probe conductivity measurement for the examination of the bulk conductivity: (i) as a function of time (left) and (ii) as a function of temperature (right). The 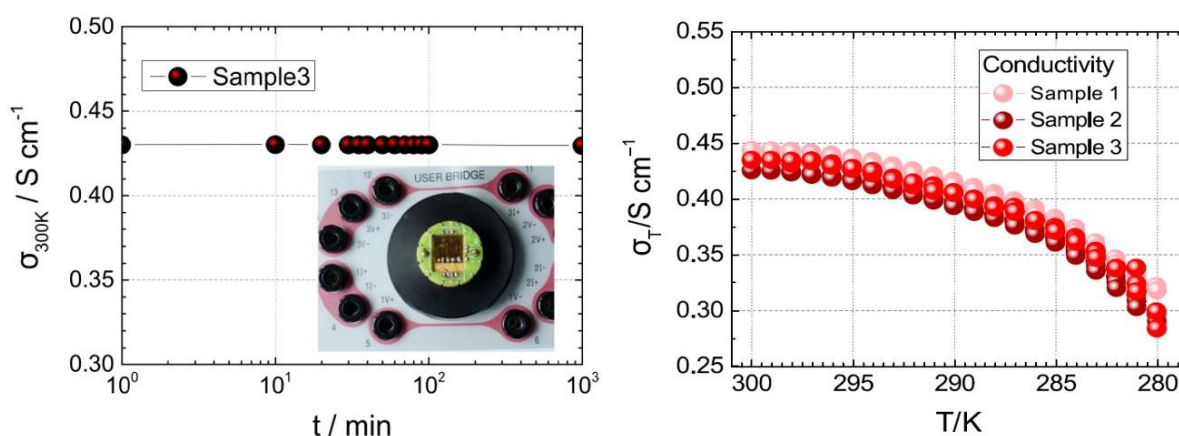stability of the electrical parameters lasted over a 1000 minutes run (17 hours). The inset displays the thin film of PDA on sapphire substrate contacted onto the testing rack of the Dynacool PPMS. Reprinted/modified from [59]. ©

The occurrence of electrical conductivity was intended by utilizing sulfuric acid as stronger oxidant. Also the higher temperature obviously directed the synthesis towards covalent C-C coupling to obtain the desired consistency of functional poly-paraphenylenes. In parallel, similar to ealier reported o-CVD polymers, the harsh conditions lead to concomitant doping. We found evidence of doping in the electrical properties and the spectroscopic signatures.[59-60]

3.1.2. Catalytic Activity of PDA as an Electrocatalyst in CO2RR

Hydrogen-bonding were discussed for electrosynthetic applications, especially utilized as non-polymeric hydrogen-bonded catalyst.[127] The frequent limitation in this concept were limited turnover and limited Faraday currents, not least because of high overpotentials. Hydrogen-bonded pigments possess characteristic insulating properties and limited ability to transport electrons.[103, 127]

In our study, we used density functional theory (DFT) calculations to investigate the interactions between the CO_2 and the proposed hydrogen-bonded catalytic active sites in PDA.[59, 128-131] We have calculated the binding energy for hydrogen- bonded sites to CO_2 in PDA. Three favored CO_2 positions were found to the amine, hydroxyl and carbonyl catalytic centers. In addition, the actual CO_2 distance between the oxygen and nitrogen atoms were calculated as 1.99 Å for CO_2 to carbonyl/hydroxyl and 2.11 Å for CO_2 to amine- slightly favoring the former. We investigated this initial finding—CO_2 nucleation over carbonyl—by in situ spectral investigations as mentioned later.[59, 132-134]
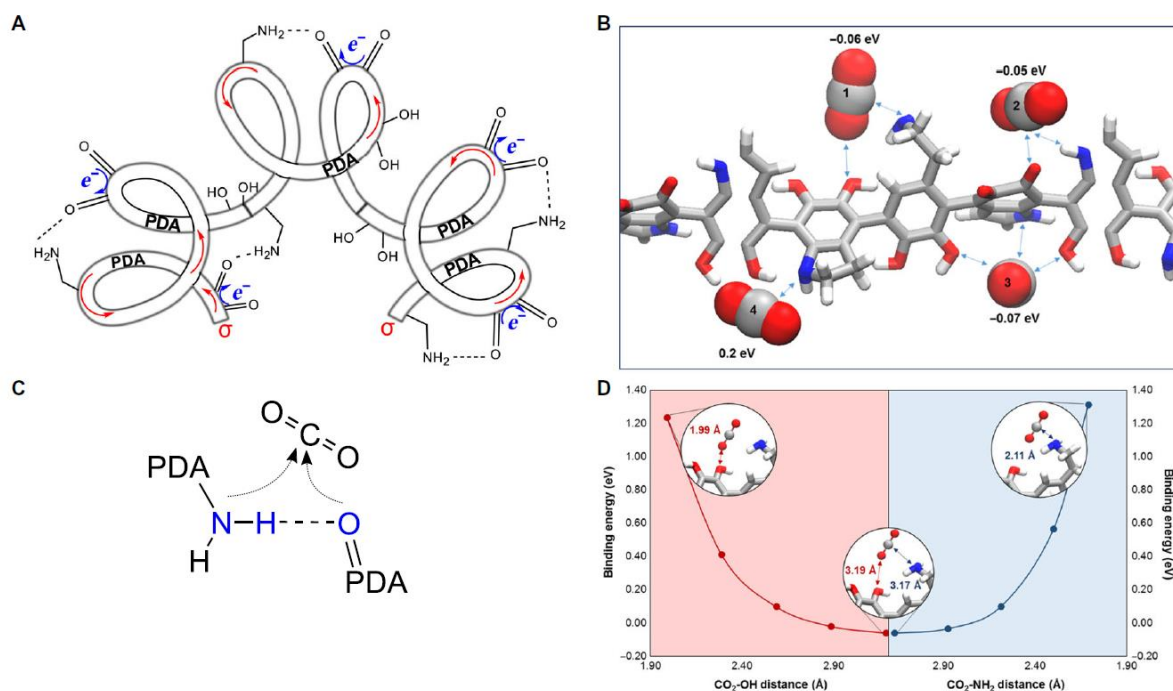
Figure 29. Hydrogen bonded functionalities as catalytic motifs for CO_2 reduction reaction. (A) Polydopamine consisting of a conjugated and conductive form with functional groups deposited on a carbon-based carrier electrode. (B-D) The functionalities drive the selective reduction of CO_2, (B) binding energies calculated by DFT at this site for CO_2, (C) amine-carbonyl hydrogen–bonded catalytically active center on polydopamine, and (D) binding energies represented as functions of the distances between the nitrogen atom and CO_2 as 1.99 Å and the oxygen atom and CO_2 as 2.11 Å, showing the most convenient energy-steric conformation. The DFT calculations were conducted through the collaboration with Toronto University by Phil De Luna. Reprinted/modified from [59]. ©

The electrochemical parameters were investigated by defining the applicable window of electrochemical potential. Thus, 0 to −1800mV versus normal hydrogen electrode (NHE) was found as the stable electrochemical potential window using an acetonitrile solution with 1 volume% water saturated with N_2 and CO_2 (0.27 M).[59] In addition, the effective CO_2 reduction reaction (CO2RR) was further improved by the geometric configuration. For this reason, the electrochemical setup was tuned and carbon felt (CF) networks were used as supporting carrier electrodes since these fiber networks offer a large surface area and a negligible catalytic activity towards the CO_2. In this manner, we were able to effectively coat the CF with conductive polydopamine to form a homogeneously covered system with maximum catalytic activity.[59] The corresponding cyclic voltammetry scans of the PDA working electrode as well as the blank CF both in N_2 and CO_2 atmosphere are shown in Figure 30. Huge reductive currents of up to 110 mA cm^{-2} at −1560 mV versus NHE were observed only in the presence of CO_2. Although this large reductive currents are highly remarkable, we denote that these values are referred to the geometric area of the CF. For this consideration, 1 cm^2 was taken into account for the sponge-type electrode area. The acetonitrile-water (2.65 mole percent H_2O) was used in order to avoid any precipitation of carbonate and unwanted side reactions going on in the anode space. By this

way, the overall electrochemical system released O_2 at the anode and the CO_2 reduction products in the cathode compartment.[59]
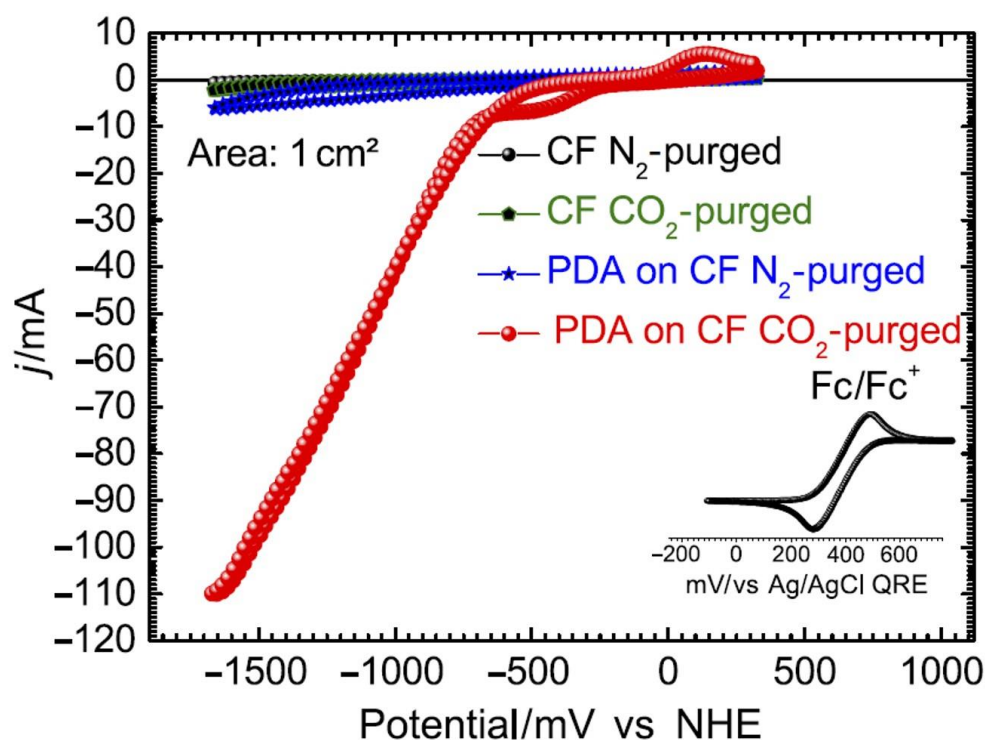

Figure 30. Polydopamine deposited onto carbon felt (CF) for the heterogenous electrocatalysis of CO_2RR. The cyclic voltammograms (CVs) of polydopamine together with the control scans as comparison under N_2 and CO_2 atmosphere. The catalytic activity is reflected in a high reductive current in acetonitrile-water electrolyte, only when purged with CO_2. Reprinted/modified from [59]. ©

Impedance analysis using an IVIUM CompactStat (Netherlands) was applied for the systematic characterization of the electrochemical setup. First of all, the electrochemical impedance of the cell was recorded by using two Pt electrodes. We measured the open circuit potential (OCP) for 30 seconds and recorded the electrochemical impedance spectrum in the range from 1 MHz to 1 Hz with a perturbation amplitude of 10 mV.[59] The high frequency range was governed by the resistive behavior of the electrolyte solution with an absolute impedance of 1.36 kΩ. In the following step, the Pt working electrode was replaced by a blank carbon felt electrode, and again the impedance was measured the same way, resulting in a value of 857 Ω. Subsequently, a carbon felt electrode coated with polydopamine catalyst (CF-PDA) was used in a three-electrode configuration using Ag/AgCl as QRE like in the usual electrosynthesis setup. The compartments were characterized individually resulting 907 Ω for Pt as counter electrode against CF-PDA as working electrode and 741 Ω for QRE against CF-PDA as working electrode. In the last step, the complete cell in Pt-CE and CF-PDA-WE configuration was characterized using a three-electrode arrangement, in which the potential at the working electrode was measured using the quasi reference electrode, and the current was measured between the counter electrode and the working electrode. To this end, the potential fall in the electrolyte solution including the membrane

with all static and kinetic losses at the counter electrode was compensated.[59] All results are summarized in Table 5.

Working electrode	Frequency	Configuration	iR (Ohms)	Counter electrode
Platinum (ref.)	1 kHz to 1 MHz	2 electrodes	1360	Pt
Carbon felt (CF)	1 kHz to 1 MHz	2 electrodes	857	Pt
Polydopa mine- carbon felt (PDA-CF)	1 kHz to 1 MHz	3 electrodes*	907 741	Pt *Ag/AgCl QRE

Table 5 The electrochemical impedance data for the applied configuration of PDA in CO2RR. Reprinted/modified from [59]. ©

3.1.3. Long term electrolysis and stability

For chronoamperometric scans an operating potential of −860 mV versus NHE was applied. At this potential the best compromise in terms of faradaic efficiency, current density, and overpotential was found. The chronoamperometry experimental runs were recorded for 16 hours (Figure 31) with frequent product analysis in parallel (cathode space only).[59]
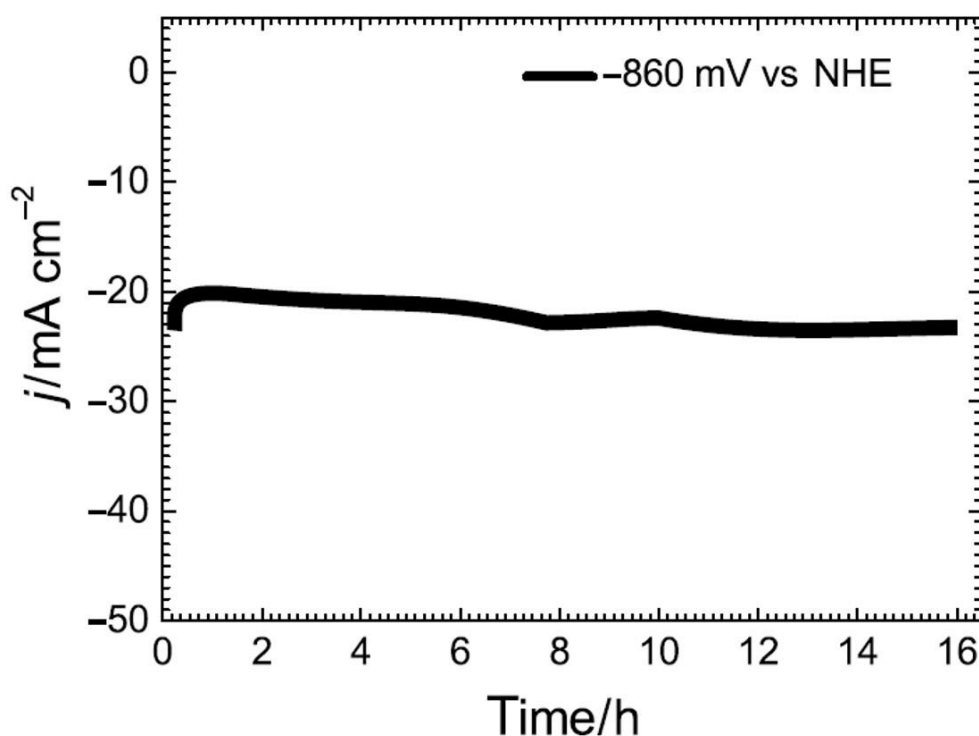
Figure 31. Long term chronoamperometric scan at the potential of −860 mV vs. NHE for sixteen hours, indicating the current stability. Reprinted/modified from [59]. ©

Insights into the fibrous structure were observed by scanning electron microscopy (SEM) before and after electrosynthesis for 8 hours (Figure 32). SEM images showed a structural roughening of the PDA surface after an applied constant potential electrolysis.[59]
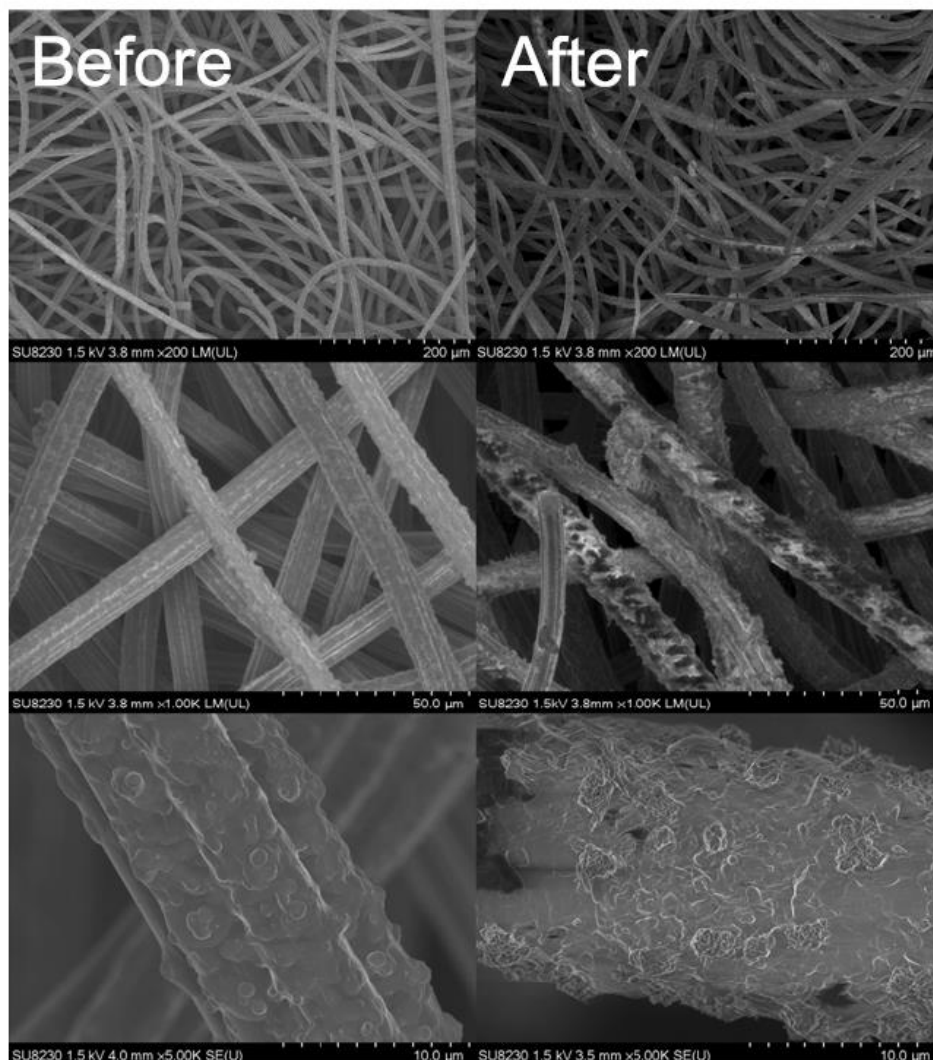
Figure 32. SEM images of the conductive polydopamine on the carbon felt fibers before and after electrocatalysis of eight hours. Reprinted/modified from [59]. ©

3.1.4. CO2RR Product Analysis

Once the chronoamperometry scans were finished, after an operating potential of −860 mV versus NHE was applied constantly for 16 hours, the product distribution was investigated by chromatographic methods. Since, possible CO_2 reduction products were of interest, only the cathode space was examined. Carbon monoxide (CO), formate ($HCOO^-$) and hydrogen (H_2) were detected as reduction reaction products (Figure 33).[59] Interestingly, by increasing reaction time a preference for formate was developed, which is attributed to the accumulation of formate and therefore the subsequent changes in the local pH. The pH value at beginning of the electrolysis was found to be 7.9 ± 1 as shown in Figure 34, however, the certainty of the measurement is

rather low in acetonitrile. While conducting a semi-continuous electrolysis at a constant potential, a trend to higher pH was observed due to the presence of formate. The yield of the liquid product formate was significantly large with 16 mM so that the concentration of the electrolyte was changed. The total faradaic efficiency overall was calculated as 95.8%, consisting of 12% hydrogen, 7.2% of carbon monoxide and 76.6% of formate) (Figure 33).[59]

By taking into consideration the standard reduction potential E^0 for CO/CO_2 in acetonitrile ($E^0_{CO;CO2;CH3CN}$ is −650 mV versus NHE) the operating potential of −860 mV versus NHE corresponded to an overpotential of 210 mV for CO. This parameter is promising and is on a par with the state-of-the-art CO2RR electrocatalysts and thus exhibits the possibility of inserting enzymatic molecular themes into electrocatalytic systems.[59]
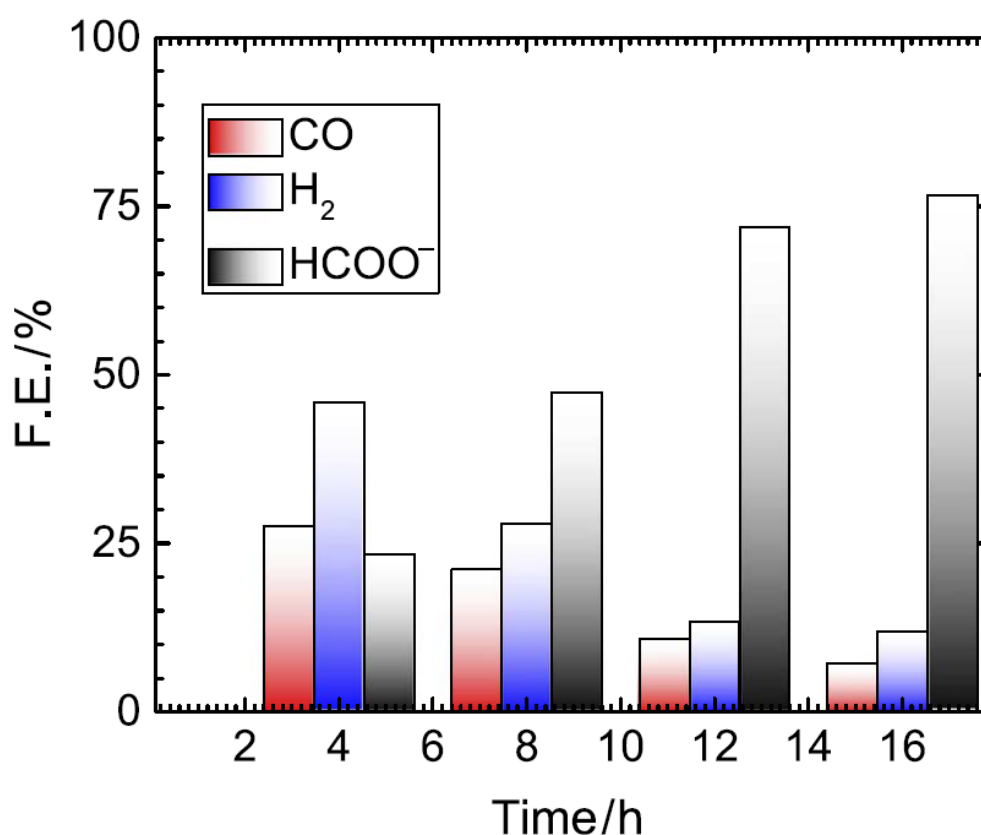
Figure 33. Faradaic efficiencies calculated from experimental data for CO, H_2, and formate as functions of different electrolysis time. Reprinted/modified from [59]. ©
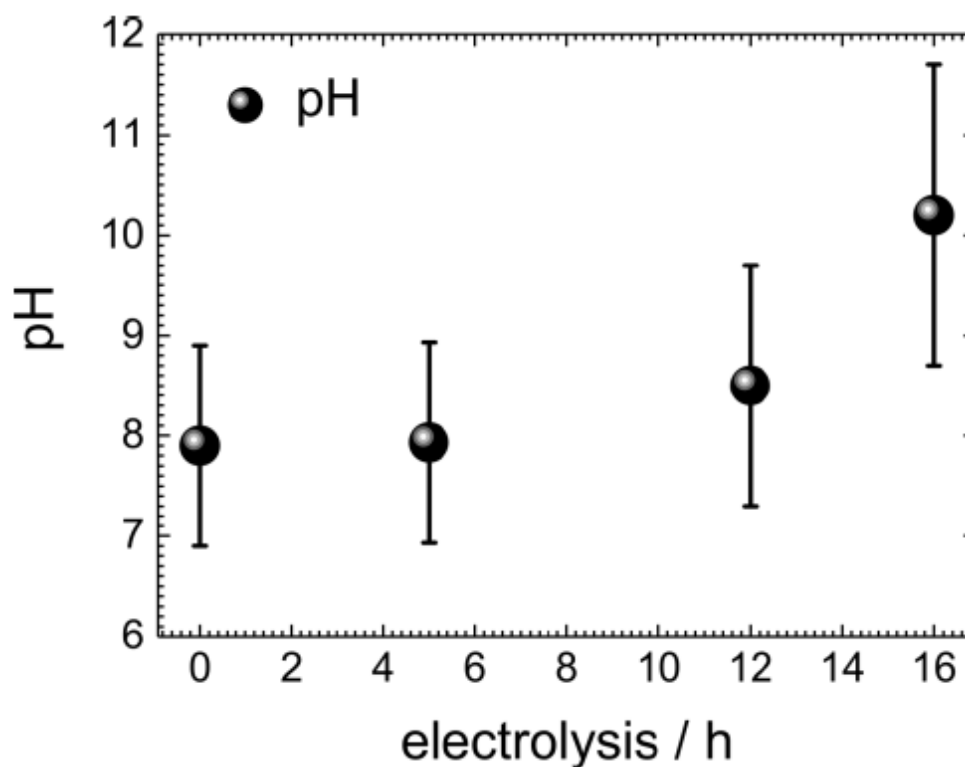
Figure 34. The pH values measured during the electrosynthesis of formate in acetonitrile-water electrolyte solution at room temperature and purged with CO_2 for 30 minutes. Reprinted/modified from [59]. ©

Since multiple latent carbon-resources besides CO_2, i.e. carbon felt electrode, acetonitrile solvent, and tetrabutylammonium-cations, were available in the electrochemical system, it was necessary to figure out the origin of electrocatalyzed CO2RR products.[59] Therefore, a separate chronoamperometry and spectral ^{13}C-NMR (Bruker Ascend 700 spectrometer equipped with a cryogenically cooled probe TXI) was performed using a marked carbon dioxide - $^{13}CO_2$ (Figure 35). For the electrochemical setup, a deuterated electrolyte solution with CD_3CN and 100 ppm D_2O was applied. The sequence of chronoamperometry was run at -1100 mV vs. Ag/AgCl for 2 hours and the spectra were recorded from the product-electrolyte sample, by using a volume of 450 µl.[59]

Three signatures of oxalate, which was the by-product of formate coupling in trace amount, formate as the main product and carbon monoxide were determined by ^{13}C-NMR. The zoom-in into the formate peak shows the D-splitting, which verified that the deuterated formate originated from $^{13}CO_2$ and D_2O and not from the above mentioned multiple latent carbon-resources. The ^{13}C-NMR spectra were utilized for qualitative evaluation only.[59]
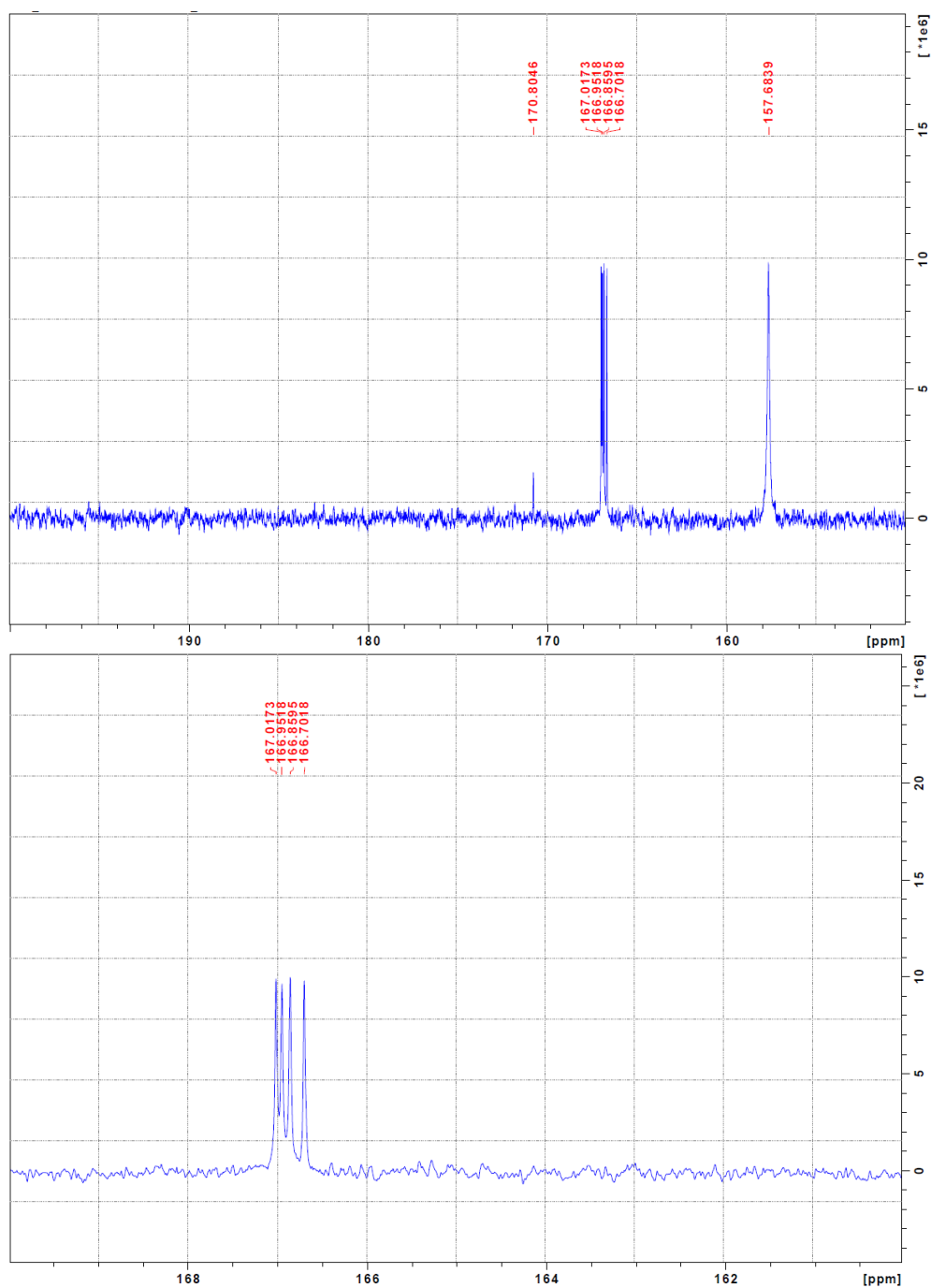
Figure 35. ^{13}C-NMR spectra exhibiting marked [13]CO_2 (acetonitrile-water, chemical shift δ = 124.8 ppm), trace amount of oxalate (157.7 ppm), formate (166.7 - 167.0 ppm) and trace amount of CO (170.8 ppm). The ^{13}C-splitting of deuterated formate (actually DCOO⁻) leading to broader peaks is shown in the chromatogramm. A zoom in into the D-splitted formate in D_2O-presence (lower chromatogramm) provides additional evidence that the product is derived from CO_2 (and D_2O). Reprinted/modified from [59]. ©

3.1.5. Mechanistic Insights by in-situ Spectroelectrochemistry

Mechanistic insights and information about the intermediate processes were gained by in situ spectroelectrochemistry (isSEC) as shown in Figure 36. This method combines electrochemistry with spectroscopy and provides useful information about the precise sequence of the electrosynthesis as a function of the applied potential.[59] By the isSEC technique it was possible to distinguish between emerging and disappearing features on the basis of the spectral peaks. The signal of carbonyl-PDA (keto-carbonyl at 1730 cm^{-1}) pointed downward in the spectrum stands for fading property while that of CO_2 and carbonyl-amide at 1650 and 1635 cm^{-1} pointed upward were newly emerging features. Based on the detailed mechanism in combination with the isSEC spectra, CO_2 firstly attached to the carbonyl functionality in polydopamine, as indicated in its subsequent depletion with increasing CO_2 concentration. The last intermediate step included the newly formed carbonyl-amide, which was generated after the attachment and subsequent reduction. These results were in agreement with the DFT calculations, which described the preferential position of the oxygen for the initial CO_2 attachment.[59] The preference for CO and formate could be explained through the subsequent reduction via the amide group and hence was exhibitive of the coupling between the amino and the carbonyl functionalities through hydrogen bonding. The enhancement in conductive PDA could be related to the active sites given by the organic functional motifs, which might have the potential to allow the large-scale electrosynthesis of C1 carbon feedstocks.[59]

The sources of renewable materials are sufficient and readily accessible in natural and bio-derived materials. In here, two attractive goals are combined: (i) eliminating expensive and rare metals and (ii) further reducing the operating potentials for enhanced energy yields in electrocatalytic CO_2 reduction. Especially, working at low overpotentials is an important concern to reduce the amount of energy that must be wasted in the form of heat at high current densities in industrial-scale electrosynthesis. Moreover, this concept can be extended to involve related enzyme-inspired molecular designs and shift the product distribution towards higher hydrocarbons or apply organic electrosynthesis for hydrogen reactions in fuel cells. Therefore, conductive and functional bio-related materials support universal approaches for developing effective electrodes for energy-related electrocatalysis.[59]
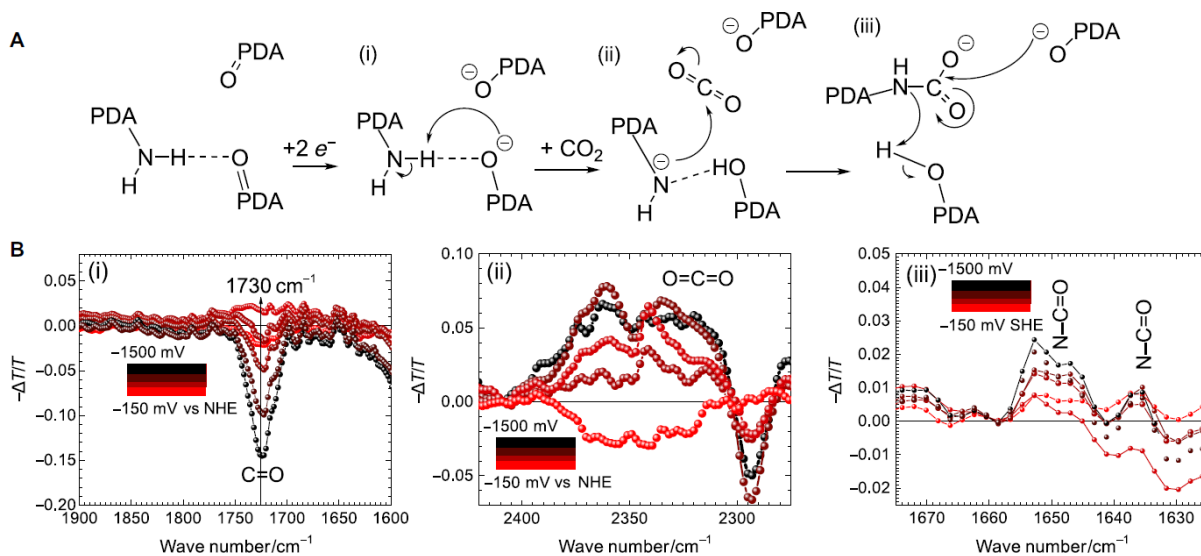
Figure 36. The electrochemical activation of amine-carbonyl bridged via hydrogen bonding to a nucleophilic center. (A) the initial steps, which drive the CO_2 reduction reaction in conductive polydopamine can be listed as the following: (i) the electrochemical activation of the carbonyl group, (ii) followed by the formation of a nucleophilic center via the amine group, and (iii) the attachment to CO_2 generating a new amide bond. (B) The isSEC-FTIR differential spectra plot the individual initial steps presented above. The negative peaks indicate the depletion of polydopamine-carbonyl feature, while the positive peaks show the emergence of new absorptions such as, CO_2-related vibrations (2350 cm^{-1}) and amide-carbonyl vibrations (1650 cm^{-1} and 1635 cm^{-1}). Reprinted/modified from [59]. ©

3.2. Polydopamine (PDA) in Hydrogen Evolution Reaction (HER)

The hydrogen evolution reaction (HER) requires an electrocatalyst with minimum binding energy for the adsorbed atomic hydrogen (further denoted as ΔG_H*). In addition, the surface configuration has to be able to sustain acidic environment, but at the same time show the thermodynamic affinity to reduce protons as measured by the exchange current i_0.[135-137] When, such requirements are met, the hydrogen evolution happens at sufficient low overpotential. This is required for the electrosynthesis at optimum energy efficiency. As such, hydrogen can be produced efficiently from water, in particular useful for industrial applications such as steady state operative electrolyzers.[138]

Presently, noble metals and some metal compounds show high electrocatalytic performances. These are metals such as platinum, rhodium, and iridium and transition metal semiconductors such as molybdenum- and cobalt compounds (e.g. carbides, phosphides, sulfides and combinations thereof).[24-43] Particularly of interest are the Mo-based systems such as MoS_2,[29, 47, 139-142] and related semiconductors of the mentioned composition. They represent the concurrently emerging alternative of the non-noble metals, mainly the Pt. They can help to make the hydrogen production from water more cost-effective.[138]

We explored the metal-free concept previously introduced by o-CVD PDA as electrocatalysts, but with a change in synthesis to promote the hydrogen reaction. The organic surfaces possess a tunability of the structure, so that catalytic sites can be re-designed for e.g. electrocatalytic HER. In this context, we sought the critical parameters, which are responsible of optimum HER. One of them is the work function: best-in-class noble metals such as Pt possess high work functions in the range of 6.0eV. So it is important to engineer the polymer, that it shows similar electronic properties to improve e.g. the i_0.[136] Also, we were interested in finding a system, where the hydrogen binding energy ΔG_H^* is similarly low as for Pt, in order to achieve an advantageous situation for the proton reduction and a similar mechanism as for Pt. In this view, o-CVD PDA were regarded as potential candidates, as they are stable in solution, particularly insoluble through their bulky functionalized polycations. The electroactivity was readily demonstrated by the CO2RR i.e. that here exists high density of functional and active sites on the surface to achieve an on-par with metal catalytic performances.[59] Furthermore, o-CVD PDA has an electrical conductivity sufficiently high for electocatalysis. Also the electronic properties render e.g. a high work functions Φ, in the range of the HOMO level close to -5.3 and -5.6 eV (caused by the p-doping). This creates an advantageous situation for electrocatalytic HER.[138]

To master the o-CVD PDA to optimize HER with high Φ and in parallel hydrogen affinity and its stability, a change in the synthesis is requisite. The hydrogen-bonded structure had to be re-designed so that motifs would be embedded that offer a minimum ΔG_H^* value similar to Pt. We apply therefore density functional theory to obtain a clear picture of the potential values on different functional system. Among the variety of hydrogen-bonded functions, we explored the keto-amine

hydrogen-bonds as the most convenient function for HER electrocatalysis. The keto-amine catalytic site is the only one in o-CVD PDA, which combines a comparatively low ΔG_H^* (calculated actually at 220 meV) and a low work function closer to Pt (e.g. 5.6eV). To enhance HER, we had to advance the o-CVD reaction to promote this catalytic theme to obtain favorable energetics, foremost to improve on the crucial and rate-determining step of hydrogen recombination on the surface as efficiently happening on Pt. However, it is demonstrated here that the production of molecular hydrogen is possible using an electrocatalyst without metallic site.[138]

The modification of o-CVD to enhance the keto-amine structure was the key-ingredient for electrocatalytic HER. The experimental method we chose to activate the desired motif in the ultimate o-CVD PDA relied on changing the reaction temperature. By increasing the reactivity effectively in the polymerization and doping step, it was possible to locally increase the oxidation power. As such, a more selective polymerization produced the o-CVD PDA with higher concentrated keto-amines.[138] This has been shown to significantly increase the electrocatalytic H_2 production. Thereby we found now experimentally, what has been hypothesized by us earlier i.e. that enrichment of keto-amines makes the surface properties close to that of noble electrocatalytic hydrogen metals, foremost similar to Ni and Pt. This results in a ΔG_H^* close to Ni on par with a work function no higher than 5.6 eV close to electrocatalytic Ir.[138] Paired with the requisite electrochemical robustness and the stability in acidic surrounding, but also the insolubility in water these polydopamine systems represent new HER electrocatalysts – hydrogen evolving polymers. They can produce continuously hydrogen gas without notable degradation in an electrolysis cell and with a performance characteristic similar to Ni.[138]

3.2.1. Optimization of Reaction Conditions for HER

To employ electroactive and hydrogen-selective functionalities for electrocatalytic HER, we presented the changes undergone in the o-CVD synthesis of PDA.[59-60] PDA was shown to have four dominating hydrogen-bonded motifs inside its structure. These vary between the amine and the corresponding and adjacent hydroxyl- or keto-function, all emerging from alternating the tri-functional monomer dopamine (DA) and its derivatives (Figure 37).[138] The derivatives are dopaminequinone (DAQ), oxidized from hydroxyl to keto-groups. Further, the next-level oxidative byproduct is the leucodopaminechrome (LDC), a condensed system with the unsaturated indole-ring. The last and highest-oxidized intermediate derivative of DA is the 5,6-dihydroxyindole (DHI) – the fully saturated functional indole (Figure 3).[60-61] These are formed during the polymerization-doping reaction, but have different concentration, e.g. in the classic synthesis presented in chapter 1.4.1, it is the DA and DAQ dominanting the structures as measured by the XPS structural investigation, foremost the N1s feature for 2/3 primary amine present.[60, 70, 118] Subsequently, we change the chemical surrounding so that the formation favors the condensated indole-structures, mainly the DHI derivative. As such, the structure is different and creates more hydrogen-bonded

motifs which are DHI-based. These are now changed in the functionality, as the nitrogen amine group in DHI is particularly different than the primary amine in DA and DAQ. These emerge the hydroxyl-amine- (OH-HN$_{DHI}$) and the corresponding keto-amine (O-HN$_{DHI}$). The earlier dominating moieties such as hydroxyl-amine from DA or DAQ are now less present in the structure. Less important are the intermediate keto-amines from of the LDC-derived amines (O-HN$_{LDC}$). The previous polymerization reactions show that the primary amines from DA and DAQ are much more present than LDC and DHI related amines.[60, 138]

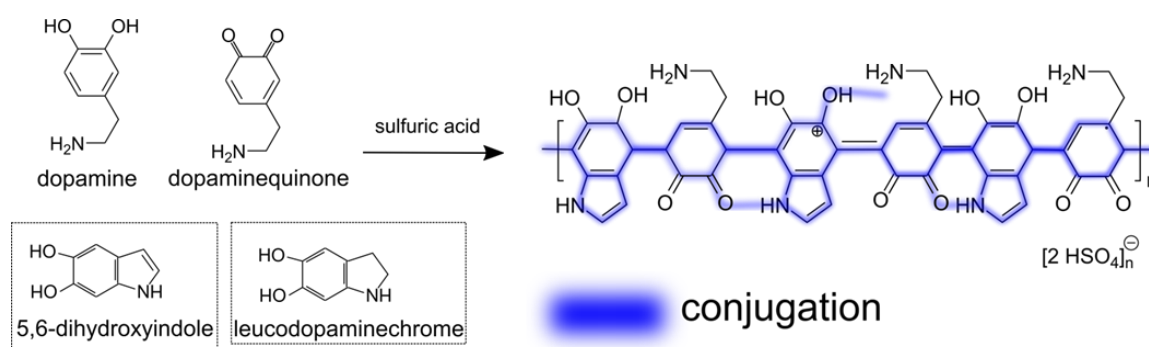

Figure 37. Four main types of hydrogen-bonded motifs of the alternating bi-functional monomer units of PDA. Reprinted/modified from [138].©

The changes between the DA and DAQ compared to LDC and DHI can be reflected by looking at the basicity of the corresponding amine groups. DA and DAQ as monomers are e.g. soluble in water and partly protonated, their pKa corresponds to 8.9 and 9.3, respectively.[138] LDC and DHI are insoluble in water, because the pKa-values are lower at 6.5 almost neutral or slightly acidic. This shift in pKa is also influencing the affinity to the hydrogen reduction – exactly this was analyzed here by DFT simulations, in detail, on each of the motifs. We derived the binding energies of all the relevant functional groups in PDA of the adsorbed hydrogen H* in a simulative calculation. The simulation depicts the affinity for the Volmer reaction and the ΔG_H^* value. Most favorable are the DHI-related secondary (acidic) amines: When they are integrated part of the keto-amine, the energy values become lower, lowest in the best case at -0.22 eV as shown by the calculation. So, in summary we had to advance the keto-amine motifs (O-HN$_{DHI}$) in PDA to derive a desirable situation for electrocatalytic HER on o-CVD processed conducting polymers (Figure 38, 2). We denote that the DFT calculations show that the Gibbs free energy of the hydrogen reaction is much lower for O-HN$_{DHI}$. Compared to the other motifs, particularly those which involve primary i.e. basic amines, the binding energy tremendously change to higher energies for DA and DAQ-based functionalities (Figure 3). So we found that the HER selectivity depends on the structure and functional groups in particular and that we had to increase DHI in the polymers, to enhance the keto-amine functional groups.[138]
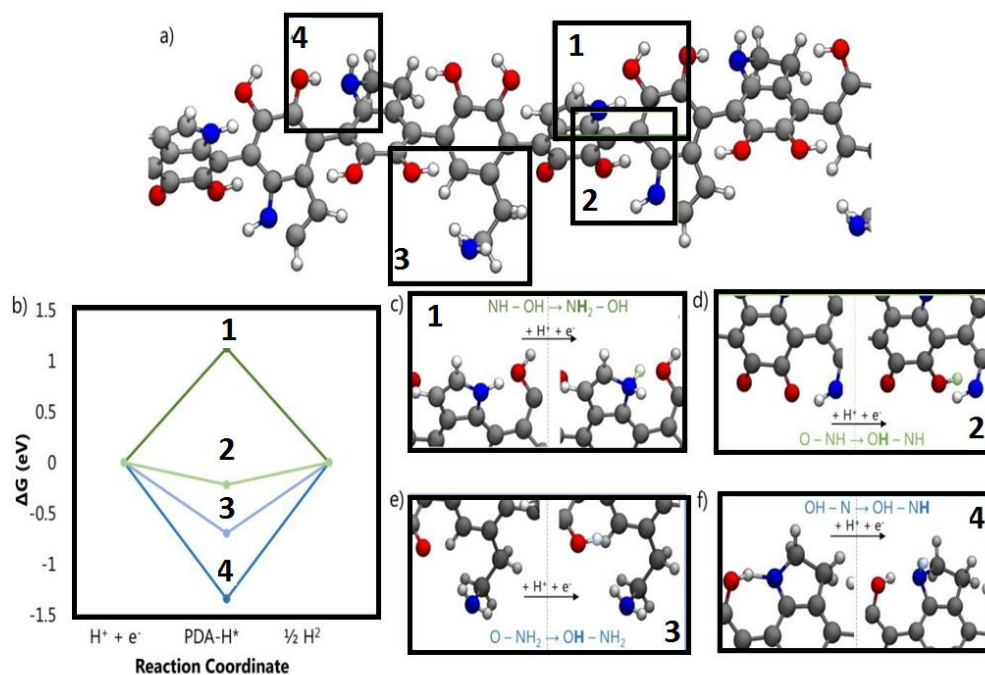
Figure 38. Density functional theory calculation for the determination of the hydrogen affinity of hydrogen bonding. (a) A representation of a PDA pattern with various functional themes. (b) The diagrams of the reaction energy for the hydrogen evolution reaction on the distinct themes. (c) The hydroxyl-amine and (d) keto-amine motifs of the dihydroxyindole (DHI), (e) the hydroxyl-amine of the dopamine, and the keto-amine of the leucodopaminechrome (LDC). The keto-amine group provides the lowest energy for ΔG_H^* of -0.22 eV, whereas the other remaining hydrogen-bonded themes own undesirable energies for the hydrogen evolution reaction. The DFT calculations were performed in collaboration with Toronto University by Phil De Luna. Reprinted/modified from [138].©

3.2.2. Electronic and Structural Properties of Polydopamine (PDA)

DHI-rich and structurally changed PDA, further called DHI-PDA, was experimentally demonstrated by a modified gas phase synthesis. Based on the experimental previously-reported oxidative polymerization, we targeted to up-concentrate the uppermost oxidation derivative of dopamine – DHI. We did so by increasing the oxidation power in the reaction zone. This was performed by increasing the temperature. All other parameters were kept constant, i.e. the oxidation reagent sulfuric acid, the pressure and the gas flow. The ΔT was 50 °C, discretely, an increase from 300 °C to 350 °C. We denote that the higher temperature did not impact the electrical conductivity significantly.[138]

Figure 39. The structural and electronic properties of the modified polydopamine (DHI-PDA). (a) The XPS results of the N1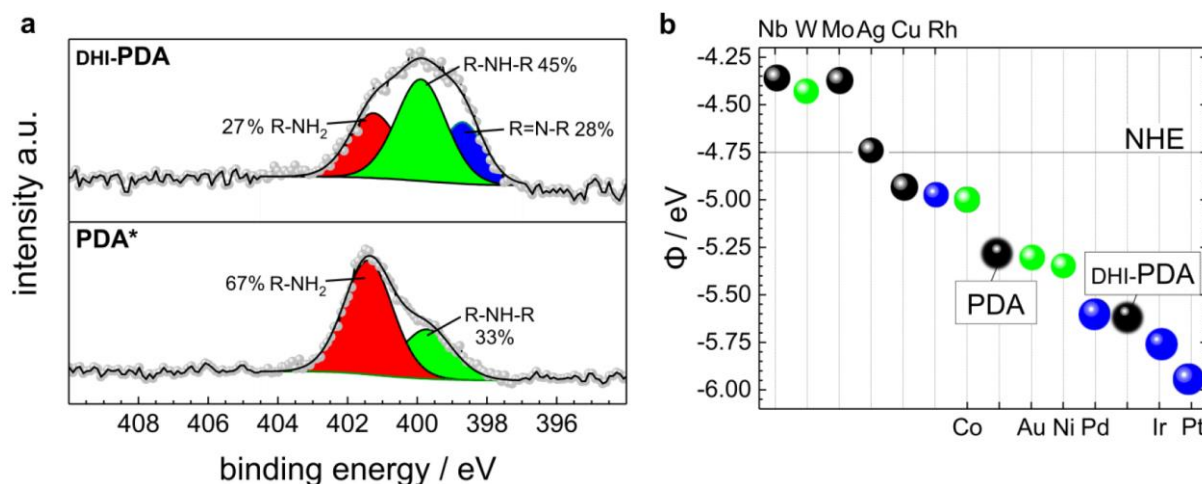s spectra of DHI-PDA compared to PDA* are shown: The result reveals a fundamental change in functional motifs, mostly on the nitrogen. While PDA contains mainly primary amines (R-NH₂ from DA and DAQ-motifs) as a major repeating unit in its structure, the DHI-PDA consists of a higher concentration of the dihydroxyindole (DHI), reflected in the dominant appearance of the secondary amine (R-NH-R) and imine (R=N-R) motifs. (b) The work functions Φ of the DHI-PDA and PDA* as compared to numerous different catalytic metals and the normal hydrogen electrode (NHE) are provided. All of the photoemission experiments shown in this thesis were measured directly on carbon felt as substrates. Reprinted/modified from [138].©

In DHI-PDA we confirmed of the higher amount of DHI from the amine, particularly from the N1s analysis (response of the high-resolution scans by XPS). We found DHI-amines i.e. secondary amines and imines are 73% of the nitrogen atoms. As compared to standard synthesized PDA (further denoted as PDA*), only 33% are effectively DHI-amines (Figure 39, a). These results show the tremendous increase and the DHI-presence inside the polymer. This changed also the work functions (DHI-PDA has 5.6 eV compared to PDA* with 5.25 eV. This is exactly between the work function of Ni (5.25 eV) and Ir (5.75 eV) (Figure 39, b). We explained the higher work function first by a higher doping level, but also by the imines in the structure (Figure 40).[138]
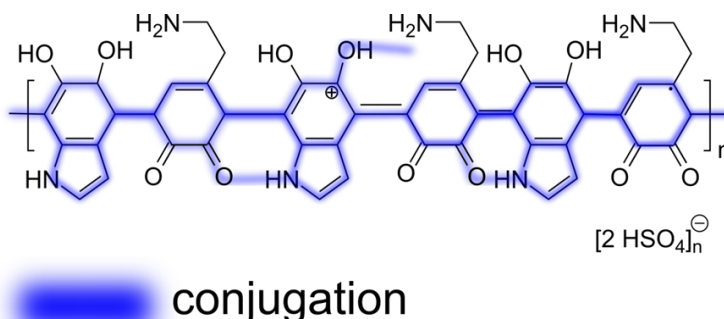

Figure 40. Modified o-CVD synthesis forms DHI-PDA with the (O-HNDHI) motif as the major hydrogen bonding functional group. Reprinted/modified from [138].©

3.2.3. Electrocatalytic Activity of PDA towards HER

As mentioned already in the above chapters, the o-CVD synthesized polydopamines enable the homogenous deposition on large and sponge-type surface area electrodes. Due to this fact, o-CVD was applied to produce structurally modified polydopamine (DHI-PDA) as electrodes for the hydrogen evolution reaction with large and 3-dimensional surface area on carbon felt to study the ongoing electrochemical reaction in detail.[138]

All polarographic and chronoamperometric scans together with the electrochemical impedance characterization were carried out using an H-cell configuration, which is separated by the anode and cathode spaces through a membrane to eliminate any crossover. A solution of 1 M trifluoromethanesulfonic acid (1M TA) was used as the electrolyte for all of the HER experiments. This electrolyte solution was preferential due to the stability of this system superior to sulfuric acid since polydopamine possessed the ability to reduce the sulfate anions of sulfuric acid. By inserting TA, any side reactions were excluded and a quantitative Faradaic yield of 100 % towards hydrogen evolution was achieved.[138]

The electrocatalytic reduction currents for the hydrogen evolution were shown in the cyclic voltammograms for both DHI-PDA and standard PDA (Figure 41). In order to have a control, the Pt-standard electrode and blank carbon felt electrode were included for comparison. The DHI-PDA delivered the threshold current density (10 mA cm^{-2}) at -190 mV versus the reversible hydrogen electrode (RHE), whereas the standard PDA* operated at +120 mV higher potential to achieve the same performance on current density. All scans were recorded with a scan rate 50 mV s^{-1} under stirring at room temperature and ambient pressure (1 atm). By analyzing the Tafel plots the higher electroactivity of DHI-PDA was confirmed as 80 mV dec^{-1} in comparison to 110 mV dec^{-1} for standard PDA*. Additionally, the Tafel plot was employed to approximate the exchange current density i_0 for both polydopamine systems. For this, i_0 was determined through the electrochemical active surface area (ECSA) in order to estimate the actual area. The ECSA was extracted from the electrochemical impedance data and calculated as A_{ECSA} = 10.625 cm^2. Our findings showed that the exchange current densities for DHI-PDA was beyond catalytic Ni metal and below Ir metal (i.e. 1.2.10^{-5} A cm^{-2}), whereas the exchange current density for standard PDA* was an order of magnitude below with 3.0.10^{-6} A cm^{-2}.[138]
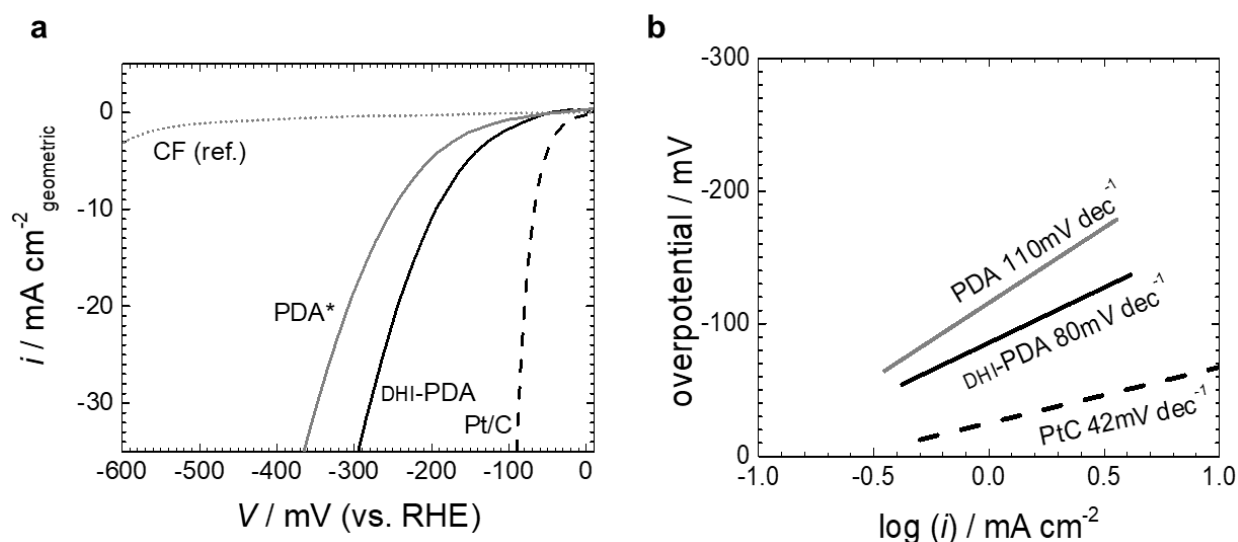
Figure 41. The electrochemical characterization results in (a) polarographic recording at 50 mV s^{-1} in 1 M TA electrolyte for hydrogen evolution reaction presenting the performance of PDA (standard) and DHI-PDA as compared to Pt as a reference (dashed line) as well as the carbon felt (CF) as blank control (dots). (b) Tafel slopes are shown in the graph. The reference overpotential η (at 10 mA cm^{-2} geometric current density) is determined as 190 mV for structurally modified DHI-PDA and as 270 mV for PDA. Reprinted/modified from [138].©

Based on the electrochemical impedance characterization of the used H-cell configuration, the appropriate cell resistances were determined from the electrolyte as 3 Ω, the membrane in between the H-cell as 30 Ω and the electrocatalyst as ΔR = 0.2 Ω, as well as the capacitance of the active area as C_i,DHI-PDA = 425 µF cm^{-2}. In order to test the electrocatalyst's stability, a representative chronoamperometric scan was performed for 168 hours continuous operation at -190 mV vs. RHE yielding in 10 mA cm^{-2} (Figure 42, a-c). The continuous hydrogen gas evolution was verified by gas chromatography. Only a decrease of 0.6 % of the overall current density, corresponding to 65 µA cm^{-2} was observed during 1 week of operation.[138] The presence of the catalyst material on the carbon felt surface was verified by SEM studies as shown in Figure 42, c.

Figure 42. The electrochemical impedance and chronoamperometric characterization are provided. (a) Bode-plot, which illustrates the frequency dependent electrochemical impedance, of 3-electrode setup shows the response of Pt-Pt as reference experiment, Pt-CF as a control experiment and Pt-CF+DHI-PDA working and counter electrodes. The resistance value between the control and DHI-PDA is found to be relatively sm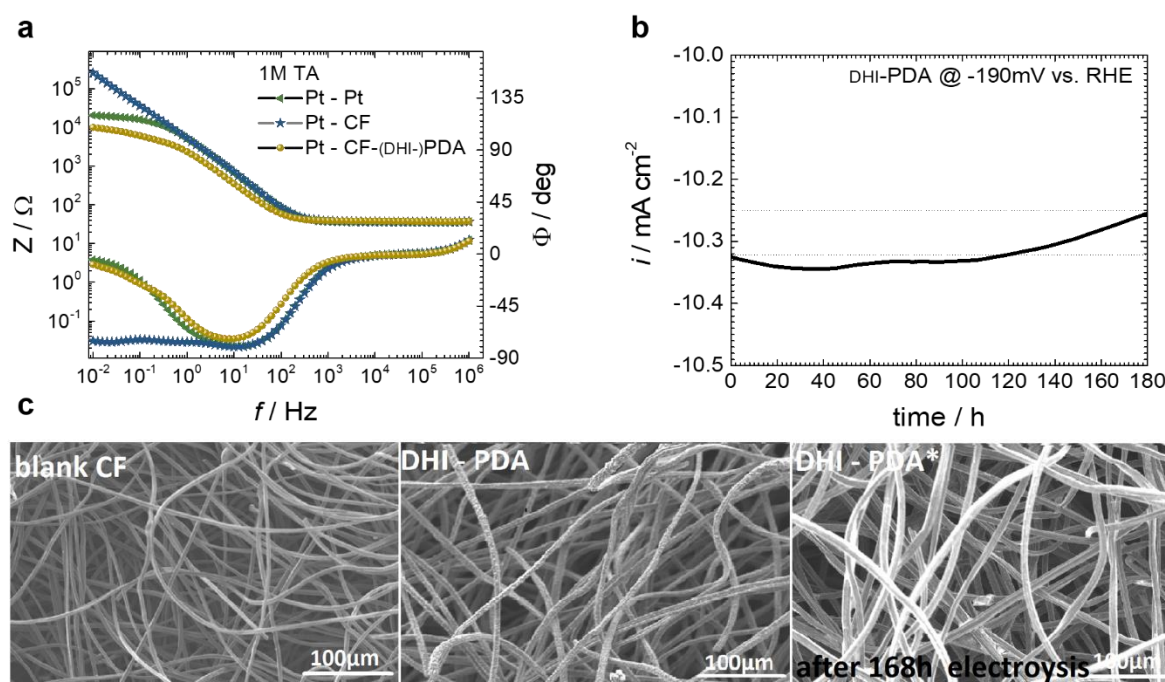all of about 0.1 Ω. (b) chronoamperometric stability scan of DHI-PDA recorded over time result in notable degradation in the catalyst system of about 0.6 % change of the total current at -190 mV vs. RHE. (c) SEM images on blank carbon felt, as well as carbon felt deposited with DHI-PDA before and after a continuous operation for 168 h. Reprinted/modified from [138].©

Combining the performance and the electrochemical stability in acidic electrolyte enabled the demonstration of a scaled electrolyser cell, in which various amounts of DHI-PDA was loaded to a carbon mesh with an area of 3 cm². Based on our observations, an increase in the catalyst load up to 2.3 mg, led to a continuous hydrogen evolution up to a current of 250 mA or 0.11 A mg^{-1} DHI-PDA related to the mass of the catalyst. As shown in Figure 43, the current increased almost linearly with the catalyst mass loaded on the carbon felt, however at this point the o-CVD technique limited the further catalysts growth due to the factors described in chapter 2.2.1.[138]

At 250 mA, which corresponds to a mass activity of 0.11A mg^{-1}, a turnover frequency (TOF) for HER was calculated at 0.2 s^{-1} (Figure 43, a). This value was obtained by taking into account the total amount of DHI units inside DHI-PDA. According to the XPS results of N1s spectrum, 73 % net DHI of the total moles monomer units was implemented in the system (Figure 43, a). By this way, 1.0 L of hydrogen was produced in a timeframe of approximately 9 hours of continuous electrolysis (Figure 43, b).[138]
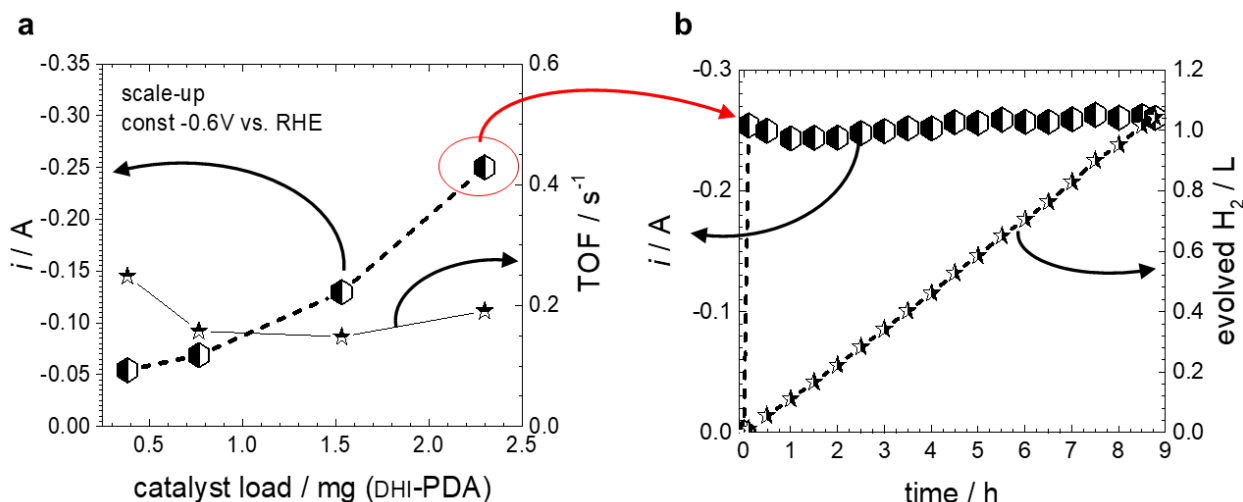
Figure 43. Presentation of a large-scale DHI-PDA electrolyzer system. Carbon felt is applied as the supporting electrode with different catalyst mass loadings and plotted against the absolute current i at -0.6 V vs. RHE. The turnover frequency (TOF) is referred to the total amount of DHI monomer building blocks and is included in the plot as well resulting in 73 % according to the XPS spectrum of N1s. By this way, at 250 mA (or mass activity of 0.11 A mg^{-1}) the continuous production of 1 L of H_2 on the basis of an electrochemical flow cell system with DHI-PDA coated carbon felt is shown. Reprinted/modified from [138].©

The conductive and functional polymer investigated in this thesis, sustained impressive performance in elelctrocatalytic HER. The DHI-PDA electrocatalyst exhibited a homogenously functionalized conductive biopolymer with enhanced keto-amine hydrogen-bonded themes. The design of a bio-originated catalyst was shown in this chapter that owns various electronic properties similarly to the catalytic metals. To sum up, these properties covered a similar work function Φ as iridium, and a similar proton adsorption energy ΔG_H^* as nickel metals, resulting in an exchange current density between those of the metals. For instance, the work function of DHI-PDA was approximately 1 eV below the standard hydrogen potential, with ΔG_H^* being 0.22 eV, and the current density at $1.2*10^{-2}$ mA cm^{-2} as presented in the volcano and Trasatti plots in Figure 44.[136] There is an analogy between the concept of volcano plots in catalysis and outer sphere electron transfer. The descending region is known as the Marcus inverted region.[138]

As a further possible improvement in the electrocatalytic activity of the biopolymer, increasing the surface density of catalytic sites, such as the fraction of DHI-fragments, might be an advantageous approach in order to reach a similar i_0 as noble metals.

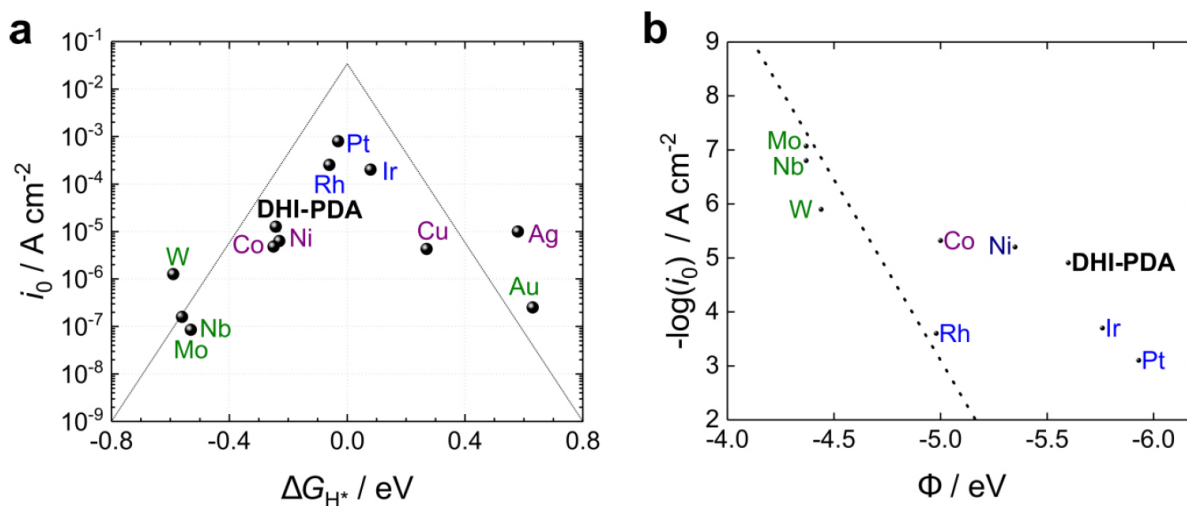**Figure 44.** (a) The Volcano plot represents the exchange current density plotted vs. adsorption energy ΔG_H^* for hydrogen and the location of the DHI-PDA electrocatalyst as compared to other metallic systems. The i_0 for DHI-PDA is found to be between Ni and Ir metals at 1.2 10^{-5} A cm^{-2} at ΔG_H^* at -0.22 eV. (b) The work function Φ of various catalytic metals against the log i_0 reveals the Trasatti´s empiric correlation. Reprinted/modified from [138].©

This chapter of the thesis showed the ability to imitate a metal-like catalyst surface utilizing bio-originated functional groups such as hydrogen-bonded themes. These have attracted great attention for numerous catalytic applications, since many systems in enzymology, such as catalytic triades, employ them for selective reactions. In here, we focused on the electrocatalysis of proton reduction and examined the affinity of such themes to act as catalyst towards HER. A two-step reduction mechanism from protons to molecular hydrogen is widely known in this field. These are the Volmer and Tafel, and in most cases in combination with Heyrovsky steps. Important for HER is the reducing of the binding energy of the adsorbed hydrogen intermediate H*. Doing so is beneficial for the overall catalytic performance. In this work, a functional motif of keto-imines in DHI-PDA was used as a catalytic reaction center, which allowed the ideal energetics for HER based on DFT calculations. Our findings revealed that these functional and conductive polymers maintain a similar adsorption energy for hydrogen as noble metals. Further, the efficient DHI-PDA electrocatalyst developed for HER yielded in quantitative Faradaic efficiency with a Tafel slope of 80 mV dec^{-1}, a low overpotential of 190 mV at a current density of 10 mA cm^{-2}, and a remarkable stability enabling the long-term electrolysis with negligible degradation for one week of continuous operation.[138] Therefore, it is highly promising for future catalyst design that bio-originated functional groups can be embedded successfully in electrocatalysis. These catalytic systems might be further advanced by tuning the functional parts, which provide high electroactive-site density as compared to best-in-class metals, insolubility in acidic electrolytes, enormous stability and quantitative selectivity.

3.3. Polyguaine (PG) in Hydrogen Evolution Reaction (HER)

Here, we investigated a novel bio-origin, bio-inspired polymer as selective HER electrocatalyst. We sought a conductive and functional polymer, which adopts a polyaniline (PANI) related structure, utilized as HER electrocatalyst: We chose guanine, the purine component of the deoxyribonucleic acid (DNA) - responsible not only for the genetic information storage but also for protein biosynthesis and energy transduction across the cells.[82-83, 85-87, 89-92, 143-148] Especially, we harnessed the presence of six functional motifs per monomer unit to allure high catalytic activity similar to platinum. For making the electrodes, we oxidatively polymerized guanine from the vapor phase in combination with sulfuric acid as an oxidant onto a surface. Similarly as in PANI, we found enhanced conductivities upon exposure of polyguanine films to different acidic environment.[149] The predominant imine, amine and carbonyl functionalities are experimentally verified by XPS and FTIR spectroscopy analysis as shown below (Figures 46- 54).[84]

To combine the electrocatalytic activity and remarkable conductivity of PG with a large electrolytic interfacial area we conducted the oxidative chemical vapor deposition (o-CVD) on the sponge-type carbon felt (CF) as a supporting 3D-electrode, a technique we developed and successfully applied to other materials before.[59-60, 96, 150] In comparison with polyaniline (PANI), PG revealed greater catalytic property towards hydrogen evolution, most probably due to the increased functional density on PG.[84]

3.3.1. Analogy between Polyaniline (PANI) and Polyguanine (PG)

Polyaniline (PANI), a representative of the family of conducting polymers, is distinguished by the others in many aspects. Due to the enhanced conductivity by proton doping, PANI is considered as an interesting platform for hydrogen evolution reaction (HER). The feature of H^+ doping provides an intimate interface between electrons and protons and thus eases the hydrogen evolution.[149, 151-154] We used this phenomenon in designing molecular HER, however PANI hardly shows electrocatalytic activity. In this study, we introduced a structural analogous to PANI with increased functional sites and thus higher catalytic activity towards HER. We depicted a unique one-step synthesis for the generation of oxidatively polymerized and doped guanine.[84]

In contrast to guanine, after undergoing the polymerization reaction, PANI occupies various oxidation states. Some of these oxidized forms are conductive while some are insulating. In Figure 45, the chemical structure of the blue Polyaniline as emeraldine base in non-conducting state and the green polyaniline as emeraldine salt in conducting form is presented. The conductivity is a result of proton doping in PANI and requires a post-treatment after the polymerization reaction of aniline.[149] However, as shown in the same Figure, the H^+ doping in polyguanine (PG) occurs subsequently after the polymerization combined in a single-step reaction form the vapor phase without compromising functional motifs embedded in the polymer backbone.[84]
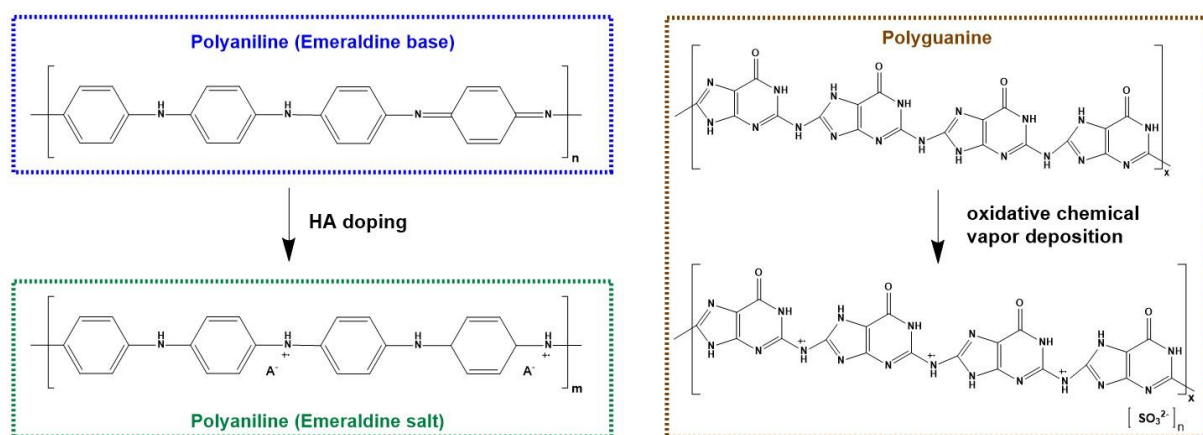
Figure 45. Structural analogy between polyaniline (PANI) and polyguanine (PG). The left side presents the H+ doping treatment in PANI to improve the conductivity. In the right, polyguanine is shown, synthesized through an oxidative chemical vapor deposition synthesis, combining the polymerization and the doping in a single step reaction, resulting in similar molecular functional substructures. Reprinted/modified from [84].©

As compared in their monomeric structure, we found a distinct similarity between aniline and guanine. Both possess primary amine functionality, which gets initialized for the polymerization by oxidation. Since the polymerization mechanism for PANI is well-known, we were able to adapt and suggest similar pathways for the polymerization of guanine.[149] Hence, we propose that the primary amine in guanine is initialized under oxidative sulfuric acid surrounding. Next, the generated radical cations couple and finally the propagation reactions take place forming a conductive and doped polyguanine at the end of the o-CVD synthesis. The proposed polymerization steps are shown in Figure 4.[84]

3.3.2. Electronic and Structural Properties of Polyguanine (PG)

We determined the elemental and surface composition of PG by the X-ray photoelectron spectroscopy (Figure 46). Based on XPS, clear differences can be depicted between the guanine monomer and polyguanine films deposited on a 10x10 mm glass substrate with Cr (8nm) / Au (80nm) contacts. Elemental concentrations of the guanine reference fits expected values from the literature.[155-156] While the C1s spectrum can be nicely fitted with five peaks of equal intensity, the N1s peak is fitted in two peaks: three amine species at higher binding energies and two imine species at lower binding energy. Based on the proposed polymerization reaction we would expect a transformation of the C8 carbon into one that has a similar BE as C2. Indeed, the C 1s spectrum of the polymer sample shows a shift in intensity from the BE region of C8 and C4 to that of C2 and C6. Compared to the monomer reference, the N 1s spectrum of the polymer shows a slightly higher intensity at higher BE, which would suggest a decrease of imino- in favour of amino-functionalities, if it were not for the possibility of side reactions involving sulphur and nitrogen. The BE of the sulphur 2p peak, as well as the distance between the S 2p and the O 1s peaks suggest a presence of sulphate as the counter ion in the polymeric structure. However, the elemental ratio of S:O (SO$_4$) was slightly below the expected 1:4 (Figures 51 and 52). All survey and high

resolution scans of guanine and polyguanine are presented in the Figures 47-53. Hence, we introduce the following potential chemical structure for polyguanine, established on the spectroscopic and structural analysis (Figure 46c).[84]
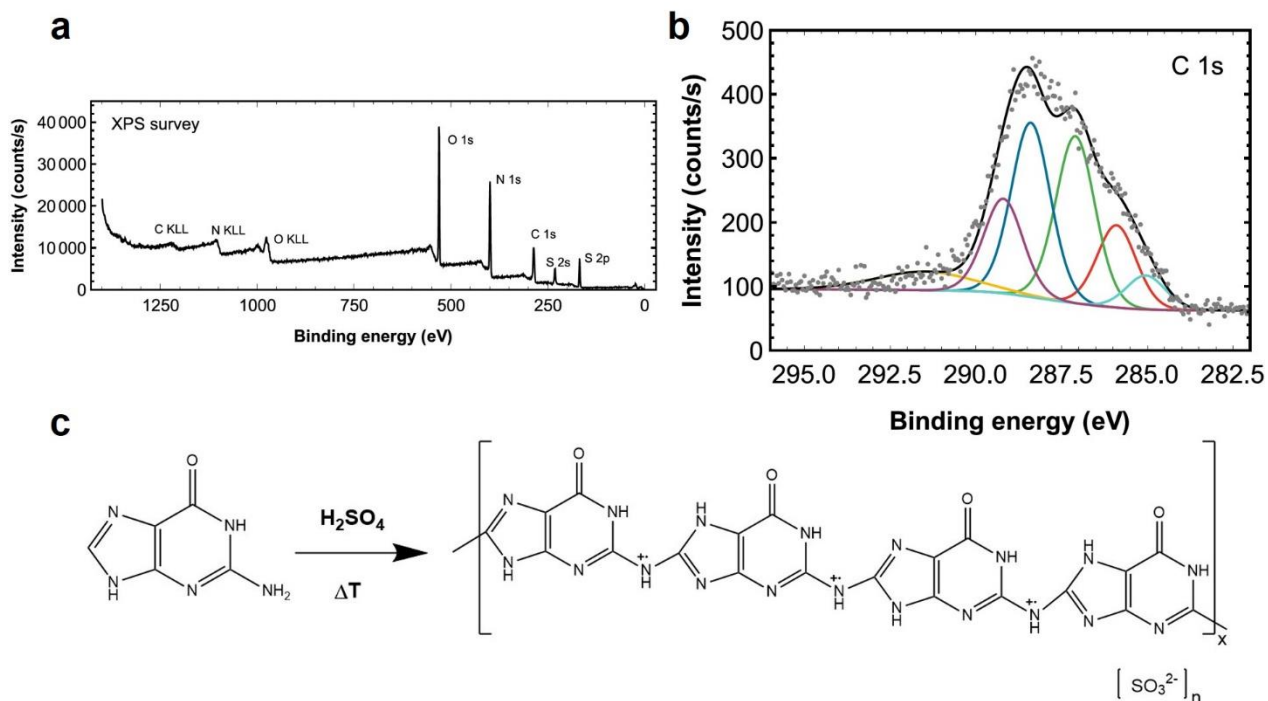
Figure 46. (a) XPS spectra of polyguanine in survey scan, (b) C1S spectrum of polyguanine, (c) potential chemical structure of PG. Reprinted/modified from [84].©
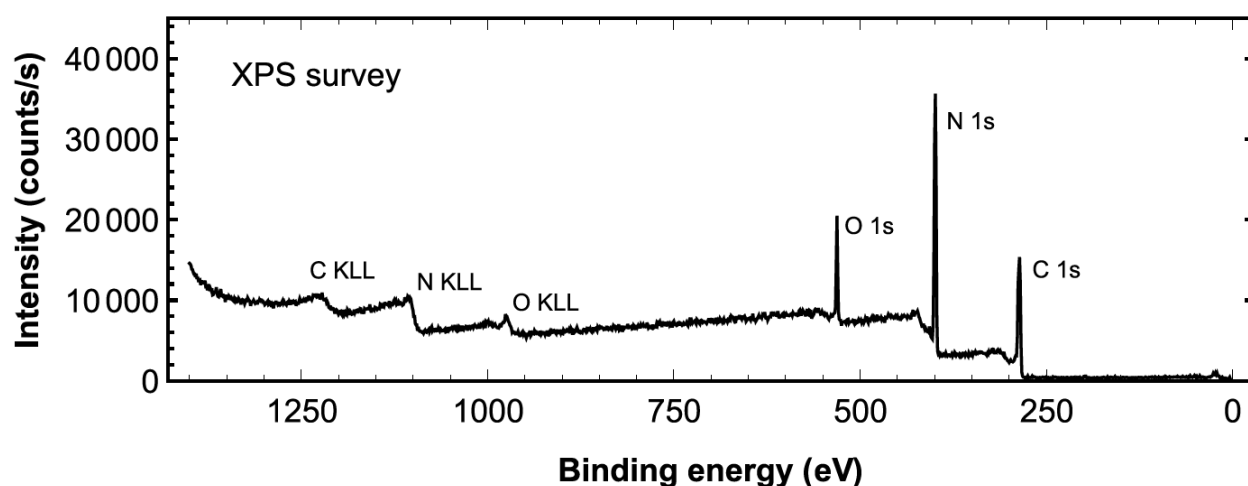
Figure 47. Survey scan of guanine powder. Carbon, nitrogen and oxygen elements were detected without any other contamination. Reprinted/modified from [84].©
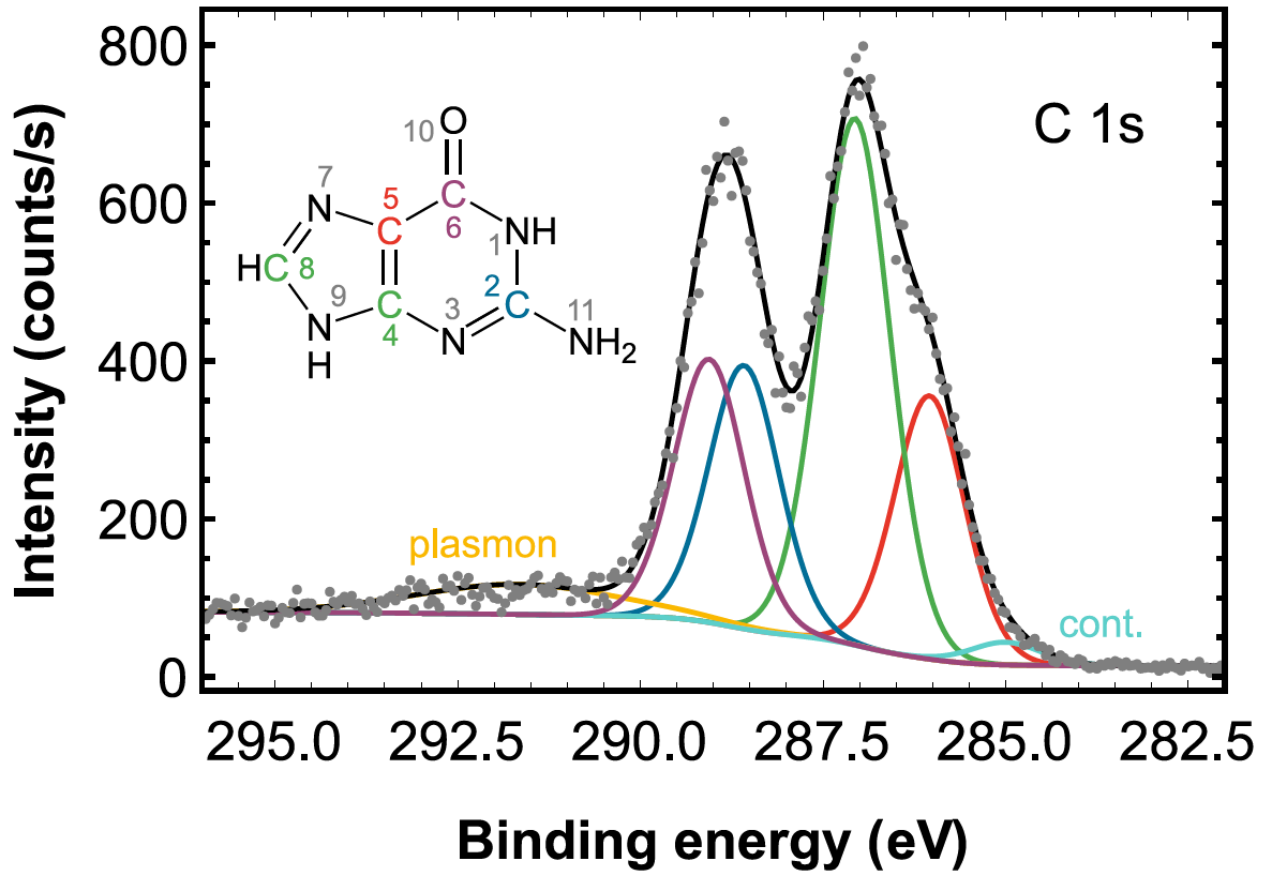
Figure 48. Carbon 1s (C1s) spectrum of guanine powder. Reprinted/modified from [84].©
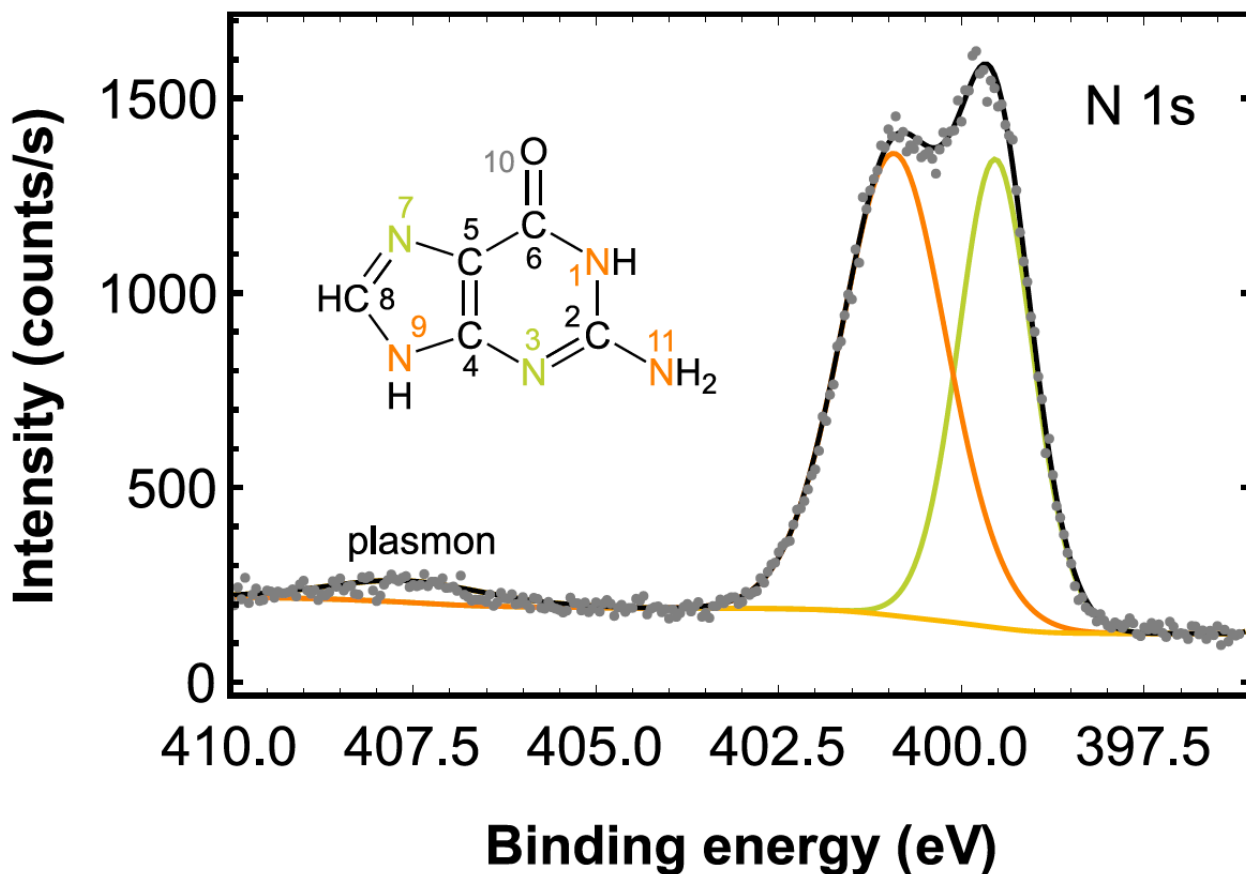
Figure 49. Nitrogen 1s (N1s) spectrum of guanine powder. Reprinted/modified from [84].©
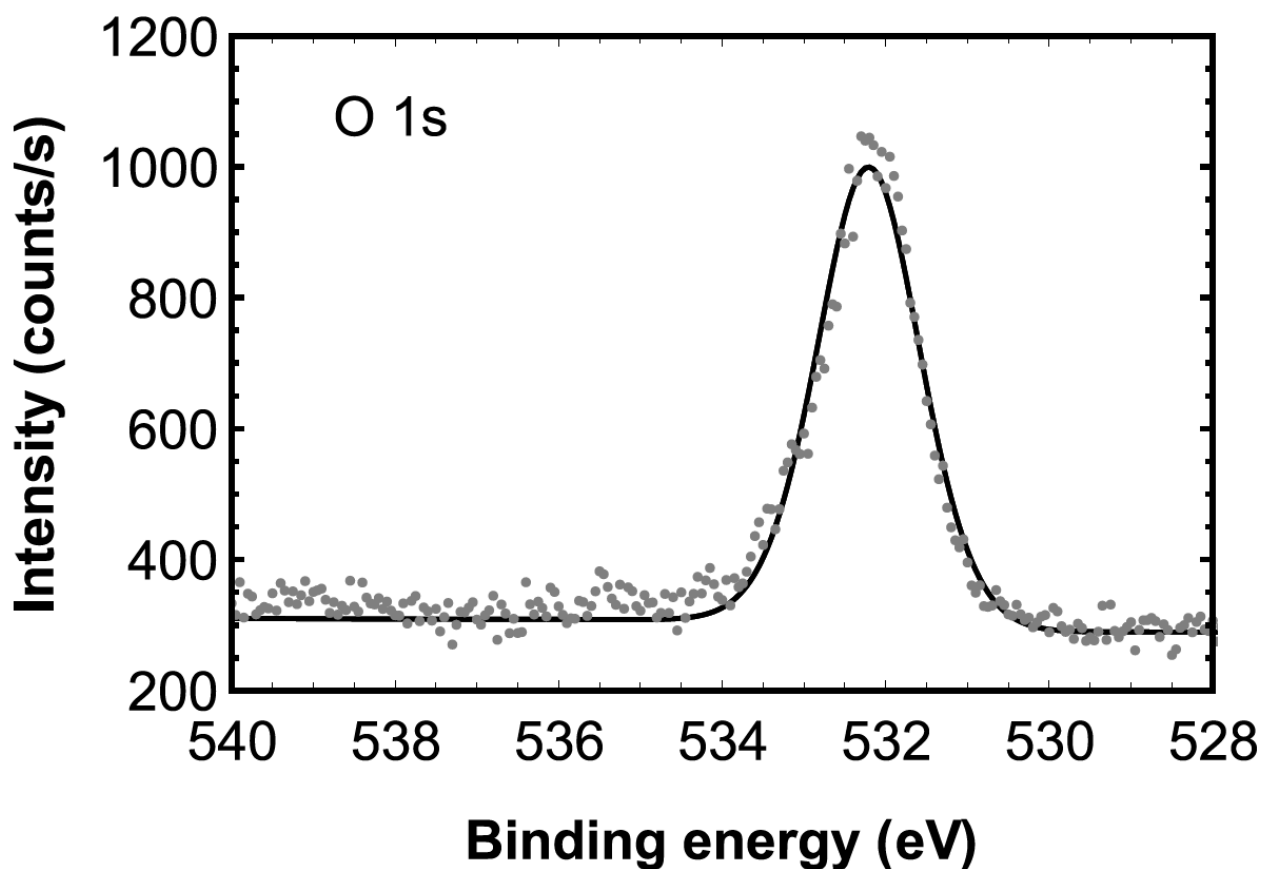
Figure 50. Oxygen 1s (O1s) spectrum of guanine powder. Reprinted/modified from [84].©
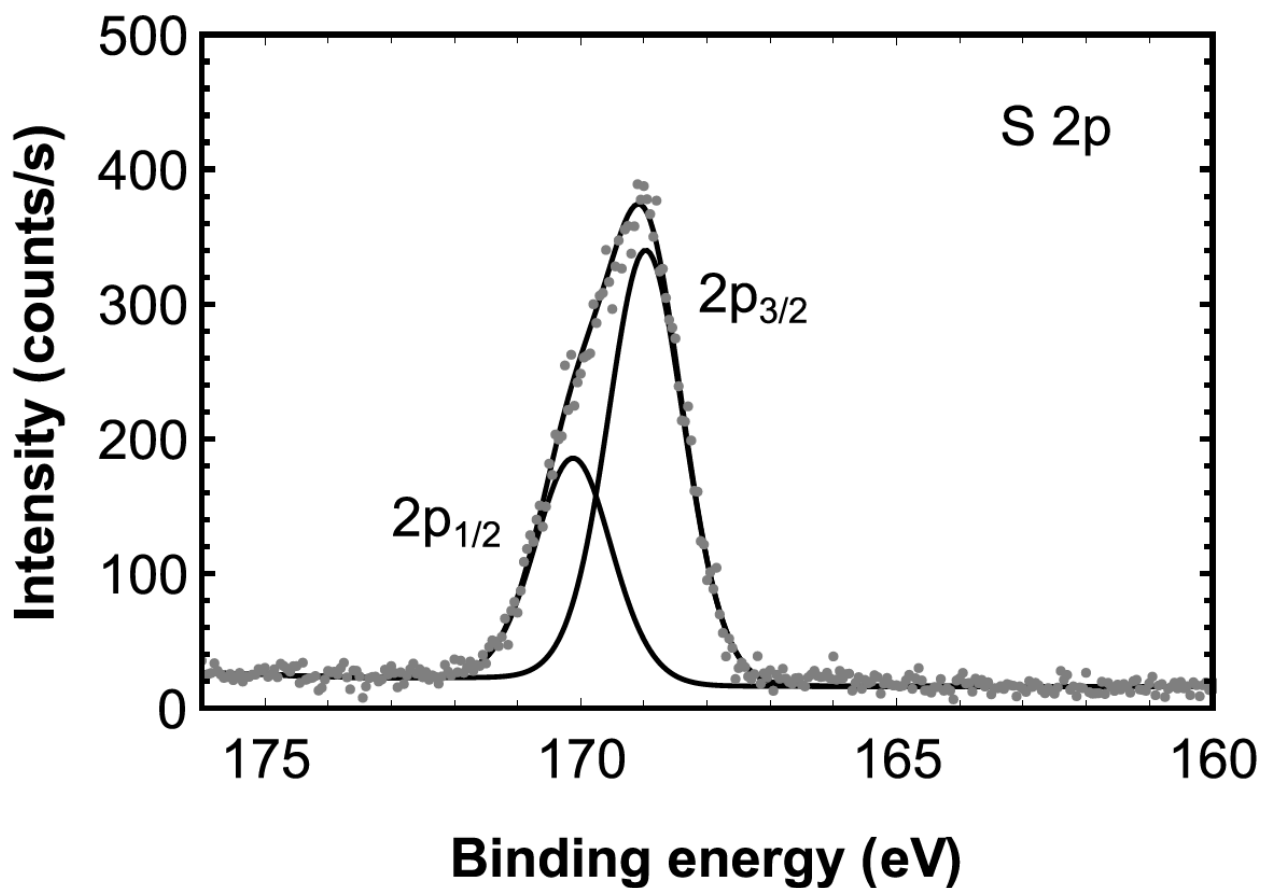
Figure 51. Sulfur 1s (S1s) spectrum of polyguanine. Reprinted/modified from [84].©
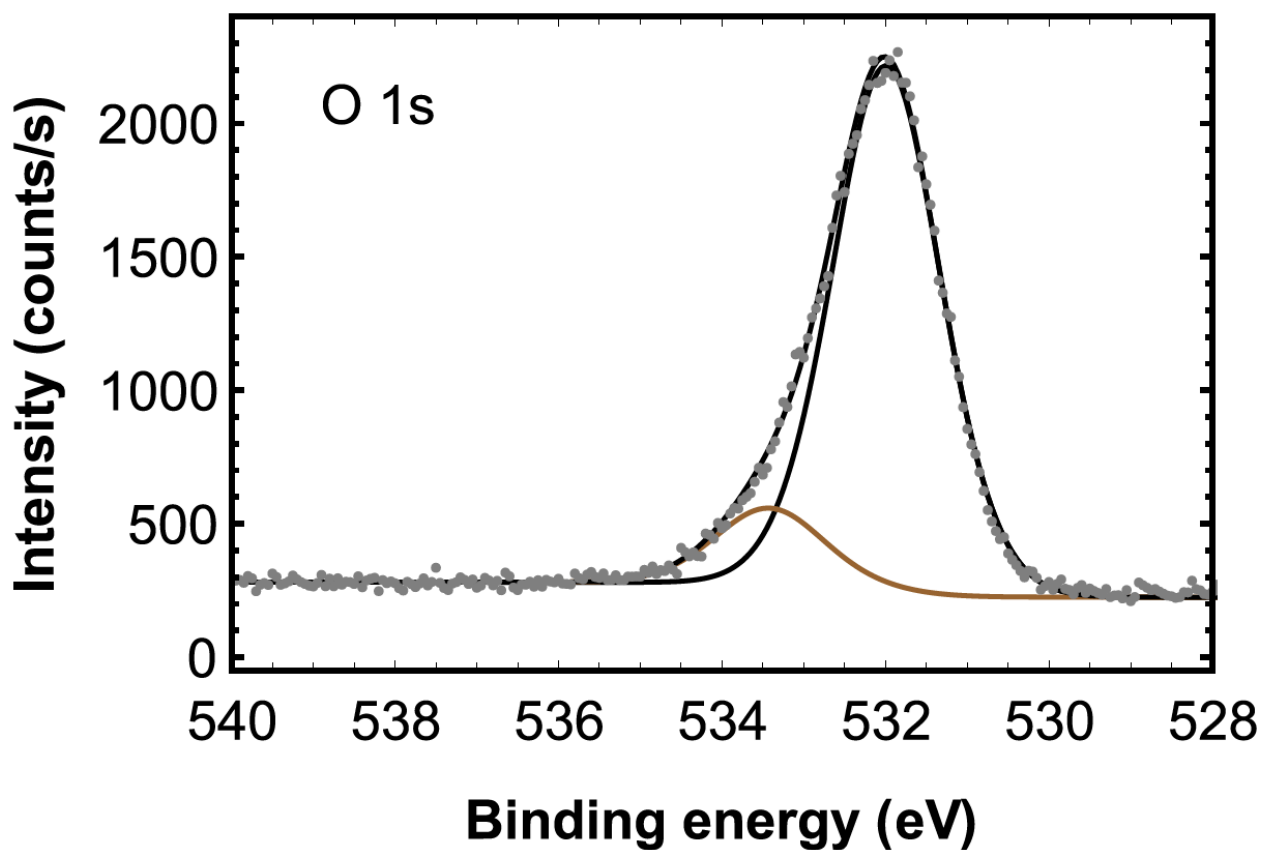
Figure 52. Oxygen 1s (O1s) spectrum of polyguanine. Reprinted/modified from [84].©
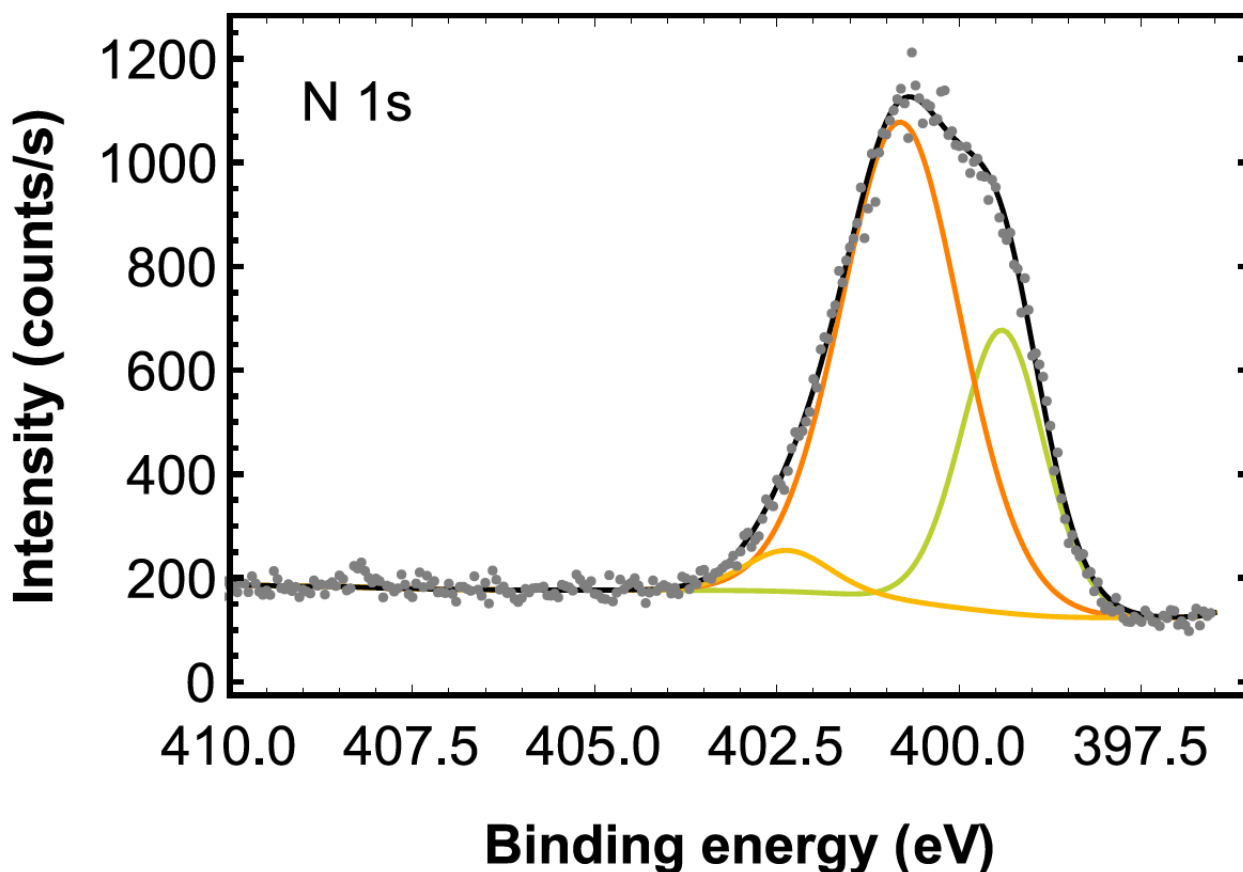
Figure 53. Nitrogen 1s (N1s) spectrum of polyguanine. Reprinted/modified from [84].©

The UV-vis spectra (Figure 54a) demonstrated the distinction between polyguanine and guanine monomer in color change. In PG, a broad absorption in the UV-vis region between 400 nm and 600 nm was obtained, explaining the light brownish appearance of the PG films on glass. Similar absorption band was not visible in the white guanine monomer film fabricated with the same method but without oxidant sulfuric acid. We also used FTIR spectroscopy to elucidate the structural variety in PG. In particular, we were interested in the structural changes induced by the new oxidative chemical vapor synthesis. To examine this, we first measured the guanine monomer powder, as well as the guanine monomer film deposited onto glass substrate fabricated with the same method but without oxidant sulfuric acid (Figure 54b).[84] The FTIR spectrum of the guanine powder was in good agreement with the literature values.[88, 157] Only small arrangements in the range between 3500 cm^{-1} to 3000 cm^{-1} and 1405 cm^{-1} were indicated, when the guanine monomer was deposited as a white film in the absence of the sulfuric acid as a mild oxidant at 360 °C. In contrast, the FTIR spectrum of the polyguanine films revealed united broad bands between 3536 cm^{-1} and 2854 cm^{-1} and between 1643 cm^{-1} to 1257 cm^{-1}, attributed to the stretching vibrations of imine, amine and carbonyl features. Additionally, hints of free charge careers along the PG chain were confirmed by the intense infrared activated vibrations (IRAVs) in the region of 1070 cm^{-1} to 840 cm^{-1}. Above all, these IRAV bands are strong indications for the conductivity in doped organic polymers, which results in the creation of new absorption features in the NIR and MIR.
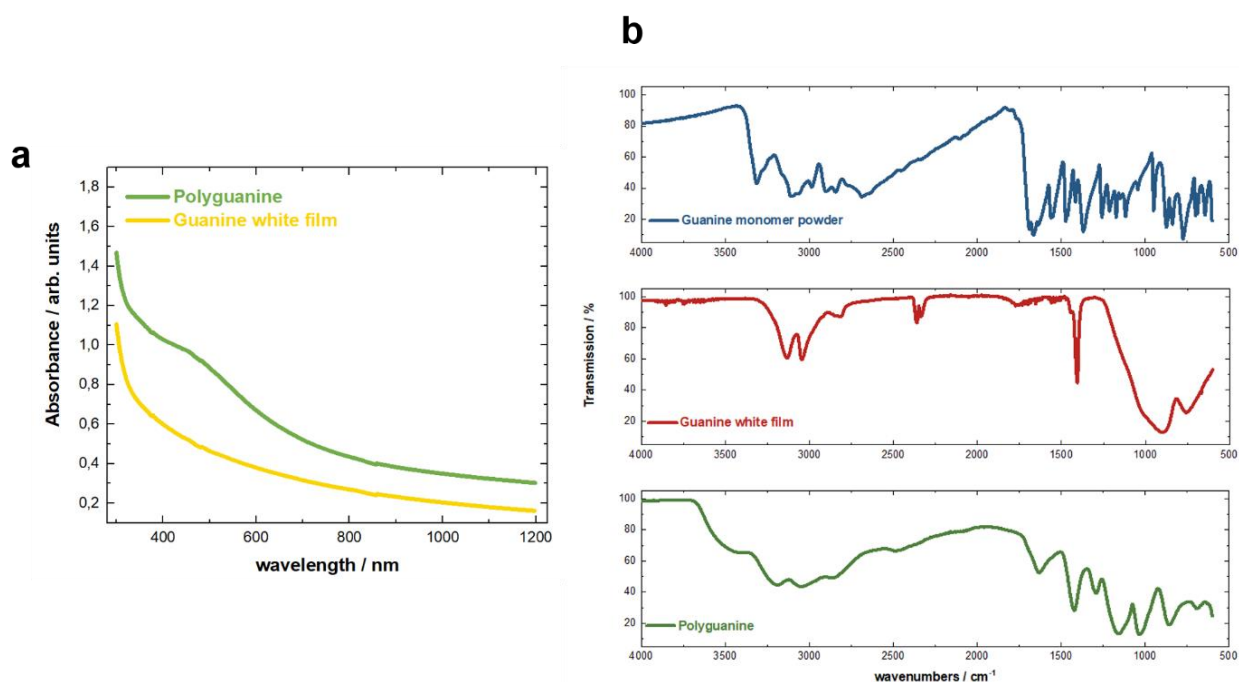
Figure 54. Spectroscopic characterization (a) UV-vis spectrum of polyguanine (light blue) and guanine monomer (yellow), (b) FTIR spectrum of guanine monomer as powder (blue), guanine monomer as film (red) and of polyguanine (green). Reprinted/modified from [84].©
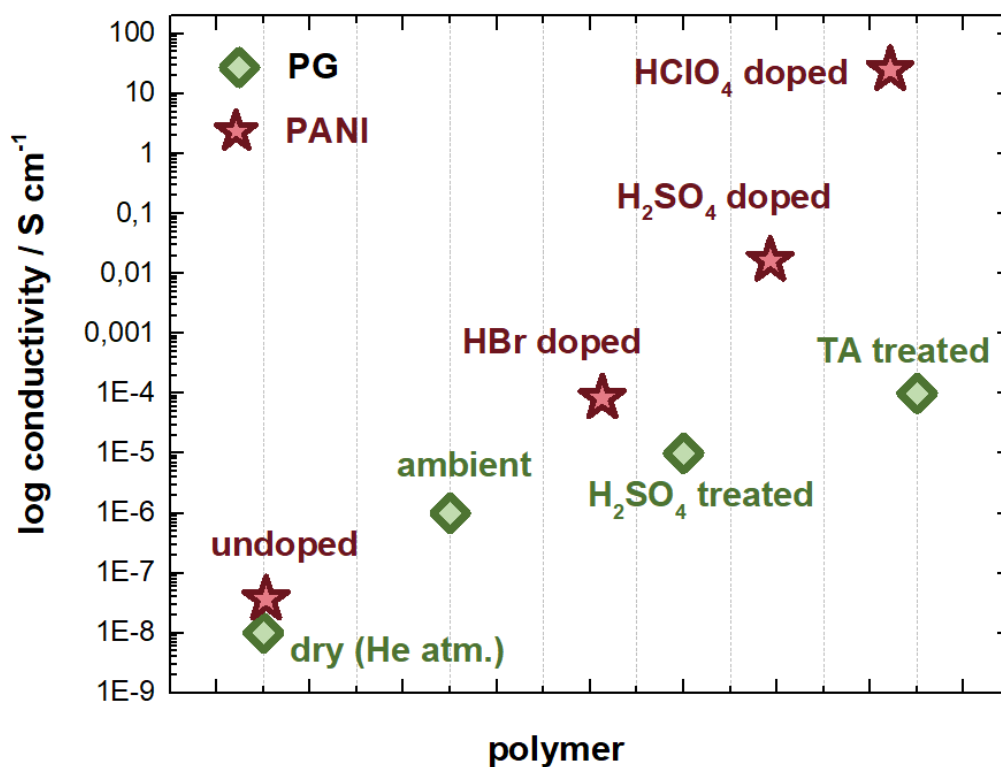
Figure 55. Conductivities of polyguanine (green) measured at different acidic environment in comparison to the conductivity values of PANI (red) in different doped and un-doped states. Reprinted/modified from [84].©

Especially, PANI was investigated in the literature with great interest due to its high electrical conductivity upon doping with acids.[50, 158-159] We found the same phenomenon of H^+ doping in polyguanine. We measured electrical conductivities of the PG films using the van-der-Pauw geometry in its (i) initial dry state under helium atmosphere, (ii) stored under ambient conditions, (iii) after treatment with concentrated sulfuric acid, (iv) and after treatment with 1M TA. Figure 55 shows the analogy between PANI and PG – the increase in conductivity upon H^+ - enriched surrounding. Even though the electrical conductivity of PG was orders of magnitude lower than PANI, its electrocatalytic HER activity was better due to improved functional density within the polymer chain.[84]

3.3.3. Electrocatalytic Activity of PG towards HER

The HER activity of the polyguanine coated CF electrode surfaces we tested in 1M TA in comparison to the PANI on CF, blank carbon felt (CF) electrodes and platinum as reference, at room temperature, and plotted as polarization scans all referred to RHE potential values.[84]
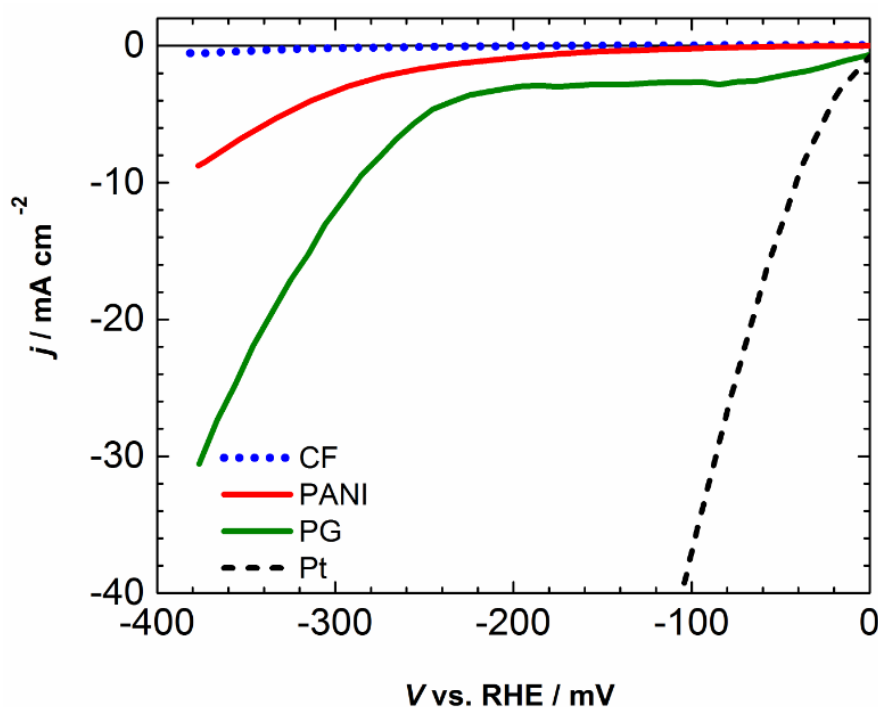
Figure 56. Electrochemical characterization including (a) polarization scans recorded at 100 mV s^{-1}. Reprinted/modified from [84].©

We refer to PANI, a representative of conducting polymers with good redox properties, easy preparation and stability. However, PANI is not catalytically active due to its conformities in style to graphite. By the utilization of PG, a PANI-like structure, was adopted with enhanced functional densities, reflected in the superior HER performance. An opportunity would be to conduct a novel PANI synthesis through o-CVD, however, the toxicity of the aniline monomer is a substantial limitation for the vapor phase deposition.[84]

In order to facilitate the two step hydrogen evolution reaction we write:[160-162]

$$H^+ + e^- \rightarrow H_{ADS} \qquad (7)$$

$$H_{ADS} + H_{ADS} \rightarrow H_2 \qquad (8)$$

Here, the HER process can be divided into the adsorption and recombination steps. First, the protons from the acidic solution are adsorbed to the catalytic sites of the electrode. In the following, the atomic hydrogen adatoms recombine to evolve H_2.[160-162]

In Figure 57, the HER overpotentials for Pt, polyguanine and polyaniline are shown as a function of the logarithm of the current density to give a plot known as a Tafel curve that is commonly used for analysis of the HER and other electrochemical reactions. Qualitatively, it is seen that the activity of PANI (168 mV dec^{-1}) was significantly lower than the PG and Pt catalytic systems. Impressively, the activity of PG (80 mV dec^{-1}) was substantially enhanced and the activity gave a Tafel plot that is as twice as that of the platinum foil (40 mV dec^{-1}). We attributed the superior performance of PG to the fact, that the different predominant amine groups in the biopolymer chain get protonated and thus exhibited a greater electron affinity towards the hydrogen evolution reactions. Although, PANI contained amine functionalities in its structure as well, the functional density of PG is higher. This difference in performance is clearly observable. The Tafel slope for platinum foil surface was in agreement with those reported in literature.[23-24, 26, 29-30, 35, 84]
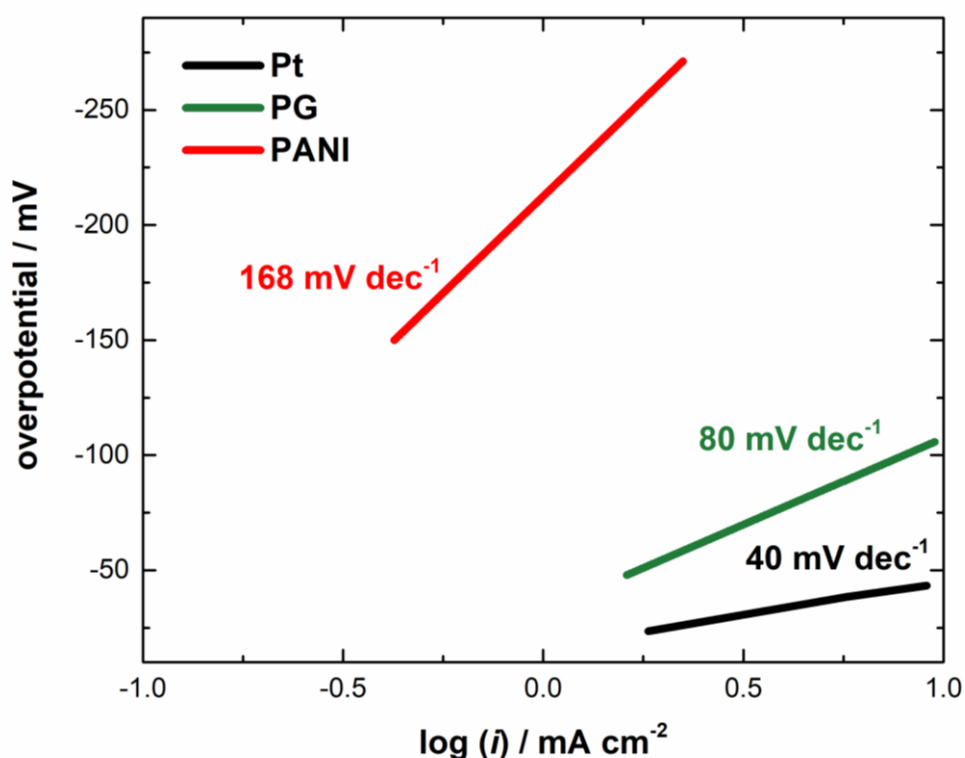
Figure 57. Tafel plots, in which the overpotential is plotted as a function of log (i) for Pt, PG and PANI systems. Reprinted/modified from [84].©

Further, the Tafel slope was used in order to extract the exchange current density i_o for PG. Hereby, the i_o value was compensated by the actual electrochemical active area, determined through electrochemical impedance measurements as 18.73 cm^2. The exchange current density for PG resulted in $3*10^{-6}$ A cm^{-2} (Figure 58).[84]
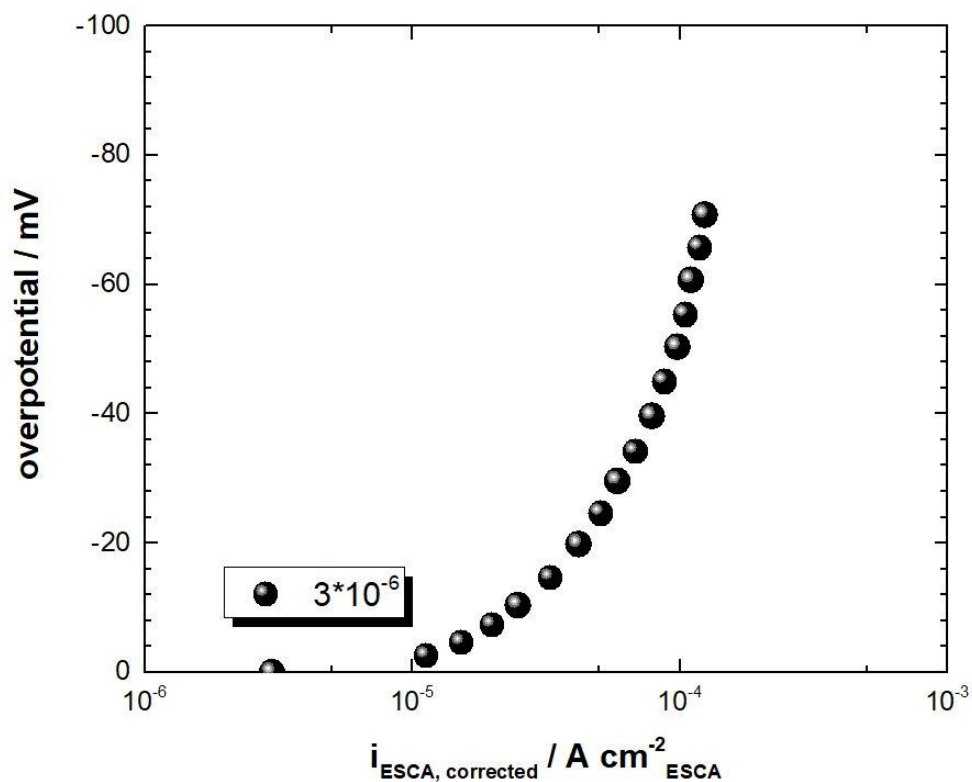
Figure 58: Corrected current density versus the overpotential (=RHE) of PG. We use the A_{ECSA} of 18.73 cm^{-2} to derive the crossover point at 0 V, which can be used as exchange current (at quasi-thermodynamic equilibrium) i_0. Reprinted/modified from [84].©

Interestingly, the electrochemical stability is especially crucial for the organic and biological systems in extreme and harsh acidic conditions. To test the long-term stability of the PG samples studied in this work, we conducted constant potential electrolysis at 290 mV vs. RHE for 80 hours. Based on the representative chronoamperometric scans (Figure 59), we found extensive durability for PG HER electrocatalyst, even after three days of continuous operation.[84]
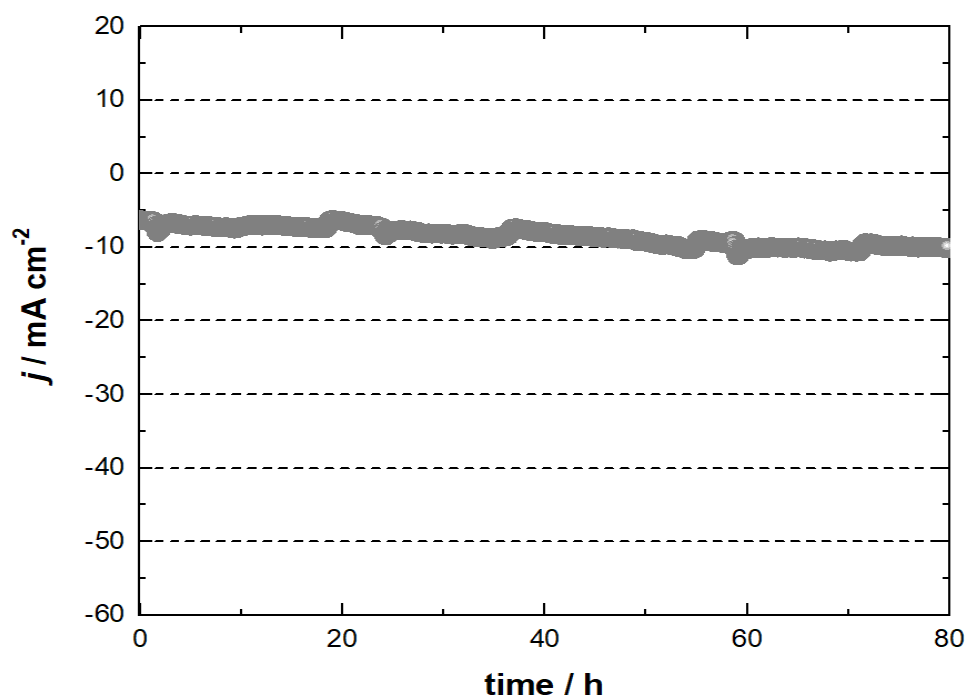
Figure 59. Constant potential electrolysis at 290 mV vs. RHE for 80 hours of operation. Reprinted/modified from [84].©

Further, we performed electrochemical impedance measurements. The Bode plot, as shown in Figure 60, was recorded in the frequency range of 1MHz to 1 kHz with a perturbation amplitude of 10 mV. We extracted the cell resistance parameters from the impedance data of the 3-electrode-system applied in HER studies together with the electrochemical active area. From the responses of the control Pt, CF and CF coated with PG, negligible cell resistance was determined.[84] The table including all cell parameters is given below (Table 4).
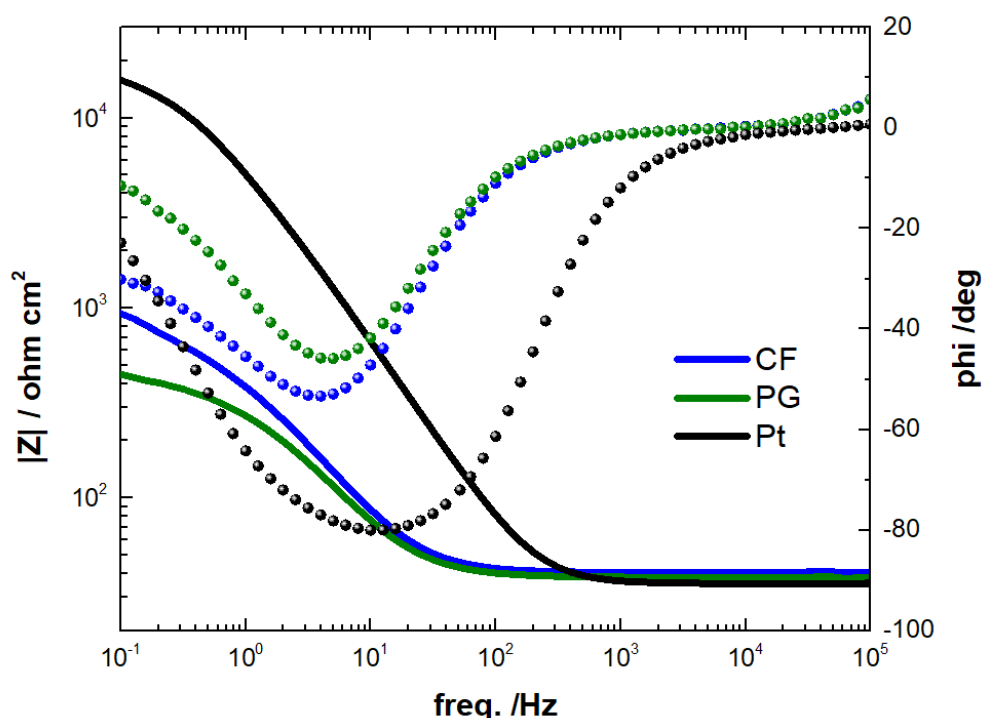
Figure 60. Electrochemical impedance characterization in the form of Bode plot, showing the responses of Pt, CF and PG samples in 3-electrode-configuration. Reprinted/modified from [84].©

The reference capacitance $C_{i,ref}$ of a flat metal electrode was measured using stainless steel (normalized to $1\,cm^2$ flat electrode). We found a value for the capacitance $40 \pm 5\,\mu F\,cm^{-2}$. The reference capacitance of PG-coated carbon felt has been measured using following equivalent circuit:
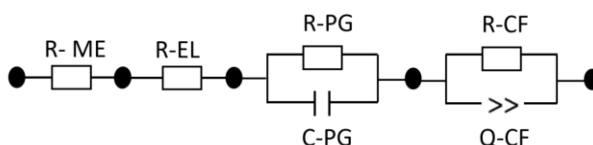
This measurement involved the characterization of the impedance versus frequency and the extraction of the resistance of the electrolyte solution (1 M TA) (R_{EL}), the resistance at the working electrode (R_{WE}), the resistance of the glass frit membrane (R_{ME}), as well as the capacitance of the

PG ($C_{i,PG}$). To compensate the porosity (non-ideal capacitance) of carbon felt, we applied the equivalent circuit using the resistance of carbon felt (R_{CF}) and the charge (Q_{CF}) expressed as the fitting parameters CTE-P and CTE-T (these are also shown for Pt-Pt, Table 6). We included the standard deviation for the measurement including the variety to determine the geometric area on CF as precisely as possible.[84]

From the measurements, we derive the electrochemical surface area A_{ECSA} as followed:

$$A_{ECSA} = \frac{C_{i,PG}}{C_{i,ref.}} = \frac{749.2 \pm 30}{40 \pm 5} = 18.73 \pm 3.23 \, cm^2 \tag{9}$$

WE	CE	R_{EL} / Ω cm^2	R_{WE} / kΩ cm^2	R_{ME} / Ω	R_{PG} / kΩ cm^2	$C_{i,PG}$ / μF cm^{-2}	CPE-T F cm^{-2}	CPE-P d.less
Pt	Pt	2	16.86	34	-	-	3.4×10^{-5}	9.5×10^{-1}
CF	Pt	3.5	1.37	34	-	-	7.4×10^{-4}	7.0×10^{-1}
CF+ PG	Pt	3.5	0.35	34	0.12	749.2	1.4×10^{-3}	7.3×10^{-1}

Table 6 Cell parameters determined via electrochemical impedance measurements. Reprinted/modified from [84].©

We finally crosschecked polyguanine deposited on carbon felt electrodes by the scanning electron microscopy. As shown in Figure 61a, before constant potential electrolysis the fiber networks were widely covered by PG, so that the electrocatalyst infiltrated into the sponge-type supporting electrode. After the long-term stability experiment it can be seen that the PG catalyst still remained on the CF fibers (Figure 61b) with some less dense regions on the CF electrode.[84]
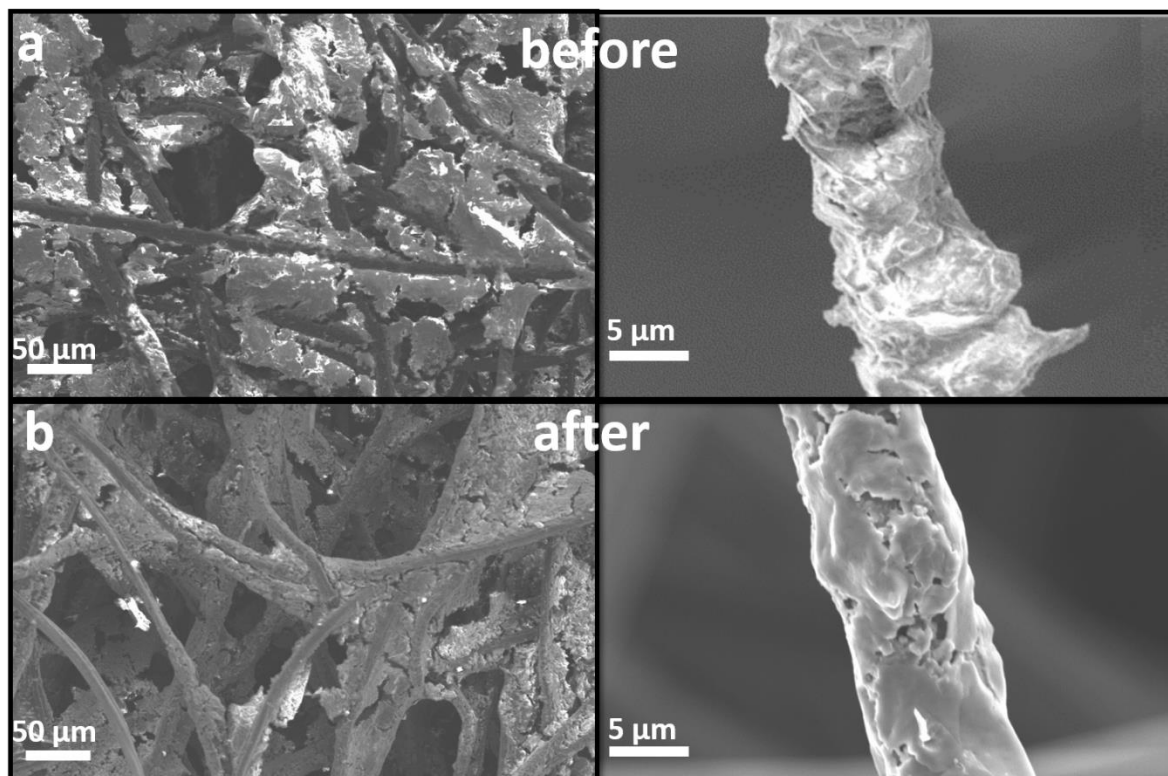
Figure 61. SEM images of polyguanine deposited on carbon felt, (a) before and (b) after constant potential electrolysis. Reprinted/modified from [84].©

In this chapter, the utilization of an alternative biopolymer, derived from guanine, one of the building blocks of the DNA macromolecule, as hydrogen cathode for HER electrocatalysis was shown. We have synthesized polyguanine (PG) from the vapor phase using the oxidative chemical vapor deposition (o-CVD) and achieved the polymerization and the oxidative doping of the resulting polymer in a facile single step reaction from the vapor phase of the guanine monomer with sulfuric acid. As compared to polyaniline (PANI), one of the well-known conducting polymers, we found analogies in structure and conductivity increase by H^+ doping. Our results suggest the fact that the prevalent amines in PG get protonated and thus have better electron affinity to accelerate the hydrogen evolution steps in ($H^+ + e^- \rightarrow H_{ADS}$) and ($H_{ADS} + H_{ADS} \rightarrow H_2$) reactions.

Indeed, paired with HER electrocatalyst performance (Tafel slope of 80 mV dec^{-1} at an overpotential of 290 mV at 10 mA cm^{-2}) and a stable operation of 80 hours in a strong 1M trifluoromethanesulfonic acid (TA) polyguanine demonstrates promising abilities as an alternative biopolymer electrocatalyst for the future.[84]

4. Summary and Outlook

This study aimed to design alternative molecular electrocatalysts. Due to the support of hydrogen-bonded, functional themes in their polymeric structure, these catalysts operate comparatively efficient like metals. Hence, two novel conductive and functional polymers from bio-organic molecules were developed and utilized as electrocatalysts in carbon dioxide reduction reaction (CO2RR) and hydrogen evolution reaction (HER) in this thesis.

By the utilization of a unique synthesis method, the oxidative chemical vapor deposition (o-CVD), two novel biopolymers were achieved.

Firstly, polydopamine (PDA), considered as a synthetic eumelanin, was synthesized by o-CVD. By this way, the bio-originated material, which was usually insulating in its nature, got polymerized and doped by this facile one-step synthesis, bringing the advantage of becoming a conductive and functional biopolymer. Having in mind, to try to mimic nature in these well-known catalytic processes such as the catalytic triades, by means of making use of organic functional themes in order to catalyze biological reactions, the o-CVD synthesized polydopamine containing a carbonyl, hydroxyl and amine functionalized polyparaphenylene type of polymer backbone was intentionally applied CO2RR. PDA is found to be as a candidate for electrocatalyst with comparable performances as compared to the best state-of-the-art metal catalysts. Combined with high geometric current densities of 18 mA cm^{-2} at 0.21V overpotential and 16 hours of continuous operation, PDA electrocatalyst produced in CO2RR 12% hydrogen and 83.8% for CO_2 reduction products of formate and carbon monoxide using a 0.1M $TBAPF_6$ aceonitrile with 1% H_2O electrolyte solution. The remarkable hydrogen production in such a low-proton electrolyte solution was a strong indication that PDA could also work as a HER electrocatalyst, if the ideal conditions would met together.

As a second approach, polydopamine was employed for HER. Based on theoretical calculations, it turned out that the keto-amine functionalities (DHI-PDA) would ease the HER performance. Therefore, the synthesis procedure was modified by increasing the initial reaction temperature from 300 °C to 350 °C in order to obtain higher degrees of keto and secondary amine groups in the modified PDA structure. The structure of new DHI-PDA was verified by spectroscopic techniques. Electrocatalytic invetigations towards HER yielded in an efficient catalyst exhibiting quantitative Faradaic efficiency with a Tafel slope of 80 mV dec^{-1}, a low overpotential of 190 mV at 10 mA cm^{-2} and a long-term stability with negligible degradation for 1 week of constant operation.

The utilization of another biopolymer, polyguanine (PG) in CO2RR showed low current densities at high overpotentials. This phenomenon was explained by to the fact, that the CO2RR preferentially takes places in organic solvents, such as acetonitrile, since the CO_2 has a better solubility in it. By choosing acetonitrile as the electrolyte, the catalytic reactions occur nearly at

neutral pH, which further limit the poor conduction in PG, leading to high operation potentials although the surface area was enhanced by carbon felt. However, its application in HER yielded in comparable results to PDA in HER (Tafel slope of 80 mV dec^{-1}, overpotential of -290 mV vs. RHE (10 mA cm^{-2}) and 80 hours of continuous electrolysis). In addition, similarly as in polyaniline PANI, a representative of the family of conducting polymers, enhanced conductivities upon exposure of polyguanine films to different acidic environment were found. Hence, we propose that the doping mechanism is analogous to PANI. In comparison with polyaniline (PANI), PG revealed greater catalytic property towards hydrogen evolution. This is further attributed to improved functional densities in PG polymer.

In this thesis, based on a series of experiments the utilization of a new material class as electrocatalysts is presented. This new material class relies on bio-originated, functional and conductive biopolymers, with the ability to catalyze various reactions over the organic and functional motifs with the aim to resemble natural phenomena. Within the timeframe of this doctoral study two novel systems, polydopamine and polyguanine, were depicted and applied in CO2RR and HER.

I consider myself lucky, since I started working on a field, in which a lot of fundamental knowledge was already available. Thinking about the engineering of a proper electrocatalyst might seem easy at the first glance, however, many critical parameters have to meet together to succeed. These are the need of abundant materials with reasonable electrical conductivity, reliable redox-stability, insolubility in the applied electrolytic system, tunable functionality and purity of the materials but also the engineering of the catalytically active large surface area. If all these properties are combined the picture of an ideal electrocatalyst is drawn. I believe that in the time this doctoral thesis has taken place, many of these conditions have been met by using these biopolymers. Compared to the previous studies, in which the functional polymers, so called third generation polymers, were used as catalysts, the biggest obstacle was the low electrical conductivity of these organic semiconductors. In case of the utilization of conductive polymers, i.e. polyaniline, the problem of low electrical conductivity has been overcome, however PANI systems were restricted to photoelectrochemical applications and mainly suffered from low current densities. Recently, enzymes immobilized on electrodes is considered as a promising approach, however, with difficulties in matching the performance with reasonable product yields. All these examples and many more show, that, material properties lonely are not enough. Finding the best electrochemical conditions, including the electrode engineering in combination with the ideal supporting electrolyte, desired products and be electrosynthesized.

As a future aspect, I believe concepts introduced in this thesis can be adapted for bio-electrochemical catalysis. Next-generation electrocatalysts, i.e. materials like other remaining nucleobases such as adenine, thymine, cytosine, uracil or many other bio-originated compounds may be candidates for future electrocatalysts. Requirements to be applicable are the conjugation

in the molecular structure as well as functional themes within the structure to enhance the catalytic performance, can be additionally supplemented to the points mentioned above.

5. References

1.   Aljabour, A.; Apaydin, D. H.; Coskun, H.; Ozel, F.; Ersoz, M.; Stadler, P.; Sariciftci, N. S.; Kus, M., Improvement of Catalytic Activity by Nanofibrous CuInS2 for Electrochemical CO2 Reduction. *Acs Appl Mater Inter* **2016,** *8* (46), 31695-31701.

2.   Asadi, M.; Kim, K.; Liu, C.; Addepalli, A. V.; Abbasi, P.; Yasaei, P.; Phillips, P.; Behranginia, A.; Cerrato, J. M.; Haasch, R.; Zapol, P.; Kumar, B.; Klie, R. F.; Abiade, J.; Curtiss, L. A.; Salehi-Khojin, A., Nanostructured transition metal dichalcogenide electrocatalysts for CO_2 reduction in ionic liquid. *Science* **2016,** *353* (6298), 467-470.

3.   Asadi, M.; Kumar, B.; Behranginia, A.; Rosen, B. A.; Baskin, A.; Repnin, N.; Pisasale, D.; Phillips, P.; Zhu, W.; Haasch, R.; Klie, R. F.; Král, P.; Abiade, J.; Salehi-Khojin, A., Robust carbon dioxide reduction on molybdenum disulphide edges. *Nature Communications* **2014,** *5*, 4470.

4.   Buss, J. A.; Agapie, T., Four-electron deoxygenative reductive coupling of carbon monoxide at a single metal site. *Nature* **2015,** *529*, 72.

5.   Gao, S.; Lin, Y.; Jiao, X.; Sun, Y.; Luo, Q.; Zhang, W.; Li, D.; Yang, J.; Xie, Y., Partially oxidized atomic cobalt layers for carbon dioxide electroreduction to liquid fuel. *Nature* **2016,** *529*, 68.

6.   Gong, Y.; Lin, J.; Wang, X.; Shi, G.; Lei, S.; Lin, Z.; Zou, X.; Ye, G.; Vajtai, R.; Yakobson, B. I.; Terrones, H.; Terrones, M.; Tay, Beng K.; Lou, J.; Pantelides, S. T.; Liu, Z.; Zhou, W.; Ajayan, P. M., Vertical and in-plane heterostructures from WS2/MoS2 monolayers. *Nature Materials* **2014,** *13*, 1135.

7.   Kas, R.; Hummadi, K. K.; Kortlever, R.; de Wit, P.; Milbrat, A.; Luiten-Olieman, M. W. J.; Benes, N. E.; Koper, M. T. M.; Mul, G., Three-dimensional porous hollow fibre copper electrodes for efficient and high-rate electrochemical carbon dioxide reduction. *Nature Communications* **2016,** *7*, 10748.

8.   Lei, F.; Liu, W.; Sun, Y.; Xu, J.; Liu, K.; Liang, L.; Yao, T.; Pan, B.; Wei, S.; Xie, Y., Metallic tin quantum sheets confined in graphene toward high-efficiency carbon dioxide electroreduction. *Nature Communications* **2016,** *7*, 12697.

9.   Lin, S.; Diercks, C. S.; Zhang, Y.-B.; Kornienko, N.; Nichols, E. M.; Zhao, Y.; Paris, A. R.; Kim, D.; Yang, P.; Yaghi, O. M.; Chang, C. J., Covalent organic frameworks comprising cobalt porphyrins for catalytic CO_2 reduction in water. *Science* **2015,** *349* (6253), 1208-1213.

10.   Liu, M.; Pang, Y.; Zhang, B.; De Luna, P.; Voznyy, O.; Xu, J.; Zheng, X.; Dinh, C. T.; Fan, F.; Cao, C.; de Arquer, F. P. G.; Safaei, T. S.; Mepham, A.; Klinkova, A.; Kumacheva, E.; Filleter,

T.; Sinton, D.; Kelley, S. O.; Sargent, E. H., Enhanced electrocatalytic CO_2 reduction via field-induced reagent concentration. *Nature* **2016,** *537*, 382.

11. Lu, Q.; Rosen, J.; Zhou, Y.; Hutchings, G. S.; Kimmel, Y. C.; Chen, J. G.; Jiao, F., A selective and efficient electrocatalyst for carbon dioxide reduction. *Nature Communications* **2014,** *5*, 3242.

12. Mistry, H.; Varela, A. S.; Bonifacio, C. S.; Zegkinoglou, I.; Sinev, I.; Choi, Y.-W.; Kisslinger, K.; Stach, E. A.; Yang, J. C.; Strasser, P.; Cuenya, B. R., Highly selective plasma-activated copper catalysts for carbon dioxide reduction to ethylene. *Nature Communications* **2016,** *7*, 12123.

13. Saberi Safaei, T.; Mepham, A.; Zheng, X.; Pang, Y.; Dinh, C.-T.; Liu, M.; Sinton, D.; Kelley, S. O.; Sargent, E. H., High-Density Nanosharp Microstructures Enable Efficient CO_2 Electroreduction. *Nano Letters* **2016,** *16* (11), 7224-7228.

14. Wang, Z.; Yang, G.; Zhang, Z.; Jin, M.; Yin, Y., Selectivity on Etching: Creation of High-Energy Facets on Copper Nanocrystals for CO_2 Electrochemical Reduction. *ACS Nano* **2016,** *10* (4), 4559-4564.

15. Xie, M. S.; Xia, B. Y.; Li, Y.; Yan, Y.; Yang, Y.; Sun, Q.; Chan, S. H.; Fisher, A.; Wang, X., Amino acid modified copper electrodes for the enhanced selective electroreduction of carbon dioxide towards hydrocarbons. *Energ Environ Sci* **2016,** *9* (5), 1687-1695.

16. Janáky, C.; Hursán, D.; Endrődi, B.; Chanmanee, W.; Roy, D.; Liu, D.; de Tacconi, N. R.; Dennis, B. H.; Rajeshwar, K., Electro- and Photoreduction of Carbon Dioxide: The Twain Shall Meet at Copper Oxide/Copper Interfaces. *ACS Energy Letters* **2016,** *1* (2), 332-338.

17. Kuhl, K. P.; Cave, E. R.; Abram, D. N.; Jaramillo, T. F., New insights into the electrochemical reduction of carbon dioxide on metallic copper surfaces. *Energ Environ Sci* **2012,** *5* (5), 7050-7059.

18. Liu, C.; Cundari, T. R.; Wilson, A. K., CO_2 Reduction on Transition Metal (Fe, Co, Ni, and Cu) Surfaces: In Comparison with Homogeneous Catalysis. *The Journal of Physical Chemistry C* **2012,** *116* (9), 5681-5688.

19. Rosen, B. A.; Salehi-Khojin, A.; Thorson, M. R.; Zhu, W.; Whipple, D. T.; Kenis, P. J. A.; Masel, R. I., Ionic Liquid–Mediated Selective Conversion of CO_2 to CO at Low Overpotentials. *Science* **2011**.

20. Aresta, M., *Carbon dioxide as chemical feedstock*. John Wiley & Sons: 2010.

21. Aresta, M., *Carbon dioxide recovery and utilization*. Springer Science & Business Media: 2013.

22.   Riduan, S. N.; Zhang, Y., Recent developments in carbon dioxide utilization under mild conditions. *Dalton Transactions* **2010,** *39* (14), 3347-3357.

23.   He, R.; Hua, J.; Zhang, A.; Wang, C.; Peng, J.; Chen, W.; Zeng, J., Molybdenum Disulfide–Black Phosphorus Hybrid Nanosheets as a Superior Catalyst for Electrochemical Hydrogen Evolution. *Nano Letters* **2017,** *17* (7), 4311-4316.

24.   Miao, M.; Pan, J.; He, T.; Yan, Y.; Xia, B. Y.; Wang, X., Molybdenum Carbide-Based Electrocatalysts for Hydrogen Evolution Reaction. *Chem-Eur J* **2017,** *23* (46), 10947-+.

25.   Kibsgaard, J.; Jaramillo, T. F., Molybdenum Phosphosulfide: An Active, Acid-Stable, Earth-Abundant Catalyst for the Hydrogen Evolution Reaction. *Angew Chem Int Edit* **2014,** *53* (52), 14433-14437.

26.   Xiao, P.; Sk, M. A.; Thia, L.; Ge, X. M.; Lim, R. J.; Wang, J. Y.; Lim, K. H.; Wang, X., Molybdenum phosphide as an efficient electrocatalyst for the hydrogen evolution reaction. *Energ Environ Sci* **2014,** *7* (8), 2624-2629.

27.   Popczun, E. J.; Read, C. G.; Roske, C. W.; Lewis, N. S.; Schaak, R. E., Highly Active Electrocatalysis of the Hydrogen Evolution Reaction by Cobalt Phosphide Nanoparticles. *Angewandte Chemie International Edition* **2014,** *53* (21), 5427-5430.

28.   Xie, J.; Zhang, H.; Li, S.; Wang, R.; Sun, X.; Zhou, M.; Zhou, J.; Lou, X. W.; Xie, Y., Defect-Rich MoS2 Ultrathin Nanosheets with Additional Active Edge Sites for Enhanced Electrocatalytic Hydrogen Evolution. *Advanced Materials* **2013,** *25* (40), 5807-5813.

29.   Voiry, D.; Salehi, M.; Silva, R.; Fujita, T.; Chen, M.; Asefa, T.; Shenoy, V. B.; Eda, G.; Chhowalla, M., Conducting MoS2 Nanosheets as Catalysts for Hydrogen Evolution Reaction. *Nano Letters* **2013,** *13* (12), 6222-6227.

30.   Voiry, D.; Yamaguchi, H.; Li, J.; Silva, R.; Alves, D. C. B.; Fujita, T.; Chen, M.; Asefa, T.; Shenoy, V. B.; Eda, G.; Chhowalla, M., Enhanced catalytic activity in strained chemically exfoliated WS2 nanosheets for hydrogen evolution. *Nature Materials* **2013,** *12*, 850.

31.   Zhang, H.; An, P.; Zhou, W.; Guan, B. Y.; Zhang, P.; Dong, J.; Lou, X. W., Dynamic traction of lattice-confined platinum atoms into mesoporous carbon matrix for hydrogen evolution reaction. *Science Advances* **2018,** *4* (1).

32.   Mollamahale, Y. B.; Jafari, N.; Hosseini, D., Electrodeposited Ni-W nanoparticles: Enhanced catalytic activity toward hydrogen evolution reaction in acidic media. *Materials Letters* **2018,** *213*, 15-18.

33.   Bose, R.; Jothi, V. R.; Koh, B.; Jung, C.; Yi, S. C., Molybdenum Sulphoselenophosphide Spheroids as an Effective Catalyst for Hydrogen Evolution Reaction. *Small* **2018,** *14* (8).

34.   Zhuang, Z.; Li, Y.; Li, Z.; Lv, F.; Lang, Z.; Zhao, K.; Zhou, L.; Moskaleva, L.; Guo, S.; Mai, L., MoB/g-C3N4 Interface Materials as a Schottky Catalyst to Boost Hydrogen Evolution. *Angewandte Chemie International Edition* **2018,** *57* (2), 496-500.

35.   Tan, C.; Luo, Z.; Chaturvedi, A.; Cai, Y.; Du, Y.; Gong, Y.; Huang, Y.; Lai, Z.; Zhang, X.; Zheng, L.; Qi, X.; Goh, M. H.; Wang, J.; Han, S.; Wu, X.-J.; Gu, L.; Kloc, C.; Zhang, H., Preparation of High-Percentage 1T-Phase Transition Metal Dichalcogenide Nanodots for Electrochemical Hydrogen Evolution. *Advanced Materials* **2018,** *30* (9), 1705509.

36.   Jing, S. Y.; Zhang, L. S.; Luo, L.; Lu, J. J.; Yin, S. B.; Shen, P. K.; Tsiakaras, P., N-Doped Porous Molybdenum Carbide Nanobelts as Efficient Catalysts for Hydrogen Evolution Reaction. *Appl Catal B-Environ* **2018,** *224*, 533-540.

37.   Li, J.; Liu, P.; Qu, Y.; Liao, T.; Xiang, B., WSe2/rGO hybrid structure: A stable and efficient catalyst for hydrogen evolution reaction. *International Journal of Hydrogen Energy* **2018,** *43* (5), 2601-2609.

38.   Fominski, V. Y.; Romanov, R. I.; Fominski, D. V.; Dzhumaev, P. S.; Troyan, I. A., Normal and grazing incidence pulsed laser deposition of nanostructured MoSx hydrogen evolution catalysts from a MoS2 target. *Optics & Laser Technology* **2018,** *102*, 74-84.

39.   Demir, E.; Akbayrak, S.; Onal, A. M.; Ozkar, S., Nanoceria-Supported Ruthenium(0) Nanoparticles: Highly Active and Stable Catalysts for Hydrogen Evolution from Water. *Acs Appl Mater Inter* **2018,** *10* (7), 6299-6308.

40.   Voiry, D.; Shin, H. S.; Loh, K. P.; Chhowalla, M., Low-dimensional catalysts for hydrogen evolution and CO2 reduction. *Nat Rev Chem* **2018,** *2* (1).

41.   Hu, J.; Huang, B.; Zhang, C.; Wang, Z.; An, Y.; Zhou, D.; Lin, H.; Leung, M. K. H.; Yang, S., Engineering stepped edge surface structures of MoS2 sheet stacks to accelerate the hydrogen evolution reaction. *Energ Environ Sci* **2017,** *10* (2), 593-603.

42.   Hu, J.; Zhang, C. X.; Meng, X. Y.; Lin, H.; Hu, C.; Long, X.; Yang, S. H., Hydrogen evolution electrocatalysis with binary-nonmetal transition metal compounds. *J Mater Chem A* **2017,** *5* (13), 5995-6012.

43.   Li, F.; Zhao, X.; Mahmood, J.; Okyay, M. S.; Jung, S.-M.; Ahmad, I.; Kim, S.-J.; Han, G.-F.; Park, N.; Baek, J.-B., Macroporous Inverse Opal-like MoxC with Incorporated Mo Vacancies for Significantly Enhanced Hydrogen Evolution. *ACS Nano* **2017,** *11* (7), 7527-7533.

44.   Rifkin, J., The hydrogen economy: the creation of the worldwide energy web and the redistribution of power on earth Tarcher. *Putnam, New York* **2002**.

45.   Kaneko, M.; Okura, I., *Photocatalysis: science and technology.* Springer: 2002.

46.   Gratzel, M., *Energy resources through photochemistry and catalysis*. Elsevier: 2012.

47.   Benck, J. D.; Chen, Z.; Kuritzky, L. Y.; Forman, A. J.; Jaramillo, T. F., Amorphous Molybdenum Sulfide Catalysts for Electrochemical Hydrogen Production: Insights into the Origin of their Catalytic Activity. *ACS Catalysis* **2012,** *2* (9), 1916-1923.

48.   Higuchi, M.; Ikeda, I.; Hirao, T., A Novel Synthetic Metal Catalytic System. *The Journal of Organic Chemistry* **1997,** *62* (4), 1072-1078.

49.   Higuchi, M.; Yamaguchi, S.; Hirao, T., Construction of Palladium-Polypyrrole Catalytic System in the Wacker Oxidation. *Synlett* **1996,** *1996* (12), 1213-1214.

50.   Huang, W.-S.; Humphrey, B. D.; MacDiarmid, A. G., Polyaniline, a novel conducting polymer. Morphology and chemistry of its oxidation and reduction in aqueous electrolytes. *Journal of the Chemical Society, Faraday Transactions 1: Physical Chemistry in Condensed Phases* **1986,** *82* (8), 2385-2400.

51.   Ugur, A.; Katmis, F.; Li, M.; Wu, L.; Zhu, Y.; Varanasi, K. K.; Gleason, K. K., Low-Dimensional Conduction Mechanisms in Highly Conductive and Transparent Conjugated Polymers. *Advanced Materials* **2015,** *27* (31), 4604-4610.

52.   Xiao, P.; Sk, M. A.; Thia, L.; Ge, X.; Lim, R. J.; Wang, J.-Y.; Lim, K. H.; Wang, X., Molybdenum phosphide as an efficient electrocatalyst for the hydrogen evolution reaction. *Energ Environ Sci* **2014,** *7* (8), 2624-2629.

53.   Zhao, Y.; Wang, C.; Wallace, G. G., Tin nanoparticles decorated copper oxide nanowires for selective electrochemical reduction of aqueous CO2 to CO. *J Mater Chem A* **2016,** *4* (27), 10710-10718.

54.   Zhang, S.; Kang, P.; Meyer, T. J., Nanostructured Tin Catalysts for Selective Electrochemical Reduction of Carbon Dioxide to Formate. *J Am Chem Soc* **2014,** *136* (5), 1734-1737.

55.   Bae, C.; Ho, T. A.; Kim, H.; Lee, S.; Lim, S.; Kim, M.; Yoo, H.; Montero-Moreno, J. M.; Park, J. H.; Shin, H., Bulk layered heterojunction as an efficient electrocatalyst for hydrogen evolution. *Science Advances* **2017,** *3* (3).

56.   Matsumoto, M.; Miyazaki, T.; Imai, H., Oxygen-Enhanced Dissolution of Platinum in Acidic Electrochemical Environments. *The Journal of Physical Chemistry C* **2011,** *115* (22), 11163-11169.

57.   Klinkova, A.; De Luna, P.; Dinh, C.-T.; Voznyy, O.; Larin, E. M.; Kumacheva, E.; Sargent, E. H., Rational Design of Efficient Palladium Catalysts for Electroreduction of Carbon Dioxide to Formate. *ACS Catalysis* **2016,** *6* (12), 8115-8120.

58.	Meredith, P.; Powell, B. J.; Riesz, J.; Nighswander-Rempel, S. P.; Pederson, M. R.; Moore, E. G., Towards structure–property–function relationships for eumelanin. *Soft Matter* **2006,** *2* (1), 37-44.

59.	Coskun, H.; Aljabour, A.; De Luna, P.; Farka, D.; Greunz, T.; Stifter, D.; Kus, M.; Zheng, X. L.; Liu, M.; Hassel, A. W.; Schofberger, W.; Sargent, E. H.; Sariciftci, N. S.; Stadler, P., Biofunctionalized conductive polymers enable efficient CO2 electroreduction. *Science Advances* **2017,** *3* (8).

60.	Coskun, H.; Aljabour, A.; Uiberlacker, L.; Strobel, M.; Hild, S.; Cobet, C.; Farka, D.; Stadler, P.; Sariciftci, N. S., Chemical vapor deposition - based synthesis of conductive polydopamine thin-films. *Thin Solid Films* **2018,** *645*, 320-325.

61.	Heeger, A. J., Semiconducting and metallic polymers: the fourth generation of polymeric materials (Nobel lecture). *Angewandte Chemie International Edition* **2001,** *40* (14), 2591-2611.

62.	d'Ischia, M.; Napolitano, A.; Ball, V.; Chen, C.-T.; Buehler, M. J., Polydopamine and Eumelanin: From Structure–Property Relationships to a Unified Tailoring Strategy. *Accounts of Chemical Research* **2014,** *47* (12), 3541-3550.

63.	Glowacki, E. D.; Coskun, H.; Blood-Forsythe, M. A.; Monkowius, U.; Leonat, L.; Grzybowski, M.; Gryko, D.; White, M. S.; Aspuru-Guzik, A.; Sariciftci, N. S., Hydrogen-bonded diketopyrrolopyrrole (DPP) pigments as organic semiconductors. *Org Electron* **2014,** *15* (12), 3521-3528.

64.	Głowacki, E. D.; Romanazzi, G.; Yumusak, C.; Coskun, H.; Monkowius, U.; Voss, G.; Burian, M.; Lechner, R. T.; Demitri, N.; Redhammer, G. J.; Sünger, N.; Suranna, G. P.; Sariciftci, S., Epindolidiones—Versatile and Stable Hydrogen-Bonded Pigments for Organic Field-Effect Transistors and Light-Emitting Diodes. *Adv Funct Mater* **2015,** *25* (5), 776-787.

65.	Glowacki, E. D.; Tangorra, R. R.; Coskun, H.; Farka, D.; Operamolla, A.; Kanbur, Y.; Milano, F.; Giotta, L.; Farinola, G. M.; Sariciftci, N. S., Bioconjugation of hydrogen-bonded organic semiconductors with functional proteins. *J Mater Chem C* **2015,** *3* (25), 6554-6564.

66.	Irimia-Vladu, M., "Green" electronics: biodegradable and biocompatible materials and devices for sustainable future. *Chemical Society Reviews* **2014,** *43* (2), 588-610.

67.	Sytnyk, M.; Głowacki, E. D.; Yakunin, S.; Voss, G.; Schöfberger, W.; Kriegner, D.; Stangl, J.; Trotta, R.; Gollner, C.; Tollabimazraehno, S.; Romanazzi, G.; Bozkurt, Z.; Havlicek, M.; Sariciftci, N. S.; Heiss, W., Hydrogen-Bonded Organic Semiconductor Micro- And Nanocrystals: From Colloidal Syntheses to (Opto-)Electronic Devices. *J Am Chem Soc* **2014,** *136* (47), 16522-16532.

68.   Dreyer, D. R.; Miller, D. J.; Freeman, B. D.; Paul, D. R.; Bielawski, C. W., Perspectives on poly(dopamine). *Chemical Science* **2013,** *4* (10), 3796-3802.

69.   Huijser, A.; Pezzella, A.; Sundström, V., Functionality of epidermal melanin pigments: current knowledge on UV-dissipative mechanisms and research perspectives. *Physical Chemistry Chemical Physics* **2011,** *13* (20), 9119-9127.

70.   Liebscher, J.; Mrówczyński, R.; Scheidt, H. A.; Filip, C.; Hădade, N. D.; Turcu, R.; Bende, A.; Beck, S., Structure of Polydopamine: A Never-Ending Story? *Langmuir* **2013,** *29* (33), 10539-10548.

71.   Liu, Y.; Ai, K.; Lu, L., Polydopamine and Its Derivative Materials: Synthesis and Promising Applications in Energy, Environmental, and Biomedical Fields. *Chemical Reviews* **2014,** *114* (9), 5057-5115.

72.   Meredith, P.; Sarna, T., The physical and chemical properties of eumelanin. *Pigment Cell Research* **2006,** *19* (6), 572-594.

73.   Mostert, A. B.; Powell, B. J.; Pratt, F. L.; Hanson, G. R.; Sarna, T.; Gentle, I. R.; Meredith, P., Role of semiconductivity and ion transport in the electrical conduction of melanin. *Proceedings of the National Academy of Sciences* **2012,** *109* (23), 8943-8947.

74.   Watt, A. A. R.; Bothma, J. P.; Meredith, P., The supramolecular structure of melanin. *Soft Matter* **2009,** *5* (19), 3754-3760.

75.   Yu, F.; Chen, S.; Chen, Y.; Li, H.; Yang, L.; Chen, Y.; Yin, Y., Experimental and theoretical analysis of polymerization reaction process on the polydopamine membranes and its corrosion protection properties for 304 Stainless Steel. *Journal of Molecular Structure* **2010,** *982* (1), 152-161.

76.   Ball, V.; Del Frari, D.; Michel, M.; Buehler, M. J.; Toniazzo, V.; Singh, M. K.; Gracio, J.; Ruch, D., Deposition Mechanism and Properties of Thin Polydopamine Films for High Added Value Applications in Surface Science at the Nanoscale. *BioNanoScience* **2012,** *2* (1), 16-34.

77.   Li, Y.; Liu, M.; Xiang, C.; Xie, Q.; Yao, S., Electrochemical quartz crystal microbalance study on growth and property of the polymer deposit at gold electrodes during oxidation of dopamine in aqueous solutions. *Thin Solid Films* **2006,** *497* (1), 270-278.

78.   Ouyang, R.; Lei, J.; Ju, H.; Xue, Y., A Molecularly Imprinted Copolymer Designed for Enantioselective Recognition of Glutamic Acid. *Adv Funct Mater* **2007,** *17* (16), 3223-3230.

79.   Lynge, M. E.; van der Westen, R.; Postma, A.; Städler, B., Polydopamine—a nature-inspired polymer coating for biomedical science. *Nanoscale* **2011,** *3* (12), 4916-4928.

80.   Pezzella, A.; Iadonisi, A.; Valerio, S.; Panzella, L.; Napolitano, A.; Adinolfi, M.; d'Ischia, M., Disentangling Eumelanin "Black Chromophore": Visible Absorption Changes As Signatures of Oxidation State- and Aggregation-Dependent Dynamic Interactions in a Model Water-Soluble 5,6-Dihydroxyindole Polymer. *J Am Chem Soc* **2009,** *131* (42), 15270-15275.

81.   Abbasi, P.; Asadi, M.; Liu, C.; Sharifi-Asl, S.; Sayahpour, B.; Behranginia, A.; Zapol, P.; Shahbazian-Yassar, R.; Curtiss, L. A.; Salehi-Khojin, A., Tailoring the edge structure of molybdenum disulfide toward electrocatalytic reduction of carbon dioxide. *ACS nano* **2016,** *11* (1), 453-460.

82.   Rad, A. S.; Aghaei, S. M., Potential of metal–fullerene hybrids as strong nanocarriers for cytosine and guanine nucleobases: A detailed DFT study. *Current Applied Physics* **2018,** *18* (2), 133-140.

83.   Yamada, T.; Shirasaka, K.; Takano, A.; Kawai, M., Adsorption of cytosine, thymine, guanine and adenine on Cu(110) studied by infrared reflection absorption spectroscopy. *Surface Science* **2004,** *561* (2), 233-247.

84.   Coskun, H.; Aljabour, A.; Hinterreiter, A.; Stifter, D.; Sariciftci, N. S.; Stadler, P., Proton assisted electron transfer in polyguanine thin films for electrocatalytic hydrogen evolution reaction. **2018**, in preparation.

85.   Arvand, M.; Sanayeei, M.; Hemmati, S., Label-free electrochemical DNA biosensor for guanine and adenine by ds-DNA/poly(L-cysteine)/Fe3O4 nanoparticles-graphene oxide nanocomposite modified electrode. *Biosens Bioelectron* **2018,** *102*, 70-79.

86.   Hinrichs, K.; Silaghi, S. D.; Cobet, C.; Esser, N.; Zahn, D. R. T., Ellipsometry from infrared to vacuum ultraviolet: Structural properties of thin anisotropic guanine films on silicon. *Phys Status Solidi B* **2005,** *242* (13), 2681-2687.

87.   Jesny, S.; Girish Kumar, K., Electrocatalytic resolution of guanine, adenine and cytosine along with uric acid on poly (4-amino-3-hydroxy naphthalene-1-sulfonic acid) modified glassy carbon electrode. *Journal of Electroanalytical Chemistry* **2017,** *801*, 153-161.

88.   Kim, M.; Ham, W. K.; Kim, W.; Hwangbo, C. K.; Choi, E. H.; Lee, G. J., Optical properties of nucleobase thin films as studied by attenuated total reflection and surface-enhanced Raman spectroscopy. *Opt Mater* **2018,** *78*, 531-537.

89.   Ks, S.; B, M.; N, K. S., Fabrication of copper oxide nanoparticles modified carbon paste electrode and its application in simultaneous electroanalysis of guanine, adenine and thymine. *Sensors and Actuators A: Physical* **2018,** *280*, 277-286.

90.   Li, W.; Jin, J.; Liu, X. Q.; Wang, L., Structural Transformation of Guanine Coordination Motifs in Water Induced by Metal Ions and Temperature. *Langmuir* **2018,** *34* (27), 8092-8098.

91.   Zhang, L.; Zhang, J., Multiporous molybdenum carbide nanosphere as a new charming electrode material for highly sensitive simultaneous detection of guanine and adenine. *Biosens Bioelectron* **2018,** *110,* 218-224.

92.   Shi, W.; Yu, J.; Katz, H. E., Sensitive and selective pentacene-guanine field-effect transistor sensing of nitrogen dioxide and interferent vapor analytes. *Sensors and Actuators B: Chemical* **2018,** *254*, 940-948.

93.   Jones, A. C.; Hitchman, M. L., *Chemical vapour deposition: precursors, processes and applications*. Royal society of chemistry: 2009.

94.   Hitchman, M. L.; Tian, F., Studies of TiO2 thin films prepared by chemical vapour deposition for photocatalytic and photoelectrocatalytic degradation of 4-chlorophenol. *Journal of Electroanalytical Chemistry* **2002,** *538*, 165-172.

95.   Crosbie, M.; Lane, P.; Wright, P.; Williams, D.; Jones, A.; Leedham, T.; Reeves, C.; Jones, J., Liquid injection metal organic chemical vapour deposition of lead–scandium–tantalate thin films for infrared devices. *Journal of crystal growth* **2000,** *219* (4), 390-396.

96.   Farka, D.; Coskun, H.; Bauer, P.; Roth, D.; Bruckner, B.; Klapetek, P.; Sariciftci, N. S.; Stadler, P., Increase in electron scattering length in PEDOT:PSS by a triflic acid post-processing. *Monatsh Chem* **2017,** *148* (5), 871-877.

97.   Farka, D.; Coskun, H.; Gasiorowski, J.; Cobet, C.; Hingerl, K.; Uiberlacker, L. M.; Hild, S.; Greunz, T.; Stifter, D.; Sariciftci, N. S.; Menon, R.; Schoefberger, W.; Mardare, C. C.; Hassel, A. W.; Schwarzinger, C.; Scharber, M. C.; Stadler, P., Anderson-Localization and the Mott-Ioffe-Regel Limit in Glassy-Metallic PEDOT. *Adv Electron Mater* **2017,** *3* (7).

98.   Aljabour, A.; Coskun, H.; Apaydin, D. H.; Ozel, F.; Hassel, A. W.; Stadler, P.; Sariciftci, N. S.; Kus, M., Nanofibrous cobalt oxide for electrocatalysis of CO2 reduction to carbon monoxide and formate in an acetonitrile-water electrolyte solution. *Appl Catal B-Environ* **2018,** *229*, 163-170.

99.   Orazem, M. E.; Tribollet, B., *Electrochemical impedance spectroscopy*. John Wiley & Sons: 2011; Vol. 48.

100.   Chang, B.-Y.; Park, S.-M., Electrochemical impedance spectroscopy. *Annual Review of Analytical Chemistry* **2010,** *3*, 207-229.

101.   Appel, A. M.; Bercaw, J. E.; Bocarsly, A. B.; Dobbek, H.; DuBois, D. L.; Dupuis, M.; Ferry, J. G.; Fujita, E.; Hille, R.; Kenis, P. J. A.; Kerfeld, C. A.; Morris, R. H.; Peden, C. H. F.; Portis, A. R.; Ragsdale, S. W.; Rauchfuss, T. B.; Reek, J. N. H.; Seefeldt, L. C.; Thauer, R. K.; Waldrop, G. L., Frontiers, Opportunities, and Challenges in Biochemical and Chemical Catalysis of CO2 Fixation. *Chemical Reviews* **2013,** *113* (8), 6621-6658.

102.   Hansen, H. A.; Varley, J. B.; Peterson, A. A.; Nørskov, J. K., Understanding Trends in the Electrocatalytic Activity of Metals and Enzymes for CO2 Reduction to CO. *The Journal of Physical Chemistry Letters* **2013,** *4* (3), 388-392.

103.   Jakešová, M.; Apaydin, D. H.; Sytnyk, M.; Oppelt, K.; Heiss, W.; Sariciftci, N. S.; Głowacki, E. D., Hydrogen-Bonded Organic Semiconductors as Stable Photoelectrocatalysts for Efficient Hydrogen Peroxide Photosynthesis. *Adv Funct Mater* **2016,** *26* (29), 5248-5254.

104.   Khadka, N.; Dean, D. R.; Smith, D.; Hoffman, B. M.; Raugei, S.; Seefeldt, L. C., CO2 Reduction Catalyzed by Nitrogenase: Pathways to Formate, Carbon Monoxide, and Methane. *Inorganic Chemistry* **2016,** *55* (17), 8321-8330.

105.   Sultana, S.; Chandra Sahoo, P.; Martha, S.; Parida, K., A review of harvesting clean fuels from enzymatic CO2 reduction. *RSC Advances* **2016,** *6* (50), 44170-44194.

106.   Zhu, Y.-P.; Liu, Y.-P.; Yuan, Z.-Y., Biochemistry-inspired direct synthesis of nitrogen and phosphorus dual-doped microporous carbon spheres for enhanced electrocatalysis. *Chemical Communications* **2016,** *52* (10), 2118-2121.

107.   Ball, V.; Frari, D. D.; Toniazzo, V.; Ruch, D., Kinetics of polydopamine film deposition as a function of pH and dopamine concentration: Insights in the polydopamine deposition mechanism. *Journal of Colloid and Interface Science* **2012,** *386* (1), 366-372.

108.   Bernsmann, F.; Ball, V.; Addiego, F.; Ponche, A.; Michel, M.; Gracio, J. J. d. A.; Toniazzo, V.; Ruch, D., Dopamine−Melanin Film Deposition Depends on the Used Oxidant and Buffer Solution. *Langmuir* **2011,** *27* (6), 2819-2825.

109.   Fu, L.; Lai, G.; Jia, B.; Yu, A., Preparation and electrocatalytic properties of polydopamine functionalized reduced graphene oxide-silver nanocomposites. *Electrocatalysis* **2015,** *6* (1), 72-76.

110.   Fu, L.; Lai, G.; Zhu, D.; Jia, B.; Malherbe, F.; Yu, A., Advanced Catalytic and Electrocatalytic Performances of Polydopamine-Functionalized Reduced Graphene Oxide-Palladium Nanocomposites. *ChemCatChem* **2016,** *8* (18), 2975-2980.

111.   Kanyong, P.; Rawlinson, S.; Davis, J., Fabrication and electrochemical characterization of polydopamine redox polymer modified screen-printed carbon electrode for the detection of guanine. *Sensors and Actuators B: Chemical* **2016,** *233*, 528-534.

112.   Murali, S.; Chang, J.-L.; Zen, J.-M., Bismuth oxide nanoparticles as a nanoscale guide to form a silver–polydopamine hybrid electrocatalyst with enhanced activity and stability for the oxygen reduction reaction. *RSC Advances* **2015,** *5* (6), 4286-4291.

113.   Palanisamy, S.; Thirumalraj, B.; Chen, S.-M.; Wang, Y.-T.; Velusamy, V.; Ramaraj, S. K., A facile electrochemical preparation of reduced graphene oxide@ polydopamine composite: A novel electrochemical sensing platform for amperometric detection of chlorpromazine. *Scientific reports* **2016,** *6*, 33599.

114.   Parnell, C. M.; Chhetri, B.; Brandt, A.; Watanabe, F.; Nima, Z. A.; Mudalige, T. K.; Biris, A. S.; Ghosh, A., Polydopamine-Coated Manganese Complex/Graphene Nanocomposite for Enhanced Electrocatalytic Activity Towards Oxygen Reduction. *Scientific Reports* **2016,** *6*, 31415.

115.   Peng, H.; Liang, C., Electrochemical determination of hydrazine based on polydopamine-reduced graphene oxide nanocomposite. *Fullerenes, Nanotubes and Carbon Nanostructures* **2017,** *25* (1), 29-33.

116.   Qu, K.; Zheng, Y.; Dai, S.; Qiao, S. Z., Graphene oxide-polydopamine derived N, S-codoped carbon nanosheets as superior bifunctional electrocatalysts for oxygen reduction and evolution. *Nano Energy* **2016,** *19*, 373-381.

117.   Yang, H.; Kang, S.; Zou, H.; Jin, J.; Ma, J.; Li, S., Polydopamine-functionalized multi-walled carbon nanotubes-supported palladium–lead bimetallic alloy nanoparticles as highly efficient and robust catalysts for ethanol oxidation. *RSC Advances* **2016,** *6* (93), 90462-90469.

118.   Zangmeister, R. A.; Morris, T. A.; Tarlov, M. J., Characterization of Polydopamine Thin Films Deposited at Short Times by Autoxidation of Dopamine. *Langmuir* **2013,** *29* (27), 8619-8628.

119.   Knowles, R. R.; Jacobsen, E. N. In *Organocatalysis Special Feature: Attractive noncovalent interactions in asymmetric catalysis: Links between enzymes and small molecule catalysts*, Proceedings of the National Academy of Science, 2010; pp 20678-20685.

120.   Lee, H.; Dellatore, S. M.; Miller, W. M.; Messersmith, P. B., Mussel-Inspired Surface Chemistry for Multifunctional Coatings. *Science* **2007,** *318* (5849), 426-430.

121.   Fei, B.; Qian, B.; Yang, Z.; Wang, R.; Liu, W. C.; Mak, C. L.; Xin, J. H., Coating carbon nanotubes by spontaneous oxidative polymerization of dopamine. *Carbon* **2008,** *46* (13), 1795-1797.

122.   Ye, W.; Wang, D.; Zhang, H.; Zhou, F.; Liu, W., Electrochemical growth of flowerlike gold nanoparticles on polydopamine modified ITO glass for SERS application. *Electrochimica Acta* **2010,** *55* (6), 2004-2009.

123.   Janotti, A.; Zhang, S.; Wei, S.-H.; Van de Walle, C., Effects of hydrogen on the electronic properties of dilute GaAsN alloys. *Physical review letters* **2002,** *89* (8), 086403.

124. Shultz, M. D.; Reveles, J. U.; Khanna, S. N.; Carpenter, E. E., Reactive Nature of Dopamine as a Surface Functionalization Agent in Iron Oxide Nanoparticles. *J Am Chem Soc* **2007,** *129* (9), 2482-2487.

125. McGinness, J.; Corry, P.; Proctor, P., Amorphous Semiconductor Switching in Melanins. *Science* **1974,** *183* (4127), 853-855.

126. McGinness, J. E., Mobility Gaps: A Mechanism for Band Gaps in Melanins. *Science* **1972,** *177* (4052), 896-897.

127. Apaydin, D. H.; Głowacki, E. D.; Portenkirchner, E.; Sariciftci, N. S., Direct electrochemical capture and release of carbon dioxide using an industrial organic pigment: Quinacridone. *Angewandte Chemie International Edition* **2014,** *53* (26), 6819-6822.

128. Blöchl, P. E., Projector augmented-wave method. *Physical review B* **1994,** *50* (24), 17953.

129. Monkhorst, H. J.; Pack, J. D., Special points for Brillouin-zone integrations. *Physical review B* **1976,** *13* (12), 5188.

130. Kresse, G.; Joubert, D., From ultrasoft pseudopotentials to the projector augmented-wave method. *Physical Review B* **1999,** *59* (3), 1758.

131. Perdew, J. P.; Burke, K.; Ernzerhof, M., Generalized gradient approximation made simple. *Physical review letters* **1996,** *77* (18), 3865.

132. Hafner, J., Ab-initio simulations of materials using VASP: Density-functional theory and beyond. *Journal of Computational Chemistry* **2008,** *29* (13), 2044-2078.

133. Humphrey, W.; Dalke, A.; Schulten, K., VMD: Visual molecular dynamics. *Journal of Molecular Graphics* **1996,** *14* (1), 33-38.

134. Perdew, J. P.; Burke, K.; Ernzerhof, M., Generalized Gradient Approximation Made Simple. *Physical Review Letters* **1996,** *77* (18), 3865-3868.

135. Seh, Z. W.; Kibsgaard, J.; Dickens, C. F.; Chorkendorff, I.; Nørskov, J. K.; Jaramillo, T. F., Combining theory and experiment in electrocatalysis: Insights into materials design. *Science* **2017,** *355* (6321).

136. Trasatti, S., Work function, electronegativity, and electrochemical behaviour of metals: III. Electrolytic hydrogen evolution in acid solutions. *Journal of Electroanalytical Chemistry and Interfacial Electrochemistry* **1972,** *39* (1), 163-184.

137. Züttel, A.; Remhof, A.; Borgschulte, A.; Friedrichs, O., Hydrogen: the future energy carrier. *Philosophical Transactions of the Royal Society A: Mathematical, Physical and Engineering Sciences* **2010,** *368* (1923), 3329-3342.

138.   Coskun, H.; Aljabour, A.; Luna, P. D.; Sun, H.; Nishiumi, N.; Yoshida, T.; Koller, G.; Ramsey, M. G.; Greunz, T.; Stifter, D.; Hassel, A. W.; Sariciftci, N. S.; Sargent, E. H.; Stadler, P., Bio-inspired hydrogen-bonded polymers mimic noble metal electrocatalysts. **2018**, submitted.

139.   Bonde, J.; Moses, P. G.; Jaramillo, T. F.; Nørskov, J. K.; Chorkendorff, I., Hydrogen evolution on nano-particulate transition metal sulfides. *Faraday Discussions* **2009,** *140* (0), 219-231.

140.   Jaramillo, T. F.; Jørgensen, K. P.; Bonde, J.; Nielsen, J. H.; Horch, S.; Chorkendorff, I., Identification of Active Edge Sites for Electrochemical H_2 Evolution from MoS_2 Nanocatalysts. *Science* **2007,** *317* (5834), 100-102.

141.   Laursen, A. B.; Kegnæs, S.; Dahl, S.; Chorkendorff, I., Molybdenum sulfides—efficient and viable materials for electro - and photoelectrocatalytic hydrogen evolution. *Energ Environ Sci* **2012,** *5* (2), 5577-5591.

142.   Li, H.; Tsai, C.; Koh, A. L.; Cai, L.; Contryman, A. W.; Fragapane, A. H.; Zhao, J.; Han, H. S.; Manoharan, H. C.; Abild-Pedersen, F.; Nørskov, J. K.; Zheng, X., Activating and optimizing MoS2 basal planes for hydrogen evolution through the formation of strained sulphur vacancies. *Nature Materials* **2015,** *15*, 48.

143.   Wang, M. L.; Cui, M. Z.; Liu, W. F.; Liu, X. G.; Xu, B. S., Facile Synthesis of Cyclodextrin Functionalized Reduced Graphite Oxide with the Aid of Ionic Liquid for Simultaneous Determination of Guanine and Adenine. *Electroanal* **2018,** *30* (5), 842-851.

144.   Gao, S. H.; Li, H. J.; Li, M. J.; Li, C. P.; Qian, L. R.; Yang, B. H., A gold-nanoparticle/horizontal-graphene electrode for the simultaneous detection of ascorbic acid, dopamine, uric acid, guanine, and adenine. *J Solid State Electr* **2018,** *22* (10), 3245-3254.

145.   Cam, E.; Tanik, N. A.; Cerkez, I.; Demirkan, E.; Aykut, Y., Guanine oxidation signal enhancement in single strand DNA with polyacrylonitrile/polyaniline (PAN/PAni) hybrid nanofibers. *J Appl Polym Sci* **2018,** *135* (3).

146.   D'Agostino, L., Native DNA electronics: is it a matter of nanoscale assembly? *Nanoscale* **2018,** *10* (26), 12268-12275.

147.   Popczun, N. J.; Breuer, L.; Wucher, A.; Winograd, N., Ionization Probability in Molecular Secondary Ion Mass Spectrometry: Protonation Efficiency of Sputtered Guanine Molecules Studied by Laser Postionization. *J Phys Chem C* **2017,** *121* (16), 8931-8937.

148.   Shi, W.; Zheng, Y. F.; Taylor, A. D.; Yu, J. S.; Katz, H. E., Increased mobility and on/off ratio in organic field-effect transistors using low-cost guanine-pentacene multilayers. *Appl Phys Lett* **2017,** *111* (4).

149.   Naveen, M. H.; Gurudatt, N. G.; Shim, Y. B., Applications of conducting polymer composites to electrochemical sensors: A review. *Appl Mater Today* **2017,** *9*, 419-433.

150.   Stadler, P.; Farka, D.; Coskun, H.; Glowacki, E. D.; Yumusak, C.; Uiberlacker, L. M.; Hild, S.; Leonat, L. N.; Scharber, M. C.; Klapetek, P.; Menon, R.; Sariciftci, N. S., Local order drives the metallic state in PEDOT:PSS. *J Mater Chem C* **2016,** *4* (29), 6982-6987.

151.   Ma, J. W.; Wang, M.; Lei, G. Y.; Zhang, G. L.; Zhang, F. B.; Peng, W. C.; Fan, X. B.; Li, Y., Polyaniline Derived N-Doped Carbon-Coated Cobalt Phosphide Nanoparticles Deposited on N-Doped Graphene as an Efficient Electrocatalyst for Hydrogen Evolution Reaction. *Small* **2018,** *14* (2).

152.   Feng, J. X.; Tong, S. Y.; Tong, Y. X.; Li, G. R., Pt-like Hydrogen Evolution Electrocatalysis on PANI/CoP Hybrid Nanowires by Weakening the Shackles of Hydrogen Ions on the Surfaces of Catalysts. *J Am Chem Soc* **2018,** *140* (15), 5118-5126.

153.   Das, S.; Ghosh, R.; Routh, P.; Shit, A.; Mondal, S.; Panja, A.; Nandi, A. K., Conductive MoS2 Quantum Dot/Polyaniline Aerogel for Enhanced Electrocatalytic Hydrogen Evolution and Photoresponse Properties. *ACS Applied Nano Materials* **2018,** *1* (5), 2306-2316.

154.   Ramohlola, K. E.; Monana, G. R.; Hato, M. J.; Modibane, K. D.; Molapo, K. M.; Masikini, M.; Mduli, S. B.; Iwuoha, E. I., Polyaniline-metal organic framework nanocomposite as an efficient electrocatalyst for hydrogen evolution reaction. *Compos Part B-Eng* **2018,** *137*, 129-139.

155.   Furukawa, M.; Yamada, T.; Katano, S.; Kawai, M.; Ogasawara, H.; Nilsson, A., Geometrical characterization of adenine and guanine on Cu(110) by NEXAFS, XPS, and DFT calculation. *Surface Science* **2007,** *601* (23), 5433-5440.

156.   Feyer, V.; Plekan, O.; Šutara, F.; Cháb, V.; Matolín, V.; Prince, K. C., Guanine adsorption on the Cu(110) surface. *Surface Science* **2011,** *605* (3), 361-365.

157.   Florian, J.; Baumruk, V., Scaled quantum mechanical force fields and vibrational spectra of solid state nucleic acid constituents. 4. N7-Protonated guanine. *The Journal of Physical Chemistry* **1992,** *96* (23), 9283-9287.

158.   MacDiarmid, A. G.; Epstein, A. J., Polyanilines: a novel class of conducting polymers. *Faraday Discussions of the Chemical Society* **1989,** *88*, 317-332.

159.   Chiang, J.-C.; MacDiarmid, A. G., 'Polyaniline': Protonic acid doping of the emeraldine form to the metallic regime. *Synthetic Metals* **1986,** *13* (1-3), 193-205.

160.   Chen, G.; Wang, T.; Zhang, J.; Liu, P.; Sun, H.; Zhuang, X.; Chen, M.; Feng, X., Accelerated Hydrogen Evolution Kinetics on NiFe-Layered Double Hydroxide Electrocatalysts by Tailoring Water Dissociation Active Sites. *Advanced Materials* **2018,** *30* (10), 1706279.

161.   Zhang, Q.; Wang, W.; Zhang, J.; Zhu, X.; Zhang, Q.; Zhang, Y.; Ren, Z.; Song, S.; Wang, J.; Ying, Z.; Wang, R.; Qiu, X.; Peng, T.; Fu, L., Highly Efficient Photocatalytic Hydrogen Evolution by ReS2 via a Two-Electron Catalytic Reaction. *Advanced Materials* **2018,** *30* (23), 1707123.

162.   Zhang, J.; Wu, J.; Guo, H.; Chen, W.; Yuan, J.; Martinez, U.; Gupta, G.; Mohite, A.; Ajayan, P. M.; Lou, J., Unveiling Active Sites for the Hydrogen Evolution Reaction on Monolayer MoS2. *Advanced Materials* **2017,** *29* (42), 1701955.

6. Curriculum Vitae

PERSONAL INFORMATION

Name	Halime
Last Name	Coskun Aljabour
Date of Birth	May 11, 1991
Email	halime.coskun_aljabour@jku.at
Birth Place	Linz, Austria
Nationality	Turkey
Contact Address	Linz Institute for Organic Solar Cells (LIOS)
	Institute of Physical Chemistry, Johannes Kepler University
	Linz, Altenbergerstr. 69, 4040 Linz, Austria

ACADEMIC QUALIFICATIONS

Nov 2015 -   **PhD student**
Johannes Kepler University (JKU), Faculty of Natural Science , Technical Chemistry, Linz, Austria

Oct 2013–Nov 2015   **Degree-Dipl.Ing:**
Johannes Kepler University (JKU), Faculty of Natural Science , Technical Chemistry, Linz, Austria

Oct 2010 –Jun 2013   **Degree- BSc:**
Johannes Kepler University (JKU), Faculty of Natural Science , Technical Chemistry, Linz, Austria

Sep 2002 – May 2010   **High School/ Science:**
Bundesrealgymnasium, Landwiedstr. 82, 4020 Linz

RESEARCH EXPERIENCE

Jul 2010   **Medical Practicum**
Dr. Andrea Gussner-Langl

Aug 2011   **Pharmaceutical Practicum**
Mag. pharm. Julia Rothenthal

Oct 2010 –Jun 2013   **Bachelor Student at JKU**

Oct 2013- Sept 2015   **Master Student at JKU**

RESEARCH PUBLICATIONS

1. Nanofibrous cobalt oxide for electrocatalysis of CO_2 reduction to carbon monoxide and formate in an acetonitrile-water electrolyte solution, A. Aljabour, **H. Coskun**, D.H. Apaydin, F. Özel, A.W. Hassel, P. Stadler, N.S. Sariciftci, M. Kus, Applied Catalysis B:Environmental, 229, 2018, 163-170.

2. Chemical vapor deposition - based synthesis of conductive polydopamine thin-films, **H. Coskun**, A. Aljabour, L. Uiberlacker, M. Strobel, S. Hild, C. Cobet, D. Farka, P. Stadler, N. S. Sariciftci, Thin Solid Films, 645, 2018, 320-325.

3. Biofunctionalized conductive polymers enable efficient CO_2 electroreduction, **H. Coskun**, A. Aljabour, P. D. Luna, D. Farka, T. Greunz, D. Stifter, M. Kus, X. Zheng, M. Liu, A. W. Hassel, W. Schöfberger, E. H. Sargent, N. S. Sariciftci, P. Stadler, Sci. Adv. 2017, 3, e1700686.

4. Anderson-Localization and the Mott–Ioffe–Regel Limit in Glassy-Metallic PEDOT, D. Farka, **H. Coskun**, J. Gasiorowski, C. Cobet, K. Hingerl, L. M. Uiberlacker, S. Hild, T. Greunz, D. Stifter, N. S. Sariciftci, R. Menon, W. Schoefberger, C. Mardare, A. W. Hassel, C. Schwarzinger, M. C. Scharber, P. Stadler, Adv. Electron. Mater. 2017, 1700050.

5. Increase in electron scattering length in PEDOT:PSS by a triflic acid post-processing, D. Farka, **H. Coskun**, P. Bauer, D. Roth, B. Bruckner, P. Klapetek, N. S. Sariciftci, P. Stadler, Monatsh Chem, 2017 148, 871–877.

6. Local order drives the metallic state in PEDOT: PSS, P. Stadler, D. Farka, **H.Coskun**, E.D. Glowacki, C. Yumusak, L.M. Uiberlacker, S. Hild, L. N. Leonat, M.C. Scharber, P. Klapetek, R. Menon, N.S. Sariciftci, *J.Mater. Chem. C*, 2016, *4*, 6982.

7. Improvement of catalytic activity by nanofibrous $CuInS_2$ for electrochemical CO_2 reduction, A. Aljabour, D.H. Apaydin, **H. Coskun**, F. Özel, M. Ersöz, P. Stadler, N.S. Sariciftci, M. Kus, *ACS Appl. Mater. Interfaces,* 2016, 8 (46), 31695–31701.

8. Bioconjugation of hydrogen-bonded organic semiconductor with functional proteins, E.D. Glowacki, R.R. Tangorra, **H. Coskun**, D. Farka, A. Operamolla, Y. Kanbur, F. Milano, L. Giotta, G.M. Farinola, N.S. Sariciftci, *J.Mater. Chem. C*, 2015, *3*, 6554.

9. Epindolidiones- Versatile and Stable Hydrogen-Bonded Pigments for Organic Field-Effect Transistors and Light-Emitting Diodes, E. D. Glowacki, G. Romanazzi, C. Yumusak, **H. Coskun**, U. Monkowius, G. Voss, M. Burian, R. T.

Lechner, N. Demitri, G. J. Redhammer, N. Sünger, G. P. Suranna, N. S. Sariciftci, *Adv. Func. Mat.,* 2015*, 25*, 5.

10. Hydrogen-bonded diketopyrrolopyrrole (DPP) pigments as organic semiconductors, E. D. Glowacki, **H. Coskun**, M. A. Blood-Forsythe, U. Monkowius, L. Leonat, M. Grzybowski, D. Gryko, M. S. White, A. Aspuru-Guzik, N. S. Sariciftci, *Organic Electronics*, 2014, *15*, 3521-3528.

RESEACH ACTIVITIES

Conferences/Workshops Attended

E-MRS, European Materials Research Society, Talk with the title: *Conductive Polydopamine for selective CO2 electroreduction*, 2017.

E-MRS, European Materials Research Society, Poster with the title: *New synthetic pathway of a naturally occurring pigment: vapor phase deposited polydopamine*, 2016.

Materials Research Society, Talk with the title: *Hydrogen-bonded pigment for transistors with stable operation directly in contact with aqueous electrolytes of pH 1-10,* 2015.

E-MRS, European Materials Research Society, Poster with the title: *Hydrogen-bonded diketopyrrolopyrrole (DPP) pigments as organic semiconductor*, 2015.

BioEL- International Winterschool on Bioelectronics, Poster with the title: *A stability study of H-bonded organic semiconductors in harsh acidic and alkaline conditions: Epindolidione versus Quinacridone*, 2015.

IWOBOE- International Workshop on Flexible Bio-and Organic Printed Electronics, Poster with the title: *Optoelectronic devices based on pristine H-bonded organic semiconductors: A comparative study of Quinacridone versus Pentacene*, 2014.

BioEL- International Winterschool on Bioelectronics, Poster with the title: *Water-stable organic transistors based on H-bonded organic semiconductors towards surface-modified transistor biodetectors,* 2014.

Solar Energy for World Peace, Poster with the title: *Hydrogen-bonded diketopyrrolopyrrole pigment semiconductors for organic electronics applications*, 2013.

JYU
JOHANNES KEPLER
UNIVERSITY LINZ

ACADEMIC TEACHING ACTIVITIES

since 2016:

Exercises in Physical Chemistry I (1.6 ECTS)

Exercises in Physical Chemistry II (1.6 ECTS)

PRIZES/ AWARDS

Sept 2017 Best Student Oral Presentation Award, E-MRS Fall Meeting, Warsaw, Poland

Mar 2018 Award for Organizing and Performing Workshop at "Lernwerkstatt für Kopf, Herz und Hand", Linz, Austria

QUALIFICATIONS

Driving Licence   B

Computing-knowledge   Microsoft-Office, Origin, ChemDraw

Mother tongue(s)   Turkish, German

Knowledge of languages:

	written	oral
English	C1	C1